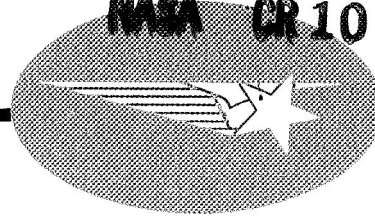


N 70 24 17 8

NASA CR 102602



CASE FILE COPY

INTERIM REPORT
STUDY OF THERMAL CONDUCTIVITY
REQUIREMENTS
VOL. I
HIGH PERFORMANCE INSULATION
THERMAL CONDUCTIVITY TEST
PROGRAM

Lockheed

MISSILES & SPACE COMPANY

A GROUP DIVISION OF LOCKHEED AIRCRAFT CORPORATION

SUNNYVALE, CALIFORNIA

LOCKHEED MISSILES & SPACE COMPANY
HUNTSVILLE RESEARCH & ENGINEERING CENTER
HUNTSVILLE RESEARCH PARK
4800 BRADFORD BLVD., HUNTSVILLE, ALABAMA

INTERIM REPORT
STUDY OF THERMAL CONDUCTIVITY
REQUIREMENTS
VOL. I
HIGH PERFORMANCE INSULATION
THERMAL CONDUCTIVITY TEST
PROGRAM

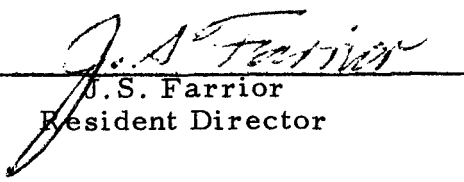
January 1969

Contract NAS8-21347

Prepared for George C. Marshall Space Flight Center
National Aeronautics and Space Administration

by
D. V. Hale

APPROVED BY: _____


J. S. Farrior
Resident Director

FOREWORD

This document presents the results of work performed by Lockheed's Huntsville Research & Engineering Center while under contract to the Propulsion & Vehicle Engineering Laboratory of NASA-Marshall Space Flight Center. This task was conducted as partial fulfillment of Contract NAS8-21347, "Study of Thermal Conductivity Requirements." Technical Monitors of the contract were Mr. John Austin and Mr. E. Haschal Hyde of the Propulsion & Vehicle Engineering Laboratory, Marshall Space Flight Center.

The interim report for "Study of Thermal Conductivity Requirements" consists of two volumes:

- Vol. I: High Performance Insulation Thermal Conductivity Test Program
- Vol. II: Multiple Docking Adapter (MDA) Thermal Model

SUMMARY

A cylindrical calorimeter was developed to measure temperature-dependent thermal conductivity for high performance insulation over a mean insulation temperature range from cryogenic temperatures to the upper temperature limit of the insulation. The device operates with a heat flux range of approximately one milliwatt to one watt per square foot of heated area and with a pressure range of 10^{-6} torr to one atmosphere. Specimen preparation costs are approximately \$400 per insulation specimen and the testing cost is approximately \$200 per data point. The ability of the device to operate accurately with a small temperature drop through the insulation (as small as 10°F) is due to its design. The apparatus is a glass fiber cylindrical tube, 3 inches in diameter, 1/16-in. thick, 3 feet long, and is wound at the center with a main test heater which is surrounded by four guard heaters. The specimen insulation is circumferentially wrapped about the cylinder. End caps of the insulation are joined to the cylindrically wrapped insulation with a diagonal-joint fit. The temperature differential is maintained across the insulation by the heaters inside and by a heated or cooled environmental shroud outside. By eliminating insulation edges with the end caps and by the electronic automation of the four guard heaters (which maintain a longitudinal temperature gradient to $\leq 0.05^{\circ}\text{F/feet}$), a thermal system results which closely approximates an infinite cylinder. The insulation backside pressure is recorded for each specimen with an ion gage installed in the calorimeter tube.

The new device was used to test the thermal conductivity of five high performance insulation materials over a temperature range of -100° to 200°F and a pressure range of 8×10^{-6} torr to one atmosphere. Samples tested were:

Specimen 1 - Unperforated double-aluminized Mylar (1/4-mil)
and 0.028-inch red polyurethane foam

- Specimen 2 - Perforated double-aluminized Mylar (1/4-mil) and 0.028-inch red polyurethane foam
- Specimen 3 - Embossed aluminized Mylar (1/4-mil)
- Specimen 4 - Embossed aluminized Mylar (1/4-mil) and Dimplar
- Specimen 5 - Embossed aluminized Mylar (1/4-mil) and nylon net.

The test results indicated a strong temperature and pressure dependence for the thermal conductivity of all five of the insulation materials. Probable errors were calculated for each data point and were included in the tables and curves for each specimen.

Gap testing was performed by cutting a circumferential slit at the center of the specimen of unperforated double-aluminized Mylar and red polyurethane foam. Room temperature tests were conducted with gap widths of 0, 1/20 and 1/10 inches, respectively. Also, a test was made with the 1/10-inch gap filled with red polyurethane foam. For a one-inch thick specimen of double-aluminized Mylar and red polyurethane foam, a 1/20-inch gap had an effective thermal conductivity of 6.82×10^{-3} Btu/hr-ft-°F while that for a 1/10-inch gap was 5.57×10^{-3} . A butt-joint test revealed a zero leak through the joint. The effective thermal conductivity for a 1/10-inch foam-filled gap was 2.96×10^{-3} Btu/hr-ft-°F. The data obtained were used to prepare engineering design curves.

Penetration tests were conducted on the Lockheed/Huntsville penetration test apparatus which is composed of a stainless steel penetration tube soldered to the center of a thick copper plate. The tests were made to compare methods of joining the high performance insulation on the plate (which represents a tank wall) to that on the penetration tube. The three methods considered were: (1) butt joint; (2) diagonal joint; and (3) buffer joint. A one-inch thick specimen of unperforated double-aluminized Mylar and red polyurethane foam was used for the tests. The plate was at liquid nitrogen temperature and the free end of

the penetration at room temperature. A thermal analysis of the diagonal joint was conducted. Good comparison (10.4% difference) was obtained between theory and test data. The tests revealed that the design which allowed minimum heat leakage to the plate through the penetration was the butt joint, (0.725 Btu/hr) followed by the diagonal joint (1.1 Btu/hr) and the buffer joint (1.45 Btu/hr).

Thermal conductivity data from six investigators for the double-aluminized Mylar and red polyurethane foam were studied, compared and presented in the form of comparative curves and tables. The study revealed that the assumption, definitions and test conditions used should be examined carefully when evaluating or comparing data between various investigators. Of particular importance were such items as layer density, surface conditions, backside pressure and boundary temperatures. When these factors were taken into account the data for the six investigators showed reasonably good comparison.

Also, various high performance insulation materials were compared on the basis of density-thermal conductivity versus mechanical load. When compared in this manner, the double-aluminized Mylar and nylon net had the lowest ρk value as well as the lowest k value in the 2×10^{-2} to 1 psi compression range for the temperatures considered. When compared on the basis of optimum layer density, the double-aluminized Mylar and Tissueglas combination was rated as the most efficient with the nylon net rating fourth. Because some fixed compressive load is generally associated with a given insulation application concept, comparison on the basis of a common compressive load is considered a necessary method of rating insulations.

CONTENTS

Section	Page
FOREWORD	ii
SUMMARY	iii
LIST OF TABLES AND FIGURES	viii
NOMENCLATURE	xii
1 INTRODUCTION	1
2 TASK I: THERMAL CONDUCTIVITY TESTING	3
2.1 Calorimeter Design and Operation	3
2.2 Environmental Control Apparatus	6
2.3 Specimen Preparation	7
2.4 Experimental Procedure	11
2.5 Theoretical Procedure and Error Analysis	12
2.6 Test Results	13
3 TASK II: INSULATION JOINT TESTING	18
3.1 Test Design	18
3.2 Thermal Analysis of the Joint Test Design	18
3.3 Experimental Results	19
3.4 Error Analysis	23
4 TASK III: INSULATION PENETRATION EFFECTS	24
4.1 Apparatus Design	24
4.2 Specimen Preparation	24
4.3 Experimental Results and Error Analysis	25

CONTENTS (Continued)

Section		Page
5	TASK IV: HIGH PERFORMANCE INSULATION DATA COMPARISON	27
	5.1 Problems Involved in High Performance Insulation Data Comparison	27
	5.2 Data Comparison of Double-Aluminized Mylar and Red Foam	29
	5.3 Comparison of Various High Performance Insulation Materials on a Basis of Mechanical Load	32
	REFERENCES	35
	APPENDIXES	
	A: Error Analysis	
	B: Kline-McClintock Probable Error Analysis Procedure	

LIST OF TABLES AND FIGURES

Table		Page
1	HREC Cylindrical Calorimeter Instrumentation Wires	37
2	Standard Thermal Conductivity Test Sequence	38
3	Test Results for Unperforated Double-Aluminized Mylar and Foam Specimen	39
4	Test Results for Perforated Double Aluminized Mylar and Red Foam Specimen	40
5	Test Results for Embossed Single Aluminized Mylar Specimen	41
6	Test Results for Dimplar and Embossed Aluminized Mylar Specimen	42
7	Test Results for Embossed Aluminized Mylar and Nylon Net Specimen	43
8	Table of Thermal Conductivity Data for 1/4-mil Double Aluminized Mylar and Red Polyurethane Foam for Various Investigators	44
9	Comparison of Various HPI Materials	46
Figure		
1	LMSC/HREC Cylindrical Calorimeter Before Application of Insulation Specimen	47
2	Schematic of LMSC/HREC Cylindrical Calorimeter Design	48
3	Insulation Application Concept	49
4	Environmental Control and Vacuum Chamber System	50
5	1/4-mil Double Aluminized Mylar and Red Polyurethane Foam Specimen	51
6	Embossed Singly Aluminized Mylar and Nylon Net Specimen	51
7	Vacuum Chamber System (View 1)	52
8	Vacuum Chamber System (View 2)	52
9	Electronic Automation Control Panel	53
10	Plot of Thermal Conductivity vs Temperature for Unperforated 1/4-mil Double-Aluminized Mylar and Red Polyurethane Foam	54

LIST OF FIGURES (Continued)

Figure		Page
11	Plot of Thermal Conductivity vs Chamber Pressure at Room Temperature for 1/4-mil Double-Aluminized Mylar and Red Polyurethane Foam Specimen	55
12	Plot of Thermal Conductivity and Chamber Pressure versus Time for 200°F Data Point for Unperforated Goodyear Insulation	56
13	Plot of Thermal Conductivity vs Temperature for Perforated and Unperforated 1/4-mil Double-Aluminized Mylar and Red Polyurethane Foam Specimen	57
14	Plot of Thermal Conductivity vs Chamber Pressure at Room Temperature for Perforated 1/4-mil Double-Aluminized Mylar and 0.030-Inch Red Foam Specimen	58
15	Plot of Pressure vs Time for 200°F Data Point for Perforated and Unperforated 1/4-mil Double-Aluminized Mylar and Red Polyurethane Foam Specimen	59
16	Plot of Thermal Conductivity versus Temperature for Embossed Aluminized Mylar at 162 Layers/Inch	60
17	Plot of Thermal Conductivity versus Chamber Pressure at Room Temperature for Embossed Aluminized Mylar at 162 Layers/Inch	61
18	Plot of Thermal Conductivity vs Temperature for Alternate Layers of Dimplar and Embossed Aluminized Mylar at 19.15 Layers per Inch	62
19	Plot of Thermal Conductivity vs Chamber Pressure at Room Temperature for Alternate Layers of 1/4-mil Embossed Aluminized Mylar and Dimplar at 19.15 Layers/Inch	63
20	Plot of Thermal Conductivity vs Temperature for Alternate Layers of 1/4-mil Embossed Aluminized Mylar and Nylon Net at 60 Layers Per Inch	64
21	Plot of Thermal Conductivity vs Chamber Pressure at Room Temperature for Alternate Layers of 1/4-mil Embossed Aluminized Mylar and Nylon Net at 60 Layers Per Inch	65
22	Insulation Gap Test Schematic	66
23	Butt Joint with 1/10-Inch Separation	67
24	Model Used for Thermal Analysis of Gap Test	68

LIST OF FIGURES (Continued)

Figure		Page
25	External Surface Temperature Distribution on 1/10-Inch Gap Test Specimen for 1/4-mil Double-Aluminized Mylar and Red Polyurethane Foam 1-In. Thick at Room Temperature	69
26	Plot of Effective Gap Width versus Gap Width for Specimen of 1/4-mil Double-Aluminized Mylar and Red Polyurethane Foam 1-In. Thick at Room Temperature	70
27	Plot of Effective Panel Thermal Conductivity versus the Ratio of Panel Area to Gap Length for Double-Aluminized Mylar and Red Polyurethane Foam 1-Inch Thick at Room Temperature	71
28	Penetration Test Apparatus	72
29	Diagonal-Joint Insulation Fit	73
30	Butt-Joint Insulation Fit	74
31	Buffer-Joint Insulation Fit	75
32	Penetration Test Apparatus During Wrapping Process	76
33	Diagonal-Joint Insulation Specimen on Penetration Test Apparatus	77
34	Open End of Penetration Test Apparatus	77
35	Backside of Penetration Test Apparatus	78
36	Buffer-Joint Insulation Specimen on Penetration Test Apparatus	79
37	Temperature Distribution Along Penetration for Diagonal-Joint Insulation Specimen	80
38	Axial Temperature Distribution Along Base of Penetration for Diagonal, Buffer and Butt Insulation Specimen	81
39	Plot of Thermal Conductivity vs Temperature for Double Aluminized Mylar and Red Polyurethane Foam as Presented by Various Investigators	82
40	Plot of Thermal Conductivity vs Layer Density for Double-Aluminized Mylar and Red Polyurethane Foam as Presented by Various Investigators	83
41	Plot of Density x Thermal Conductivity vs Mechanical Load for Various HPI Materials at 0°F	84

LIST OF FIGURES (Continued)

Figure		Table
42	Plot of Density x Thermal Conductivity vs Mechanical Load for Various HPI Materials at 400°R and 40°R Boundary Temperatures	85
43	Plot of Thermal Conductivity vs Mechanical Load for Various HPI Materials at 0°F	86
44	Plot of Thermal Conductivity vs Mechanical Load for Various HPI Materials of 400°R and 40°R Boundary Temperatures	87

NOMENCLATURE

A_c	calorimeter tube cross section
C_p	specific heat
d	error in a quantity
I	test section current
k	thermal conductivity
L	calorimeter test section length
m	mass
P	test section power
q	heat flux through insulation on test section
q_l	longitudinal heat flow from test section
q_s	heat stored in test section
r	insulation specimen radius
t	calorimeter tube thickness
T	temperature
ΔT	$(T_i - T_o)$
V	test section voltage

Greek

δ	gap width
θ	time
ρ	insulation density

NOMENCLATURE (Continued)

Subscripts

i	inside of insulation
ins	insulation
o	outside of insulation
1	glass fiber tube
2	copper heater wires

Section 1

INTRODUCTION

The need for extremely high performance insulation (HPI) has accelerated the development of insulation composites that are capable of operating in the thermal conductivity range of 10^{-4} to 10^{-5} Btu/hr-ft- $^{\circ}$ R. With the availability of such efficient insulation and with the constant development of new and improved composites, the problems associated with insulating missile systems and components efficiently would seem to be solved; however, problems remain that cannot be solved simply by developing insulations that have even lower thermal conductivity values. Significant problems which remain are applying the insulation and predicting the performance of the applied insulation.

The thermal conductivity of evacuated multilayer insulation materials has in the past been obtained by using a flat-plate or guarded-tank type of calorimeter. When one of these devices is used, material is tested by imposing large temperature differentials across the insulation specimen. As a result of these tests, an effective thermal conductivity for the boundary temperatures used is obtained.

A new testing technique has been developed which permits accurate temperature dependent thermal conductivity measurement due to the small temperature differential required across the specimen. This new technique employs a glass fiber tube wound with a main test heater and two guard heaters on each side of the main test section. The use of guard heaters virtually eliminates longitudinal temperature gradients and permits data to be obtained with a driving temperature potential of only a few degrees ($\geq 10^{\circ}$ F). The basic test apparatus was discussed previously in Ref. 1; however, at the time of that writing, the device was operated manually. Since then, the operation of the apparatus has been completely automated. As a result, personnel attendance time has been reduced from 24 hours per

day to 3-5 hours per day. Furthermore, automating the system has resulted in greater accuracy in the data generated.

The apparatus also has application to the study of insulation gaps and joints. These gaps, which occur where panels of insulation are joined, can result in heat leakage which is a significant part of the total. The joint studies conducted on the apparatus are discussed in Task II.

Heat leakage through penetrations was also considered to be of significance because of the magnitude of heat that can be attributed to it. Tests conducted on the Lockheed/Huntsville penetration apparatus are discussed in Task III.

The presentation of information obtained during this study is as follows:

Section 2 - Thermal Conductivity Testing (Task I)

Section 3 - Insulation Joint Testing (Task II)

Section 4 - Insulation Penetration Effects (Task III)

Section 5 - High Performance Insulation Data Comparison (Task IV)

Each section of this report presents all the information pertinent to that particular subject including results, excepting references, tables and figures, which are found on pages 36 through 87.

Section 2

TASK I: THERMAL CONDUCTIVITY TESTING

2.1 CALORIMETER DESIGN AND OPERATION

The Lockheed/Huntsville cylindrical calorimeter was developed in 1967 under Contract NAS8-21134 for the purpose of obtaining thermal conductivity of highly anisotropic materials. Considerations that led to the specific design chosen for the apparatus are discussed in detail in Section 3 of Ref. 1, which is the final report for that contract. Primary considerations were accuracy and ease of specimen preparation. During the present contract, major improvements were made on the apparatus and its associated equipment. Although these improvements do contribute to the system's accuracy and ease of specimen preparation, the major value of the improvements were in the area of reducing the cost per data point. Testing that once required 24 hours a day of personnel attendance now requires only 3 to 5 hours per day. Included in this section of the report are a description of the calorimeter design and operation, the environmental control apparatus, the specimen preparation procedure, the test procedure, the theoretical procedure and the test results.

A photograph of the basic calorimeter is shown in Fig. 1 and a schematic drawing in Fig. 2. The calorimeter consists of a 1/16-in. thick, 3-in. outside diameter, 38-in. long silicone glass fiber tube, wound continuously and covered completely by five heaters which consist of 6-mil copper magnet wire. The primary or test heater, 1 foot in length, is located at the geometric center of the tube. On either side of the test heater is a 1-ft "longitudinal" heater, and beyond each of these there is a 1-in. end heater. (These heater systems serve a purpose similar to the guard heaters used on flat plate calorimeters.) Four fine differential thermocouples (3-mil copper and constantan) connect each adjacent pair of the five thermocouple junction points (Fig. 2) and are used to monitor the temperature difference between these junction points.

The entire calorimeter is wrapped with a specimen of the insulation to be tested. The longitudinal portion of the calorimeter is wrapped circumferentially, and the ends are covered with end discs of insulation. Figure 3 shows the diagonal joint at which the circumferential panels meet the end caps of insulation. The instrumentation wires exit the insulation at these diagonal joints. The insulated calorimeter is placed in an environmental shroud to control the outside of the insulation at a uniform, desired temperature, and the combined system is then placed in a vacuum chamber. The inside of the insulation is maintained at a slightly higher temperature than the outside by supplying power to the five internal heaters. The temperature drop from inside to outside is measured by a differential thermocouple. The known power, temperature drop, insulation thickness and area enable thermal conductivity of the insulation to be determined.

An ion pressure transducer gage was installed inside the calorimeter at one end to measure the gas pressure inside the calorimeter during testing. This is a meaningful measurement due to the outgassing of some of the insulation materials tested. Occasionally, the internal pressure was two orders of magnitude higher than the pressure on the outside of the insulation.

An electronic automation system was the major new feature added to the system. The five calorimeter heaters are now controlled automatically as well as the environmental control apparatus which is discussed in the next section. The longitudinal heaters and end heaters are controlled by using the emf outputs from the four differential thermocouples discussed previously as input to four high-gain (10^6) amplifiers which directly drive the four heaters. Fine amplifier adjustments assure precise control of the longitudinal temperature. It is important to note that the longitudinal heaters and the end heaters serve distinctly different functions, as is discussed in the following paragraphs.

After several months of operating the system, the following operational concept has evolved. The longitudinal heaters are used to assure a zero temperature difference between the center of the test heater and the centers of the longitudinal heaters. The end heaters are not used as might be expected

to maintain a zero-temperature difference between the centers of the longitudinal heaters and the centers of the end heaters. Instead, they are used to maintain a power distribution in the longitudinal heaters which is approximately the same as that in the test heater. That is, the goal is to avoid a temperature or power discontinuity between the test heater and the longitudinal heaters since the overall objective is to attain an infinite cylinder effect near the test section. To attain the power balance, it is necessary occasionally to have a significant temperature discontinuity between the longitudinal heaters and the end heaters. Fine adjustments of the amplifier offset resistors make possible the end heater temperature adjustments necessary to attain power density similarity. Conservation of energy implies that whenever the power density and temperature in a longitudinal heater is equal to that in the test heater, no net heat flows longitudinally between the two. A substantially higher power density always exists in the end heaters than is present in the test or longitudinal heaters. This is due to the heat loss from the ends of the calorimeters. The end heat loss is kept to a minimum by the end caps of insulation and by using the fine instrumentation wires discussed previously.

Even though the total system is automated, the test heater itself can be operated automatically or manually. In the automatic mode, the test heater temperature is held constant, while under the manual mode, the test heater power is held constant. The fixed temperature under the automatic mode is attained by having a variable reference voltage in series with a thermocouple as input to a high-gain amplifier. The output from the amplifier drives the test heater. The thermocouple measures the temperature between a liquid nitrogen reference bath and the test heater. The variable reference voltage is set to match the thermocouple emf which would correspond to the temperature desired. This will maintain the temperature of the heater at the value prescribed.

The fixed-power capability is desirable because under the extremely high-gain conditions of the amplifier, instability causes power fluctuations

which make accurate measurement of the output test power difficult. Therefore, after equilibrium is reached, the output voltage is monitored on a Sanborn recorder, and the average value is estimated and dialed in under the fixed voltage (or power) mode. Minor adjustments may be required before near steady state is attained. The known thermal capacity of the calorimeter provides for rapid convergence. The final steady state power is that used for determining thermal conductivity.

2.2 ENVIRONMENTAL CONTROL APPARATUS

In preparation for this contract, Lockheed/Huntsville constructed a vacuum chamber for conducting thermal conductivity tests on HPI systems. The chamber was designed specifically to meet the requirements of the thermal tests with the two primary criteria: (1) precise thermal control and (2) speed of operation. This chamber, shown in Fig. 4, is a major improvement over the larger and less ideally designed vacuum chamber that was used for testing under the previous contract. The nominal dimensions are 17.5 in. inside diameter and 52 in. long. The chamber was constructed by butting a stainless steel, right circular cylinder chamber 23 in. long, against a glass bell jar chamber 30 in. long (including access within the chamber). An aluminum shroud 14 in. inside diameter and approximately 47 in. long is used to provide a controllable thermal environment for the test specimen. A copper coil encloses the aluminum shroud, and the fluid is circulated through the coil for thermal control of the shroud. The shroud and coil are enclosed in an HPI blanket to minimize heat leakage between the shroud and the chamber.

The shroud can be either heated by hot water or cooled by liquid nitrogen. Heated water is supplied to the shroud coil by a closed fluid loop containing a liquid pump and heater. The heater power is set at a value sufficient to maintain the shroud at the desired temperature. A thermocouple located in the fluid loop is used as input to a temperature controller which controls a relay. The relay activates or deactivates the heater power as required. This system maintains the shroud at almost constant temperature ($\pm 4^{\circ}\text{F}$).

For the cooling mode, LN₂ is supplied by a 25-gal dewar situated near the vacuum chamber. A thermocouple in series with a variable reference voltage is used as input to an amplifier which controls a relay, which in turn actuates a valve in the LN₂ supply line. The thermocouple measures the temperature difference between an LN₂ bath and the environmental shroud. The reference voltage is set to match the emf that the thermocouple would produce when the shroud is at the temperature desired. The LN₂ is vented to the atmosphere after it passes through the shroud coil. By having a short supply line between the dewar and the shroud, the temperature variations of the shroud during operation are held to a minimum ($\leq 8^{\circ}\text{F}$). The HPI blanket around the shroud minimizes the number of LN₂ flow cycles. A typical cycle is two to three hours. However, the oscillations in the shroud temperature are impressed on the outside of the specimen insulation requiring that the average ΔT across the insulation be used in calculating a data point. The ΔT , therefore, must be much greater than the temperature variation of the shroud. A ΔT of 30°F or greater is sufficient.

2.3 SPECIMEN PREPARATION

Five HPI materials were tested for their thermal conductivity as a function of temperature. They were:

1. Unperforated double-aluminized Mylar (1/4-mil) and 0.028-in. red polyurethane foam
2. Perforated double-aluminized Mylar (1/4-mil) and 0.028-in. red polyurethane foam
3. Embossed singly aluminized Mylar (1/4-mil)
4. Alternate layers of 1/4-mil embossed singly aluminized Mylar and Dimplar
5. Alternate layers of 1/4-mil embossed singly aluminized Mylar and nylon net.

Basically, two methods were used in preparing these specimens. The first method, used on the first two specimens, was to apply alternate single

layers of Mylar and foam until the desired thickness was achieved. A butt joint with no bonding was used on the foam while an overlap joint secured with Mylar tape was used on the Mylar layers. The end caps were applied simultaneously with the side layers. The second method was to wrap the insulation continuously on the tube until the desired thickness was attained, after which all the end caps were applied as a group. The outermost end cap was secured to the outermost side layer with Mylar tape.

On all five specimens the layers were joined diagonally at the ends of the calorimeter (Fig. 3). This eliminated any thermal shorting between layers. The calorimeter and insulation, weighing approximately 2 lb, were supported in the vacuum chamber by a thin nylon cord connected to each end of the glass fiber tube and passed through the insulation at the 45-deg joint to a support rod above the specimen. Heat loss was, therefore, limited to that passing through the instrumentation wires and the nylon cords. Adjustable end power compensated for this heat loss.

The thermocouples used on this equipment are listed in Table 1. The four differential thermocouples discussed in Section 2.1 are those used to control the temperatures of the longitudinal and end heaters. Two of the absolute thermocouples are used to measure the temperature of the test heater. (They are referenced to an LN_2 bath.) One of these is also used as input to the automation control system on the test heater. The other two thermocouples listed in the table are used to measure the temperature difference between the inside and the outside of the insulation. They are redundant as are the two above to protect against failure. Each is referenced to junctions on the outside of the insulation specimen which are not shown on Fig. 2.

After the calorimeter is wrapped with the specimen insulation in one of the ways described above, and the outside thermocouple is attached to the insulation, the entire package is suspended in the chamber by the support rod and support brackets. The shroud and chamber are then closed and testing is begun.

2.3.1 Unperforated Double-Aluminized Mylar (1/4-mil) and 0.028 In. Red Polyurethane Foam

A specimen of double-aluminized Mylar (1/4-mil Mylar and 600 angstroms aluminum on each side) and 0.028 in. polyurethane red foam insulation was prepared by Goodyear Aerospace Corporation, Akron, Ohio, according to the procedures they commonly use in applying their insulation. Figure 5 shows the specimen as it was received from Goodyear (except for the joint at the center which is discussed in a later section). The specimen contained 24 layers of Mylar and 23 layers of foam and has a total thickness of 1 in. Each layer of Mylar and foam was cut to size so that the foam forms a butt joint and the Mylar overlaps slightly so that it could be taped with transparent Mylar tape. Each successive layer of Mylar and foam was applied completely including the end caps before the next layer was started. Each Mylar end cap was large enough to allow a 3/4-in. overlay on to the side Mylar layer.

Because of the rigidity of the foam and the layer density chosen (24 layers per in.), no sagging resulted. The specimen was uniformly 1-in. thick. Extreme care was used by Goodyear personnel in preparing the specimen.

2.3.2 Perforated Double-Aluminized Mylar (1/4-in.) and 0.028 In. Red Polyurethane Foam

A perforated specimen of double-aluminized Mylar (1/4-mil Mylar and 600 angstroms of aluminum on each side) and 0.028-in. red polyurethane foam insulation was prepared by Goodyear Aerospace Corporation to exactly the same specifications as was the unperforated specimen described previously. The only difference in the two specimens was the perforations in the Mylar. The perforations were 0.085 in. in diameter on 3/8 in. centers.

2.3.3 Embossed Singly Aluminized Mylar (1/4-mil)

A continuous sheet of embossed aluminized Mylar was cut long enough and wide enough to wrap a calorimeter continuously with 1 in. of insulation and a total of 70 layers. No spacer was used in this lay-up. The material was so loose at this layer density that it compressed to 1/2 in. at the top and sagged to 1-1/2 in. at the bottom. Under this condition no meaningful tests could be made; therefore, the same sheet was wrapped again on the calorimeter, this time at the minimum layer density for which there would be no significant sagging. The result was that the sheet was wrapped to 1/2-in. thick with 81 layers of insulation. The resulting layer density was 162 layers per inch. Discs of the same material varying in diameter from 3 in. (the size of the calorimeter) to 4 in. were used to insulate the ends of the calorimeter.

2.3.4 Embossed Singly Aluminized Mylar (1/4-mil) and Dimplar

A sheet of Dimplar and a sheet of embossed aluminized Mylar were placed together and cut to the size necessary for wrapping at 22 layers and 1-in. thick. Marks were made along the edges at the proper positions so that when these marks were aligned the insulation would be smoothly applied. After the insulation was applied, the final diameter measured 5.15 in. At 22 layers, the resulting layer density was 19.15 layers per inch. End caps of the material were applied as discussed in Section 2.2.3.

2.3.5 Embossed Singly Aluminized Mylar (1/4-mil) and Nylon Net

A sheet of embossed aluminized Mylar and a sheet of white nylon net were placed together and cut to a size that would provide for 70 layers of insulation at 1-in. thick. The insulation was not applied to this exact layer

density, however. Instead, it was applied on the minimum layer density for which there would be no appreciable sagging. The result was that the specimen laid up at 1-in. thick and 60 layers per inch. End caps were applied in the manner described in previous sections. Figure 6 shows the completed specimen.

2.4 EXPERIMENTAL PROCEDURE

After a specimen was prepared and the lead wires checked for continuity, the entire assembly was suspended from a support rod (Fig. 4), and hung inside the environmental shroud. Figures 7 and 8 show views of the vacuum chamber after the shroud was closed, the protective HPI applied and the bell jar set in place. To the right side of Fig. 7 is the control panel for the heated water environmental control system. To the lower left of Fig. 8 is the LN₂ portable storage dewar for use in cooling the environmental control system. Figure 9 shows the control panel for the electronic automation system.

Table 2 shows the basic test sequence used for testing each specimen. After the -100°F data point was reached, the temperature within the calorimeter could be increased without changing the chamber pressure. This was accomplished by dialing in a large power on the five calorimeter heaters until the new temperature was attained. The calorimeter cannot be cooled to -100°F at low pressures, however, because of the low thermal conductivity of the insulation.

A typical test procedure is as follows:

- Evacuate the chamber to approximately 10^{-3} torr Hg.
- Purge the system with gaseous helium preheated to 250°F for one hour at approximately one atmosphere.
- Begin chamber evacuation and simultaneously begin establishing the required temperature gradient through the insulation. This is accomplished with the five heaters and the environmental control system by setting the reference voltages on the test and shroud automation systems.

- When the ultimate pressure ($\leq 8 \times 10^{-8}$ torr) and the temperature profile are attained, record the temperature drop through the insulation, the longitudinal gradients on the calorimeter and the power level of the test and longitudinal heaters. A data point is attained when the following conditions are met:
 1. The test power and temperature are near steady for at least three hours such that $dT/d\theta \leq 0.02^\circ\text{F/hr}$ and $dP/d\theta = 0$ (fixed power mode).
 2. The longitudinal powers are near the same value as the test heater (within 10%).
 3. The longitudinal heaters are the same temperature as the test heater (within $1/20^\circ\text{F}$).

(The latter two conditions can be attained by offset adjustments on the four control amplifiers. The first condition is attained only by waiting for the transients to settle and dialing in the correct fixed voltage.)
- When the data point is complete, read the pressure inside the calorimeter.

The test current and voltage provide the test power. This along with the ΔT through the insulation and the specimen dimensions provide the insulation thermal conductivity. A typical data point requires approximately three days of test time.

2.5 THEORETICAL PROCEDURE AND ERROR ANALYSIS

The conduction equation used to calculate the thermal conductivity of insulation on the cylindrical calorimeter is

$$k(T) = \frac{q \ln \left(\frac{r_o}{r_i} \right)}{2 \pi L \Delta T}$$

where

$$T = \frac{T_i + T_o}{2}$$

The specimen parameters r_o , r_i and L are measured before the specimen is tested, while ΔT and q are measured as described in Section 2.4 at thermal equilibrium. An equilibrium q is obtained simply by knowing P , the power ($V \times I$), in the test section. If heat is flowing into or out of the test section in a longitudinal direction, however, or if the test section is storing or releasing heat, then q becomes

$$P \pm q_l \pm q_s$$

Errors in r_o , r_i , L and ΔT must be examined as well to arrive on the probable error in $k(T)$. Appendix A has a complete error analysis to determine the error in $k(T)$. The results from that analysis are used to obtain the error on each data point. That error is presented in the test results. A typical test error at room temperature and 10^{-5} torr for one inch of insulation thickness is $\pm 10\%$.

2.6 TEST RESULTS

Test results for the thermal conductivity data are presented in Figs. 10 through 21 as curves of thermal conductivity as a function of temperature and pressure. The data are also presented in Tables 3 through 7.

2.6.1 Unperforated Double-Aluminized Mylar and Red Foam

Table 3 presents in chronological order the data that were obtained for the unperforated double-aluminized Mylar and red foam insulation specimen. Figures 10 and 11 show, respectively, the temperature-dependent data taken at pressures of $\leq 8 \times 10^{-6}$ torr Hg and the pressure-dependent data taken at room temperature. Also on Fig. 10 is plotted, for the purpose of comparison, the data obtained for the unperforated Goodyear insulation tested under contract NAS8-21134. The only difference in the two specimens was the layer densities. The earlier specimen had a layer density of 21

layers per inch, while this one had a density of 23 layers per inch. This difference was due to a slight difference in the foam thicknesses used for the two specimens. The figure shows a favorable comparison, especially considering the layer density differences. Error bands on the figures correspond to the probable errors listed in the table. Also on Fig. 10 is data taken by Dynatech for a 24-layer-per-inch specimen using 30-mil foam. The Dynatech data also were taken with small temperature differentials across the insulation. Again, the comparison is favorable. The room temperature pressure-dependent data are plotted as a function of chamber pressure because the ion gage installed inside the tubular calorimeter and used to record the insulation backside pressure did not read above the 10^{-4} torr pressure range. At all but the very low pressure ranges ($\leq 10^{-3}$ torr), however, the backside pressure was assumed equal to the chamber pressure. It should be noted that the low pressure room temperature point reveals two orders-of-magnitude difference between the chamber and the backside pressures. Table 3 further indicates that for points below room temperature, the difference was more like one order of magnitude. For points above room temperature, the insulation backside pressure was too high to read. The one point of particular interest is the 104.5°F point which has a very low insulation backside pressure considering its temperature. The reason for this low pressure is discussed fully in the following paragraphs.

An interesting phenomenon occurred at the two high temperature data points, 140.2°F and 202.5°F . Long-term outgassing of the insulation occurred with an accompanying decrease in thermal conductivity during the same period. Figure 12 shows chamber pressure and thermal conductivity versus time for the 202.5°F point. Figure 12 indicates that even after five days the specimen was still outgassing and, accordingly, the thermal conductivity was still decreasing. The 140.2°F data point was run for just one day, and as a result the insulation did not have sufficient time to outgas. At the time it was not expected that this long-term outgassing phenomenon would be present at this temperature. This accounts for the high value of thermal conductivity for this data point as shown in Fig. 10. The

high chamber pressure listed in the table for this data point tends to substantiate the theory that sufficient outgassing was not allowed.

After five days of outgassing the specimen at 200°F, additional data were run at lower temperatures to determine if the outgassing at the 200°F point would affect the thermal conductivity at lower temperatures. The effect was found to be present just as it was for this insulation specimen in the previous series of tests. This is shown clearly for both series of tests in Fig. 10. The effect seemed more prominent for the previous series of tests than it does for the current series. The only point to test the effect for the current series was the 104.5°F point shown in Fig. 10 and Table 3. While the thermal conductivity value is not too much lower than for those points taken before outgassing, a more realistic story is told by the insulation backside pressure. The backside pressure was an order of magnitude lower at 104.5°F than it was for 88.5°F, whereas it would be expected to be much higher had outgassing not occurred. Indeed, there appears to be a long-term insulation outgassing effect which occurs at certain temperatures for the specimen tested.

One data point was run with a large ΔT so that results could be compared with results of thermal conductivity tests performed by other investigators. This point is the last listed in Table 3. It compares quite favorably with data taken by other investigators as detailed in Section 5.2. Absolute comparison is not possible, however, because the boundary temperatures used, 78°F and -161°F, were not matched by any other experimentalists.

2.6.2 Perforated Double-Aluminized Mylar and Red Foam

Table 4 presents in chronological order the data obtained for the perforated double-aluminized Mylar and red foam insulation specimen. Figs. 13 and 14 show, respectively, the temperature-dependent data taken at pressures of $\leq 8 \times 10^{-6}$ torr Hg and the pressure-dependent data taken at room temperature. Figure 13 also shows the data for the unperforated

specimen for comparison. As expected the radiation heat leakage through the perforations resulted in an increase in the measured thermal conductivity.

The error bands on Figs. 13 and 14 correspond to probable errors listed in Table 4. Figure 15 presents the outgassing of the perforated Goodyear insulation at 200°F. Also plotted is the outgassing curve at 200°F of the unperforated specimen tested previously. The curves show the chamber pressure plotted as a function of time. Although the test conditions may have been slightly different for the two, it is evident that perforations do permit better outgassing during high temperature baking.

2.6.3 Embossed Singly Aluminized Mylar

Table 5 presents in chronological order the data obtained for the embossed singly aluminized Mylar specimen. Figures 16 and 17 show, respectively, the temperature-dependent data taken at pressures of $\leq 8 \times 10^{-6}$ torr Hg and the pressure-dependent data taken at room temperature. The relatively large probable errors are due to having an insulation thickness of 1/2 in.

2.6.4 Embossed Singly Aluminized Mylar and Dimplar

Table 6 presents in chronological order the data obtained for the embossed aluminized Mylar/Dimplar specimen. Figures 18 and 19 show, respectively, the temperature-dependent data taken at pressures of $\leq 8 \times 10^{-6}$ torr Hg and the pressure-dependent data taken at room temperature. The error bands on the figures correspond to probable errors listed in Table 6.

2.6.5 Embossed Singly Aluminized Mylar and Nylon Net

Table 7 presents in chronological order the data obtained for the 1/4-mil embossed singly aluminized Mylar and nylon net specimen. Figures 20

and 21 show, respectively, the temperature-dependent data taken at pressures of $\leq 8 \times 10^{-6}$ torr Hg and the pressure-dependent data taken at room temperature. The error bands on the figures correspond to probable errors listed in Table 7.

Section 3

TASK II: INSULATION JOINT TESTING

3.1 TEST DESIGN

A simple yet effective means of isolating the thermal effects of joints and gaps in HPI was desired. Specifically, knowledge of the heat loss through gaps of various widths was needed. A means was devised whereby the Lockheed/Huntsville cylindrical calorimeter was used for this purpose without modifications to the calorimeter itself. The concept involved testing a specimen of 1/4-mil double-aluminized Mylar and red polyurethane foam on the calorimeter with no joint present to get a basis of comparison and then testing the same specimen after a circumferential joint was cut in the insulation at its center. Figures 22 and 23 show the gap schematically and pictorially. The gap was tested at various widths by simply displacing the insulation panels longitudinally.

As before, the power in the fine wire heaters was monitored as a measure of the heat flux passing through the insulation. Because the insulation gap was at the center of the middle or "test" heater, the power distribution required by the test heater was expected to be greater than that required for the two adjacent or "longitudinal" heaters in order that a flat temperature distribution was maintained. Equal power distributions were observed in testing for which no gaps were present. When the test heater power for the same insulation with and without a joint was compared, the extent of heat loss through the gap was isolated.

3.2 THERMAL ANALYSIS OF THE JOINT TEST DESIGN

Before testing was done using this concept, a computer analysis of the device was conducted to assure that the temperature depression would

not propagate down the insulation beyond the general region of the gap. Therefore, a mathematical thermal model was formulated to represent the insulation gap test device. This model was constructed for use in the Mark 5C Thermal Analyzer Computer Program to obtain the insulation surface equilibrium temperatures.

In the formulation of the thermal model it was assumed that the surface temperatures would be independent of circumferential location. The thermal model would thereby be simplified to a two-dimensional dependency. A 40-in. long, 45-deg wedge with adiabatic end plates was chosen as the model (Fig. 24), with a nodal breakdown of 52 longitudinal increments and 10 radial increments. The path was constructed, and resistance values were calculated. The radiation view factors of the nodes in the gap were calculated by Lockheed's View Factor Computer Program.

Nodal equilibrium temperatures were obtained and the distribution on the outermost layer of the insulation is shown in Fig. 25. The effect of the gap on the surface temperatures is appreciable within the regions 1-1/2 inches either side of the gap. The conclusion is that the disturbance does not propagate beyond the test section of the calorimeter.

3.3 EXPERIMENTAL RESULTS AND CONCLUSIONS

All gap testing was conducted at room temperatures. Figures 22 and 23 show a 1/10 in. gap separation. As seen in Fig. 23, care was used to assure a clean, straight cut. Three other configurations were tested, a 1/20-in. gap, a zero-separation gap and a 1/10-in. foam filled gap. The test results for the zero-gap-width butt-joint revealed that no discernible heat loss occurred at the joint. The heat loss through the insulation was observed to be equal to that before the cut was made. This was apparently due to the clean "joint" that was made. It was concluded from this zero-gap-width butt-joint test that the miter joint would result in zero heat loss through the joint. This is because a miter joint is essentially a stepped butt-joint.

When the joint was separated to 1/20-in. and 1/10-in., respectively, however, the heat loss through the gap became significant. Calculations were performed to determine the total heat loss emitted through the two gaps and to ascertain an "effective" gap width for both. The steady-state power output from the one-foot long "test" heater and the ΔT across the insulation for the three cases was as follows:

$$\begin{aligned} P_0 &= 9.7 \text{ mW} & \Delta T_0 &= 543 \mu V \equiv 23.64^\circ F \\ P_{1/20} &= 10.22 \text{ mW} & \Delta T_{1/20} &= 460 \mu V \equiv 20.04^\circ F \\ P_{1/10} &= 13.2 \text{ mW} & \Delta T_{1/10} &= 530 \mu V \equiv 23.10^\circ F \end{aligned}$$

Since the three tests were at different values of ΔT , two of them must be adjusted to match the third. Therefore, the 1/20-in. and the 1/10-in. gaps are adjusted to match the ΔT of the zero-width separation.

$$\begin{aligned} P'_{1/20} &= 10.22 \frac{543}{460} = 12.08 \\ P'_{1/10} &= 13.2 \frac{543}{530} = 13.53 \end{aligned}$$

Furthermore, since the gaps are 0.05-in. and 0.1-in. and the test heater is 12 in. long, only 11.95 and 11.9 in. of the test heater, respectively, are covered by insulation for the two gap tests. A meaningful comparison of the two required adjusting for these differences. Therefore

$$\begin{aligned} P''_{1/20} &= P'_{1/20} \frac{12}{11.95} = 12.08 \frac{12}{11.95} = 12.12 \\ P''_{1/10} &= P'_{1/10} \frac{12}{11.9} = 13.53 \frac{12}{11.9} = 13.65 \end{aligned}$$

The actual heat loss through the gaps is the difference between P_0 and $P''_{1/20}$ and $P''_{1/10}$, respectively. Therefore,

$$P_{\text{gap}_{1/20}} = 12.12 - 9.7 = 2.42 \text{ mV}$$

$$P_{\text{gap}_{1/10}} = 13.68 - 9.7 = 3.95 \text{ mV}$$

The effective thermal conductivity of the gap is now calculated for both cases

$$k = \frac{q \ln \frac{r_o}{r_i}}{2\pi L (T_i - T_o)}$$

$$k_{1/20} = \frac{2.42(.511)(.003414)(12)}{2\pi \frac{1}{20} (23.64)} = 6.82 \times 10^{-3}$$

$$k_{1/10} = \frac{3.95(.511)(.003414)(12)}{2\pi \frac{1}{10} (23.64)} = 5.565 \times 10^{-3}$$

The ratio of the effective thermal conductivity of the gap to that of the insulation is now calculated.

$$\frac{k_{1/20}}{k_{\text{ins}}} = \frac{6.82 \times 10^{-3}}{0.114 \times 10^{-3}} = 77.4$$

$$\frac{k_{1/10}}{k_{\text{ins}}} = \frac{5.565 \times 10^{-3}}{0.114 \times 10^{-3}} = 48.8$$

This ratio also represents the ratio of the insulation width required to emit the same amount of heat as that passing through the gap to the gap width itself. An "effective" gap width is therefore calculated for each gap which represents the length of tube covered with insulation which would pass the same amount of heat as the open gap.

$$\delta_{\text{eff}1/20} = \delta \frac{k_{1/20}}{k_{\text{ins}}} = 0.05(77.4) = 3.87 \text{ in.}$$

$$\delta_{\text{eff}1/10} = \delta \frac{k_{1/10}}{k_{\text{ins}}} = 0.1(48.8) = 4.8 \text{ in.}$$

A plot of δ_{eff} vs δ is shown in Fig. 26.

The foam filled 1/10-in. gap test resulted in

$$P_{1/10 \text{ foam}} = 11.3 \text{ mW} \quad \Delta T_{1/10 \text{ foam}} = 525 \mu\text{V} = 22.78^\circ\text{F}$$

As before, the power is adjusted to match the ΔT of the zero-gap test.

$$P'_{1/10 \text{ foam}} = 11.3 \frac{543}{525} = 11.7$$

and adjusted again for the length of the test heater covered by the insulation

$$P''_{1/10 \text{ foam}} = 11.7 \frac{12}{11.9} = 11.8$$

Therefore, the actual heat loss through the gap is the difference between P_0 and $P''_{1/10 \text{ foam}}$, or

$$P_{\text{gap}1/10 \text{ foam}} = 11.8 - 9.7 = 2.1 \text{ mW}$$

The effective thermal conductivity of the gap is

$$k_{1/10 \text{ foam}} = \frac{2.1(.511)(.003414)(12)}{(2\pi)(1/10)(23.64)} = 2.96 \times 10^{-3}$$

The ratio of the effective thermal conductivity of the gap to that of the insulation is now calculated

$$\frac{k_{1/10 \text{ foam}}}{k_{\text{ins}}} = \frac{2.96 \times 10^{-3}}{0.144 \times 10^{-3}} = 20.6$$

Again, this ratio also represents the ratio of the insulation width required to emit the same amount of heat as that passing through the gap to the gap width itself. As before, then, the effective gap width is

$$\delta_{\text{eff } 1/10 \text{ foam}} = \delta \frac{k_{1/10 \text{ foam}}}{k_{\text{ins}}} = 0.1 (20.6) = 2.06 \text{ in.}$$

This value is shown on Fig. 26 as a square at the $\delta = 1/10$ coordinate. This shows pictorially the comparison between the foam filled 1/10-in. gap and the void 1/10-in. gap. The improvement gained by adding the foam to the 1/10-in. gap is a 57% reduction in heat leakage.

The above data were used to plot a curve (Fig. 27) of effective panel thermal conductivity versus the A/ℓ ratio of an insulation panel. In the A/ℓ ratio, A is the total insulation area for some insulated system and ℓ is the total length of all gaps. In determining the effective thermal conductivity, the total heat leak through the gap and through the insulation is used instead of that through the insulation only as is normally done. The curve shown is valid only for a specimen of 1/4-mil double-aluminized Mylar and red polyurethane foam 1 in. thick at room temperature. The heat leakage for a panel can be reduced by reducing the gap width or by increasing the A/ℓ ratio.

3.4 ERROR ANALYSIS

Since the insulation thickness was the same for all four of the above cases, the normal error associated with measuring insulation thickness is eliminated. There was, however, a probable error of considerable magnitude in measuring gap width in each case. The best estimate of this error was $\pm 10\%$. This error propagates through the equations linearly so that δ_{eff} also has a probable error of $\pm 10\%$ for each case. These errors are presented in Fig. 26 but not Fig. 27.

Section 4

TASK III: INSULATION PENETRATION EFFECTS

4.1 APPARATUS DESIGN

The need for comparison data for various methods of HPI joint construction at the base of a penetration tube led to the development of a simplified penetration test apparatus. The penetration calorimeter as seen in Fig. 28 is a 24-in. diameter, 1/16-in. thick, copper plate cooled on the backside by copper tubes carrying LN_2 . The penetration is a stainless steel tube measuring 1-in. o.d. and 42-in. long and penetrates at the front face of the copper plate. Insulation is tested on the calorimeter by covering the entire plate and all but the free end of the penetration tube as shown in the figure. Heat passing into the plate through the penetration is measured at the base of the penetration by a differential thermocouple. Temperatures along the penetration are monitored by thermocouples referenced to an LN_2 bath.

Insulation can be applied at any thickness on the apparatus and with any type of joint configuration at the base of the penetration.

4.2 SPECIMEN PREPARATION

In all three of the tests conducted, the same insulation material and the same insulation thickness were used. The three joint configurations used were the diagonal joint, the butt joint and the buffer joint. These three are shown in that order in Figs. 29, 30 and 31.

The insulation material was alternate layers of 1/4-mil double-aluminized Mylar and red polyurethane foam, and it was wrapped to a thickness of 1 in. It was composed of 22 layers of aluminized Mylar and 21 layers of foam. Figure 32 shows the penetration test apparatus after

a layer of red foam was applied. Figures 33, 34 and 35 show the apparatus after it was wrapped, in this case, in the diagonal-joint configuration.

In the case of the diagonal joint (Fig. 29), each successive layer on the tube was overlapped and taped to its corresponding layer on the plate. For the butt joint and the buffer joint, the layers of insulation were applied to touch but no tape was used. The buffer material was a block of foam of the same material as the foam spacers. As can be observed in Fig. 31, it was doughnut shaped with inside radius of $1/2$ in., outside radius of $2-1/2$ in. and thickness of 1 in. Figure 36 shows the buffer joint construction just before testing was done.

4.3 EXPERIMENTAL RESULTS AND ERROR ANALYSIS

After the diagonal joint configuration was tested, a comparison was made between the temperature distribution along the penetration as observed from the test and the same as predicted by computer analysis of the test apparatus. Figure 37 shows this comparison. The intent was to determine just how reasonable were the data being generated by the apparatus. The comparison in the figure was considered to be reasonable.

The heat rate into the copper plate from the penetration at the base of the penetration was measured indirectly by measuring the temperature drop across a known distance at the base of the penetration with the differential thermocouple. With this and the known thermal conductivity of the stainless steel at that temperature and the cross section area of the tube, the heat rate was determined to be 1.23 Btu/hr for the diagonal joint case. This compares with 1.10 Btu/hr predicted by the computer analysis. The difference is 10.4%, a close comparison.

The heat leak through the base of the penetration for the butt-joint was 0.817 Btu/hr; for the buffer joint it was 1.68 Btu/hr. As for the diagonal-joint case, the heat rates were determined from the temperature slope at

the base of the penetration. The temperature slopes and the heat rates are shown in Fig. 38. It had been expected that the diagonal-joint case would allow the smallest heat leakage to the plate. Instead, the butt-joint case had the smallest leakage. No explanation for this was found.

A possibility exists that the small 0.15-in. differential thermocouple had been disturbed or shifted prior to the third test. This possibility was checked after the test, and no problem was noted except that one junction of the differential couple was not in firm contact with the stainless steel tube. However, there was no assurance that the junction was in firm contact during the previous tests either. Furthermore, there would be no immediate logical explanation of how the failure to have contact would affect the reading from the thermocouple. Conduction in the thermocouple intermediate metal itself, the constantan, would be a possible explanation of the apparent temperature-difference suppression in the couple. Again, this explanation would be dependent on this not having occurred in the previous tests.

An error analysis was conducted to determine the error in the heat flow at the base of the penetration (q on Fig. 37). The 8% error was a result of errors in measuring the area of the tube, the length of the 1/8-in. differential thermocouple, the thermal conductivity of the steel and the emf of the thermocouple. All three of the q values have approximately the same errors since the error in ΔT is only an insignificant part of the 8%.

Based on the above, it is suggested that further testing be conducted before any conclusions be reached about the relative rankings of the three test configurations. The data already generated are, however, valuable from the standpoint of general quantitative value. The q values presented indicate general values of heat leakage through a stainless steel penetration.

Section 5

TASK IV: HIGH PERFORMANCE INSULATION DATA COMPARISON

5.1 PROBLEMS INVOLVED IN HIGH PERFORMANCE INSULATION DATA COMPARISON

In recent years the number of investigators studying the thermal conductivity of HPI has increased substantially. Similarly the types and varieties of experimental apparatus used for testing have increased. Not only the physical characteristics of the calorimeter but also the test procedures used strongly affect the resulting data because for multilayer insulation (MLI) materials an "effective" thermal conductivity is being measured rather than a true thermal conductivity. Standardization of equipment and procedures is not practical, because each calorimeter is designed to do a certain task optimally, and the test procedure must comply with this custom design.

As these increased quantities of data are generated by different investigators and on different apparatus, a need is created for a standard of comparison. Direct comparison of thermal conductivity may reveal apparent discrepancies in the test data. Close examination of the test equipment and procedures could reveal the sources of discrepancies. One good example of a source of data discrepancy is in the definition of the number of layers per inch of multilayered insulation material. Some investigators measure the distance between the two extreme layers and divide that distance into the total number of layers, including the two extreme layers. Others do not include the two extreme layers in the total number, considering those to be boundaries instead of layers. For a 10-layer specimen, a 20% apparent error in layer density is observed between the data for the two investigators. A more correct method would be to count only one of the extreme layers, which would be the same as counting the spacers. It is really just a matter of definition, however. Since thermal conductivity is a strong function of layer density for all MLI systems, it is important that the respective

definitions of layer density used by different investigators are properly understood. Only by so doing can layer densities be correctly compared between investigators.

Another factor which should be considered in comparing data is the surface conditions. For example, a flat plate calorimeter (FPC) is constructed so that the insulation test specimen is bounded by two flat plates -- a hot plate on the bottom and a cold plate on the top. The bottom layer of the MLI is in uniform contact with the bottom (hot) plate due to gravity. The top layer, however, is not necessarily in contact with the top plate. Conceivably, the top plate could be suspended above the insulation so that no contact exists. It could be lowered to barely touch the top layer without making uniform contact, or it could be allowed to compress the insulation somewhat to have uniform contact. Certainly, consideration must be given to which of the cases exist since a space (or partial space) between the top layer and plate causes one additional "radiation resistance" between the two plates. For an insulation system consisting of 10 radiation shields, the one additional resistance represents 10% of the total number and can therefore cause 10% comparative discrepancy. Technically speaking, if a space does exist, then the cold plate temperature should not be considered as the boundary temperature; instead, the temperature of the top layer of insulation should be. Other types of calorimeters, such as the Lockheed/Huntsville cylindrical calorimeter, do not have "plates" as such. Instead, the cold surface of the insulation (or perhaps both surfaces) is maintained at its desired temperature by radiative interchange with an environmental control shroud. In this case, the outermost layer of insulation is considered to be the boundary temperature.

Another parameter which should not be ignored is the insulation backside pressure. Since convective heat transfer can occur where sufficient insulation evacuation does not exist, the insulation internal or backside pressure is important. Data discrepancies could conceivably be traceable to insulation systems having different internal pressures while being exposed to the same test chamber pressure. Factors such as duration of pump-down,

exposure to heat, presence of condensation inside the insulation, cleanliness of insulation, prior conditioning of the insulation and others contribute to the internal pressure.

Data discrepancies can also be due to actual quantitative measurement errors. A particular example is the measurement of insulation thickness. Most MLI systems are highly susceptible to sagging. This results in a non-uniform insulation thickness. Another primary potential error is in determining heat losses through "edge" effects. The highly anisotropic nature of MLI makes this a most critical problem. Methods used by each investigator for assuring that edge effects have been properly accounted for should be examined.

5.2 DATA COMPARISON OF DOUBLE-ALUMINIZED MYLAR AND RED FOAM

With the above concepts in mind, a data comparison was conducted for data presented by six independent investigators for the 1/4-mil double-aluminized Mylar and red polyurethane foam composite. The comparison was made both as an exercise in data comparison to check out the arguments presented above and also because there was need for a meaningful comparison on Goodyear HPI data due to its anticipated use on various vehicle components in the near future. Table 8 presents data taken by the six investigators. References 1 through 7 are indicated on the figure. In reading the table it is important to note that an entry applies to all data lying below it until the next entry is made. Dittos and arrows were not used. The table shows that two of the investigators (Lockheed and Dynatech) took data as a function of mean temperature with the layer density at or near its optimum value, while the other four investigators took their data as a function of layer density with the boundary temperatures fixed at ambient and cryogenic temperatures. Figure 39 presents the data for all six investigators as a function of mean temperature. The Lockheed and Dynatech data are reasonable values of "effective" thermal conductivity due to their small ΔT values. Caution should be used in interpreting the other data on Fig. 39 due to the large ΔT

values involved (two of the Lockheed points are also at large ΔT values). Since the k vs T of HPI is not linear, the effective value of k for a data point with a large ΔT does not correspond exactly to the local k value for the insulation at the mean temperature of the large ΔT point. The effective values will be slightly above the true k value because the k vs T curve is concave upwards. To determine the exact extent of the discrepancy, the k vs T curve would have to be integrated between the boundary temperatures. The layer densities and foam thicknesses are indicated in the legend of Fig. 39. The solid line on Fig. 39 is Eq. (1.18) of Lockheed Report K-17-68-5, which was solved for a layer density value of 21 layers per inch (and a converged set of boundary temperatures). The two dotted lines are a band on the total data plotted. The solid points are data that were taken on an out-gassed or baked (at 200°F) specimen of insulation.

Figure 40 shows the k vs layer density data for the four investigators that took their data in terms of layer density. It should be noted that three of the investigators used LN_2 as the cold boundary; the fourth investigator used LH_2 . The boundary temperatures are indicated on the figure along with the foam thickness.

Proper use of Figs. 39 and 40 requires careful study of Table 8. For example, items such as chamber pressure and helium purge are not indicated on the figures.

As emphasized previously, the method of determining layer density is an important consideration, and it was for this reason that this information was presented in the table. In each figure the layer density values were adjusted so that each one would be based on the same definition. In Fig. 40 where the X coordinate was layer density, the correction brought the data in line much better.

The previous discussion concerning the surface condition is significant in two of the sets of data. On Fig. 40 the three points for the NASA/MSFC

and the Lockheed/Sunnyvale data with the lowest layer density were taken with the top plate of the flat plate calorimeter suspended above the insulation specimen. Data in the table reveal that this is the case. The significance of this, as discussed previously, is that there is an additional radiation resistance between the top plate and the top of the insulation specimen. A more subtle discrepancy inherent in presenting this data as shown in Fig. 40 (this is how it is always presented) for these 6 points is that the true layer density is really identically equal to the uncompressed value due to the large space above the insulation. The concept of counting layers and dividing by "plate separation" is somewhat misleading when that separation is greater than the uncompressed thickness.

The insulation backside pressure is most significant in the case of insulation systems that do not have edges open to the vacuum. This was the case on the Lockheed/Huntsville cylindrical calorimeter and for that reason the backside pressure was measured and presented. A backside pressure higher than the chamber pressure indicates the average effective gas pressure between the layers is not identified by the chamber pressure alone. The strong pressure dependence of the insulation thermal conductivity is well known. The phenomenon of a varying pressure through the insulation thickness should be considered in evaluating data taken on unperforated insulation with unexposed edges.

The aspect of quantitative measurement errors of insulation dimensions, ΔT , q , etc., is a difficult one to deal with as it relates to this data comparison because an error analysis was not conducted for each of the six cases. In addition, no data were presented from which an error analysis could be conducted. Ignoring the previously outlined discrepancies between testing concepts, the normal probable errors on thermal conductivity data are on the order of 10 to 25%. On that basis, the data presented in Fig. 39 show reasonably good comparison. It should be kept in mind that the darkened data points are those made on outgassed, or baked, specimen.

Conclusions that were reached are:

- Care should be used when comparing data taken by various investigators.
- The foam data generated by several different sources compared reasonably well considering the factors discussed above.

5.3 COMPARISON OF VARIOUS HIGH PERFORMANCE INSULATION MATERIALS ON A BASIS OF MECHANICAL LOAD

In order to make a valid thermal comparison between different high performance insulation materials, it is essential to use reasonable criteria of comparison. For example, a common yet perhaps unreasonable method for comparing materials is to compare the thermal conductivities of the materials at their respective optimum values of layer density and for the same boundary temperatures. The optimum value of layer density is the value to which the minimum thermal conductivity corresponds. Comparing at the same boundary temperatures is essential, since the conditions of the proposed application must be used. However, comparing values of thermal conductivity may not represent reasonable criteria of comparison. Also, comparison at optimum values of layer density may not be reasonable.

In designing missile components there are two primary constraints on the components. Either the HPI is space limited or weight limited, and either the HPI space or weight must be minimized. Weight limitation is the common practice. If this is the case, instead of minimizing the thermal conductivity, k , the density-thermal conductivity product, ρk , should be minimized. In this way, the least heat flow per unit weight of insulation can be obtained.

The practice of comparing insulations at optimum values of layer density is predicated on all insulation materials having the same ease of application and the same reliability at their respective optimum values of layer

density. This assumption is usually not valid. For example, double-aluminized Mylar and 0.030 in. red foam has a high degree of structural integrity and proven fabrication techniques at its optimum layer density of approximately 22 layers per inch. On the other hand, the double-aluminized crinkled Mylar and Tissueglas composite is highly compressible and requires parallel tension constraint for fabrication at its optimum layer density of approximately 80 layers per inch. In fact, just sitting in a 1-g field, it will compress considerably over 80 layers per inch under its own weight. A more reasonable standard of comparison is to compare the materials at the same value of compression. In an application concept for which the insulation is held on by lacing or circumferential wrapping, there is a hoop tension. This tension is equivalent to a normal mechanical load or a compression. Unless each insulation layer is individually mechanically supported at its edges, there will more than likely be some compression associated with holding the layers in place. A reasonable assumption at this point is that the same application concept be used for all materials to be compared.

The conclusion from the above is that a plot of ρk versus p , or mechanical compression, is needed when meaningful comparison of HPI materials is made. Using data already available in Ref. 4, Table 9 and Figs. 41 and 42 were generated. The curves were developed by cross plotting data which were presented in the form of curves of pressure vs layer density, and density vs layer density on pages 1-68 through 1-70 of Ref. 4, and equations of thermal conductivity versus layer density on pages 1-68 through 1-70 of Ref. 4 and equations of thermal conductivity versus layer density on pages 1-49 to 1-50 of Ref. 4. It should be noted that the equations referred to on pages 1-49 and 1-50 are semi-empirical correlations arrived at by using observed data taken with ambient and cryogenic boundary temperatures. It is assumed, however, that these equations can be extended to the boundary temperature condition used in Figs. 41 and 42. The table presents the information used from Ref. 4, as well as that used in Figs. 41 and 42. The two sets of boundary

conditions were chosen as representative cases. The 400°R and 40°R case was representative of the large temperature difference case and of a typical Multiple Docking Adapter operational condition. The 460°R case ($T_{\text{hot}} = T_{\text{cold}}$) was chosen to represent a small ΔT situation.

For the purpose of comparison, curves of k versus mechanical compression are presented in Figs. 43 and 44 for the same materials and boundary temperatures as in Table 9 and Figs. 41 and 42.

REFERENCES

1. Hale, D. V., et al., "A Study of Thermal Conductivity Requirements," LMSC/HREC A784841, Lockheed Missiles & Space Company, Huntsville, Ala., 13 October 1967, pp. 38-39.
2. Lockheed Missiles & Space Company, "Study of Thermal Conductivity Requirements — Monthly Progress Report," LMSC/HREC A791861, Huntsville, Ala., 18 October 1968, pp. 6-7.
3. Letter from J. G. Austin, Jr., Contracting Officer's Representative, NASA, R-P&VE, to D. V. Hale, Lockheed/Huntsville, 6 November 1968; Subject: Contract NAS8-21347, DCN 1-8-52-10145.
4. Brogan, J. J., "Investigations Regarding Development of a High-Performance Insulation System — Third Quarterly Progress Report," K-17-68-3, Lockheed Missiles & Space Company, Sunnyvale, Calif., 15 April 1968, pp. 1-25 through 1-58.
5. Dynatech Corporation, "The Thermal Conductivity of Two Thermal Insulating Materials," Reference: NAS-23, Palo Alto, Calif.
6. Burkley, R. A., et al., Goodyear Aerospace Corp., "Development of Materials and Materials Application Concepts for Joint Use as Cryogenic Insulation and Micro-Meteoroid Bumpers," GER 11676 S/36 Annual Summary Report, 30 June 1967, pp. 8-11.
7. Arthur D. Little, Inc., "Advanced Studies on Multi-Layer Insulation Systems," ADL 67180-00-04, 1 June 1966, p. II-32.

TABLES
AND
ILLUSTRATIONS

Table 1
HREC CYLINDRICAL CALORIMETER INSTRUMENTATION WIRES

Component	Number of Wires	Size	Composition
Thermocouples			
Differential (4)	8	3 mil	Copper
Absolute (4)	4	3 mil	Copper
	4	3 mil	Constantan
Heaters (5)	10	6 mil	Copper
Ion Cage	7	(No. 26 Wire)	Copper
Total	33		

Table 2
STANDARD THERMAL CONDUCTIVITY TEST SEQUENCE

Data Point	Approximate Mean Insulation Temperature (°F)	Chamber Pressure (torr)
1	-100	8×10^{-6}
2	0	8×10^{-6}
3	100	8×10^{-6}
4	100	10^{-2}
5	100	10^0
6	100	760
7	200	8×10^{-6}

Table 3

TEST RESULTS FOR UNPERFORATED DOUBLE-ALUMINIZED MYLAR AND FOAM SPECIMEN

Mean Insulation Temperature ($^{\circ}\text{F}$)	ΔT ($^{\circ}\text{F}$)	Chamber Pressure (torr)	Insulation Backside Pressure (torr)	Thermal Conductivity ($\times 10^5$) (Btu/hr-ft- $^{\circ}\text{R}$)	Probable Error Bands (%)
-104.9	46.75	3×10^{-6}	2×10^{-5}	5.89	12.0
-40.9	49.48	4×10^{-6}	3.7×10^{-5}	6.3	11.8
19.7	42.36	4×10^{-6}	6×10^{-5}	9.75	10.6
88.5	25.30	7.4×10^{-6}	7×10^{-4}	13.1	10.8
83.1	8.34	—	1×10^{-2}	47.7	10.2
84.8	1.22	—	1	5200	8.3
90.5	2.67	—	1.6×10^2	7570	8.3
140.2	38.52	2×10^{-5} *	$> 1.5 \times 10^{-3}$	24.6	8.6
202.5	39.34	1.4×10^{-5}	$> 1.5 \times 10^{-3}$	28.1	8.6
104.5	43.0	3.6×10^{-6}	7.5×10^{-5}	12.2	9.4
**	239.0	1.5×10^{-6}	—	7.05	8.4

*Sufficient time for outgassing was not allowed.

** $T_{\text{hot}} = 78^{\circ}\text{F}$; $T_{\text{cold}} = -161^{\circ}\text{F}$.

Table 4
TEST RESULTS FOR PERFORATED DOUBLE ALUMINIZED
MYLAR AND RED FOAM SPECIMEN

Mean Insulation Temperature (°F)	ΔT (°F)	Chamber Pressure (torr)	Insulation Backside Pressure (torr)	Thermal Conductivity (x 10 ⁵) (Btu/hr-ft-°F)	Probable Error Bands (%)
-100.0	63.1	2.5 x 10 ⁻⁶	2.0 x 10 ⁻⁶	6.78	9.9
- 8.95	65.9	2.4 x 10 ⁻⁶	~2.0 x 10 ⁻⁶	9.70	9.1
99.6	38.3	2.5 x 10 ⁻⁶	*	16.5	9.1
97.0	32.5	2.2 x 10 ⁻²	2.2 x 10 ⁻²	80.5	8.3
85.0	3.7	1	1	5280	8.3
83.5	3.09	200	200	6370	8.3
207.2	53.5	6.9 x 10 ⁻⁶	1 x 10 ⁻⁴	34.8	8.4

* Pressure not recorded.

Table 5
TEST RESULTS FOR EMBOSSED SINGLE ALUMINIZED MYLAR SPECIMEN

Mean Insulation Temperature (°F)	ΔT (°F)	Chamber Pressure (torr)	Insulation Backside Pressure (torr)	Thermal Conductivity ($\times 10^5$) (Btu/hr-ft-°F)	Probable Error Bands (%)
-61.6	60.4	2.8×10^{-6}	8.4×10^{-5}	1.86	21.3
5.7	52.7	4.6×10^{-6}	2.4×10^{-5}	2.10	21.3
100.0	38.8	3.4×10^{-6}	$< 2.0 \times 10^{-4}$	3.53	20.3
85.5	7.3	3×10^{-1}	—	266	18.0
84.0	9.7	1×10^{-2}	—	13.3	20.6
84.0	1.4	≈ 760	—	8630	18.0
205.71	51.6	2.8×10^{-6}	4.0×10^{-5}	6.06	18.5
*	266.0	2.3×10^{-6}	—	2.18	18.2

* $T_{HOT} = 72^\circ F$; $T_{COLD} = -194^\circ F$

Table 6
TEST RESULTS FOR DEMPLAR AND EMBOSSED ALUMINIZED MYLAR SPECIMEN

Mean Insulation Temperature (°F)	ΔT (°F)	Chamber Pressure (torr)	Insulation Backside Pressure (torr)	Thermal Conductivity ($\times 10^5$) (Btu/hr-ft-°F)	Probable Error Bands (%)
-100.2	37.7	2.5×10^{-6}	5.5×10^{-5}	13.5	9.6
1.3	38.5	1×10^{-6}	6×10^{-5}	19.9	8.9
*	237.3	3.8×10^{-6}	7.5×10^{-5}	14.0	8.3
99.5	32.2	3.8×10^{-6}	—	29.7	8.7
83.9	7.85	1×10^{-2}	—	71.5	9.4
90.6	8.87	1.0	—	1100	8.3
94.7	16.15	360	—	1690	8.3
199.8	36.5	3.3×10^{-6}	1.4×10^{-4}	29.7	8.6

* $T_{HOT} = 62.7$

$T_{COLD} = -173.3$

Table 7
TEST RESULTS FOR EMBOSSED ALUMINIZED MYLAR AND NYLON NET SPECIMEN

Mean Insulation Temperature (°F)	ΔT (°F)	Chamber Pressure (torr)	Insulation Backside Pressure (torr)	Thermal Conductivity ($\times 10^5$) (Btu/hr-ft-°F)	Probable Error Bands (%)
-112.7	59.4	3×10^{-6}	—	8.17	9.6
- 11.58	44.8	3.3×10^{-6}	4.7×10^{-4}	16.6	8.9
*	258.0	6×10^{-7}	7.2×10^{-4}	14.6	8.3
99.40	33.1	5.6×10^{-6}	7.2×10^{-4}	32.4	8.6
9.187	20.05	9.5×10^{-3}	—	56.2	8.6
97.25	10.5	7.0	—	2010	8.3
94.5	13.0	760	—	1740	8.3
201.5	37.7	7.2×10^{-6}	—	26.5	8.6

* $T_{\text{hot}} = 73.0$

$T_{\text{cold}} = -185.0$

Investigator	Calorimeter Type	Spacer Thickness (in.)	Mean Temp. (°F)	ΔT (°F)	Plate Separation (or) Insulation Thickness (in.)	No. of Layers	Layer Density (l/in.)	Chamber Pressure (torr)	Insulation Backside Pressure (torr)	Thermal Conductivity (Btu/hr-ft-°F) (x 10 ⁵)	Method of Determining Layer Density	Insulation Load (psi)	Helium Purge	Uncom-pressed Thickness (in.)	Instrumentation
LMSC/HREC (Ref. 1) (data presented in order taken)	HREC Cylindrical Calorimeter	0.030	76.0 104.9 154.0 55.8 72.3 198.6 - 58.6 174.7 132.6 74.9 - 46.5	9.8 10.1 10.5 10.9 11.4 11.2 270.0 13.2 12.4 10.3 9.2	1.0	22 shields 21 spacers	21	≤8x10 ⁻⁶	Not recorded (assumed outgassed)	12.7 14.1 30.8 8.14 11.3 30.1 5.10 18.4 9.62 6.03 4.68	Total No. of spacers divided by total thick-ness	Small hoop tension to dis-allow sagging	Before test starts, 1 hr at 250°F	Approx. 1 inch	TC taped to calorimeter coil with My-lar tape at hot face; TC taped to outside shield at cold face
LMSC/HREC (Ref. 2) (data presented in order taken)	HREC Cylindrical Calorimeter	0.028	-104.9 - 40.9 19.7 88.5 140.2 202.5 104.5 - 41.5	46.8 49.5 42.4 25.3 38.5 39.3 43.0 239.0	1.0	24 shields 23 spacers	23	3x10 ⁻⁶ 4x10 ⁻⁶ 4x10 ⁻⁶ 7.4x10 ⁻⁶ 2x10 ⁻⁵ 1.4x10 ⁻⁵ 3.6x10 ⁻⁶ 1.5x10 ⁻⁶	2x10 ⁻⁵ 3.7x10 ⁻⁵ 6x10 ⁻⁵ 7x10 ⁻⁴ ≥1.5x10 ⁻³ ≥1.5x10 ⁻³ 7.5x10 ⁻⁵ Not presented	5.89 6.30 9.75 13.1 24.6 28.1 12.2 7.05	Total No. of spacers divided by total thick-ness	Small hoop tension to dis-allow sagging	Before test series starts, 1 hr at 250°F	Approx. 1 inch	TC taped to calorimeter coil with My-lar tape at hot face; TC taped to outside shield at cold face
NASA/MSFC (Ref. 3)	ADL Model 12 Flat Plate Calorimeter	0.030	-125 T _H =70 T _C =-320	390 (LN ₂)	0.76 0.65 0.55 0.55 0.50 0.50 0.475 0.475 0.450 0.450	10 shields 11 spacers	13.2 15.4 18.2 18.2 20.0 20.0 21.1 21.1 22.2 22.2	Not pre-sented	Not appli-cable (as-sumed out-gassed)	8.0 6.1 5.1 5.0 4.9 6.4 6.9 11.7 11.3 19.5 17.6	Total No. of shields divided by plate sep-eration	Not presented	Not presented	0.5	Hot and cold plates instru-mented
LMSC/Sunnyvale (Ref. 4)	LMSC/Sunnyvale Flat Plate Calorimeter	0.03-0.034	-120 T _H =60 T _C =-320	390 (LN ₂)	Not presented (can be computed from layer den-sity and No. of layers)	10 shields 11 spacers	21.0 25.0 29.0 32.0 39.0 22.0 25.0 29.0 33.0 42.0	≤4x10 ⁻⁶	Not appli-cable (as-sumed out-gassed)	11.7 15.5 19.5 35.0 64.0 15.8 17.0 27.5 36.5 78.0	Total No. of shields divided by plate sep-eration	Not presented	Not presented	0.49 0.73	Hot and cold plates instru-mented

Table 8
Table of Thermal Conductivity Data for 1/4-mil Double Aluminized Mylar and Red Polyurethane Foam for Various Investigators

[illegible]

Table 8 (Continued)

Table 9
COMPARISON OF VARIOUS HPI MATERIALS

Material	Mechanical Load (psi)	Layer Density (shields/in.)	Density (lbm/ft ³)	$(T_h = T_c = 0^\circ\text{R})$ $(k \times 10^5)$ (Btu/hr-ft- ^o F)	$(T_h = T_c = 0^\circ\text{R})$ $(\rho k \times 10^5)$	$(T_h = 400^\circ\text{R}, T_c = 40^\circ\text{R})$ $(k \times 10^5)$ (Btu/hr-ft- ^o F)	$(T_h = 400^\circ\text{R}, T_c = 40^\circ\text{R})$ $(\rho k \times 10^5)$ (Btu/hr-ft- ^o F)
Superfloc	1	950	19.8	1340	26500	640	12700
	0.1	520	10.8	403	4360	193	2090
	0.025	330	6.86	146	1000	70.4	482
Mylar & Nylon	1	100	3.20	2.48	7.91	0.95	3.04
	0.1	80.0	2.56	2.19	5.59	0.78	1.99
	0.025	76.0	2.43	2.16	5.25	0.75	1.82
Mylar & Silk	1	90.0	4.20	5.49	23.1	2.30	9.70
	0.1	72.0	3.35	4.76	15.9	1.90	6.33
	0.025	69.0	3.23	4.65	15.0	1.85	5.95
Mylar & Red Foam	1	31.6	2.36	58.8	139	27.4	64.6
	0.1	29.0	2.18	38.0	82.6	17.4	37.8
	0.025	27.0	2.04	25.7	52.4	11.4	23.2
Crinkled Mylar & Tissueglas	1	395	9.09	34.7	315	16.5	149
	0.1	237	5.45	12.5	68.0	5.79	31.6
	0.025	160	3.68	6.24	23.0	2.73	10.1
Mylar & Tissue-glas	1	492	11.3	21.3	245	10.1	116
	0.1	353	8.11	10.8	87.7	5.07	41.0
	0.025	267	6.14	6.49	39.8	2.96	18.1
NRC-2	1	1060	14.8	305	4520	146	2160
	0.1	490	6.86	65.5	449	31.1	214
	0.025	290	4.06	23.6	96.0	11.1	45.0

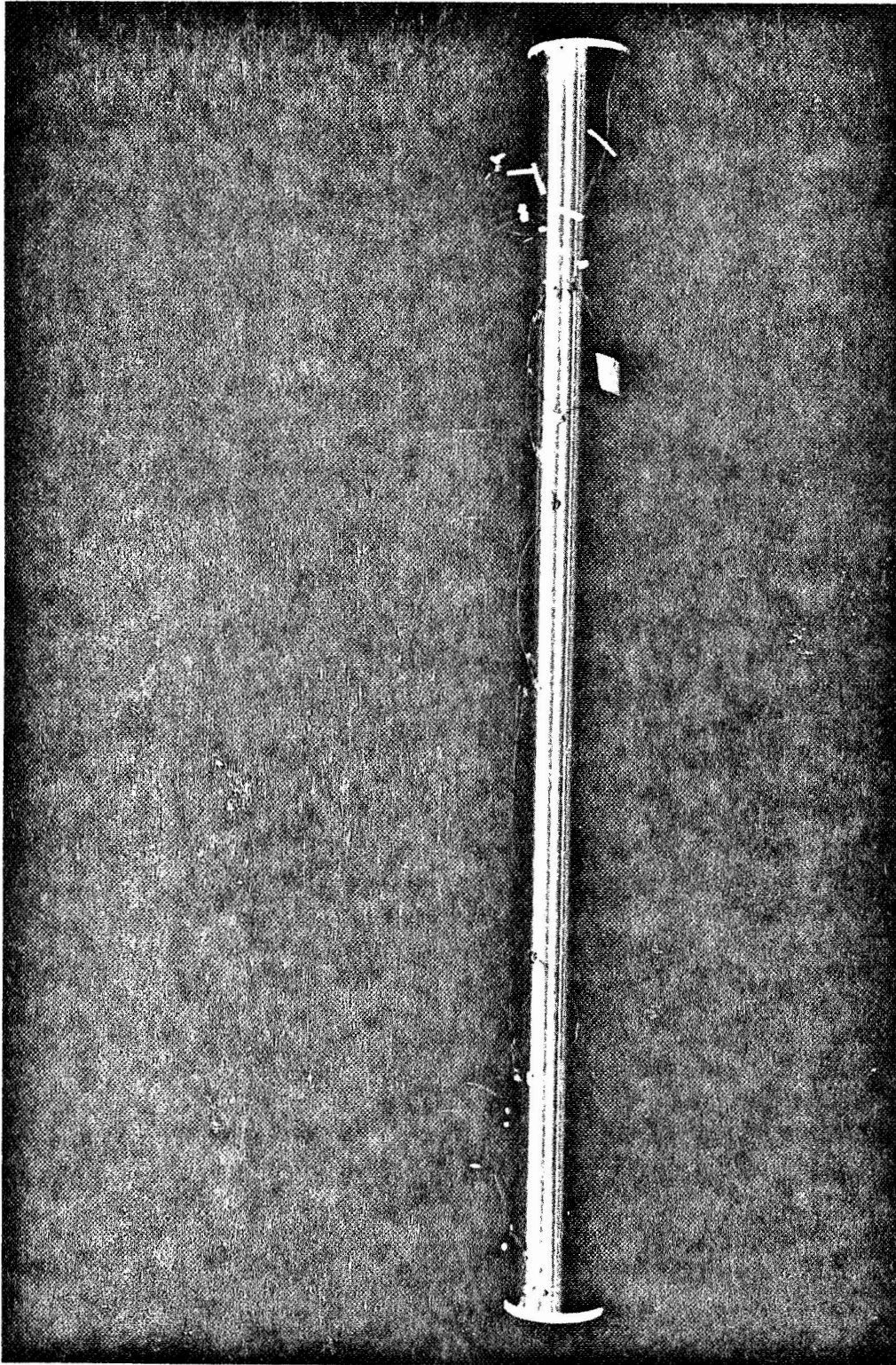


Figure 1
LMSC/HREC Cylindrical Calorimeter Before Application of Insulation Specimen

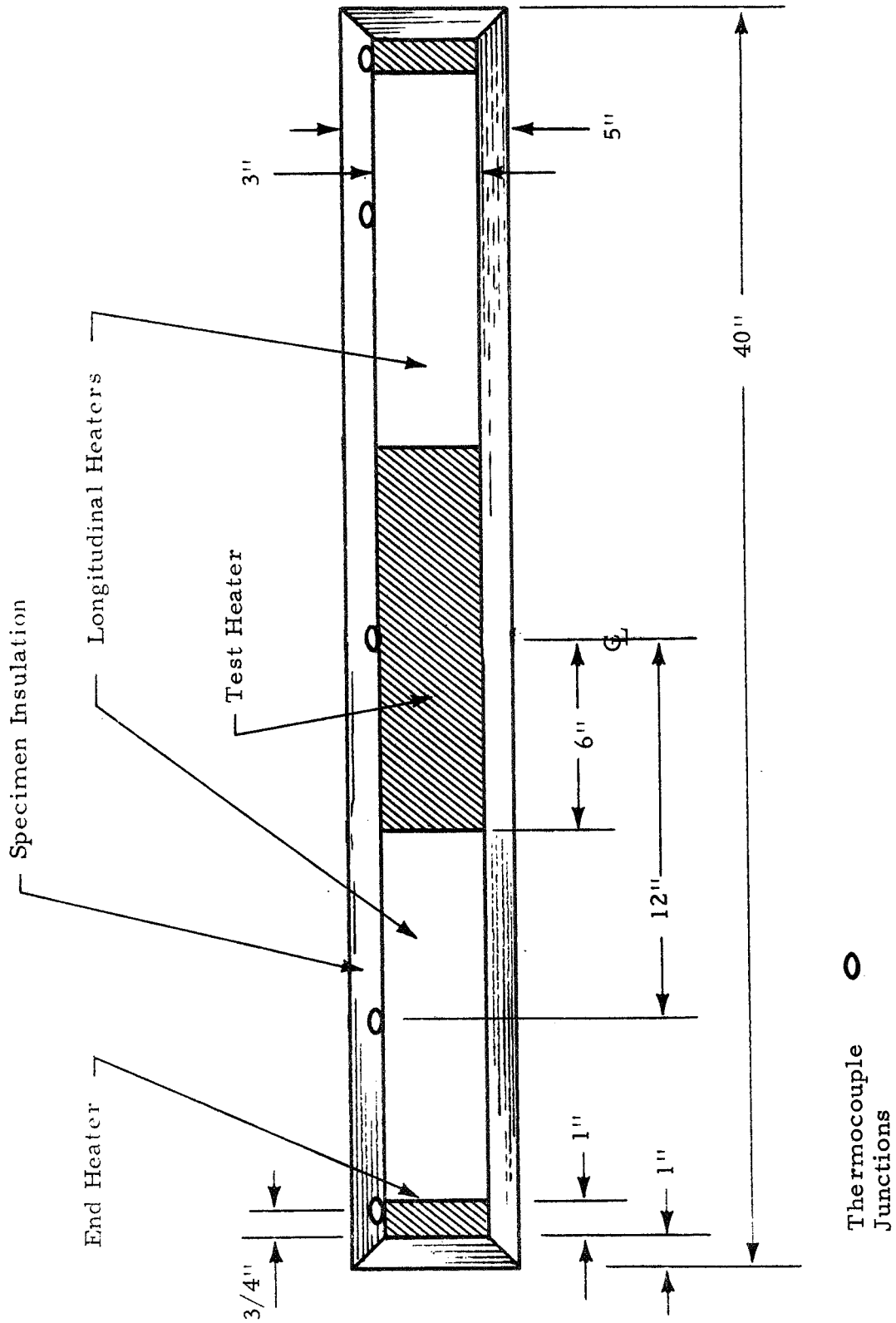


Figure 2 - Schematic of LMSC/HREC Cylindrical Calorimeter Design

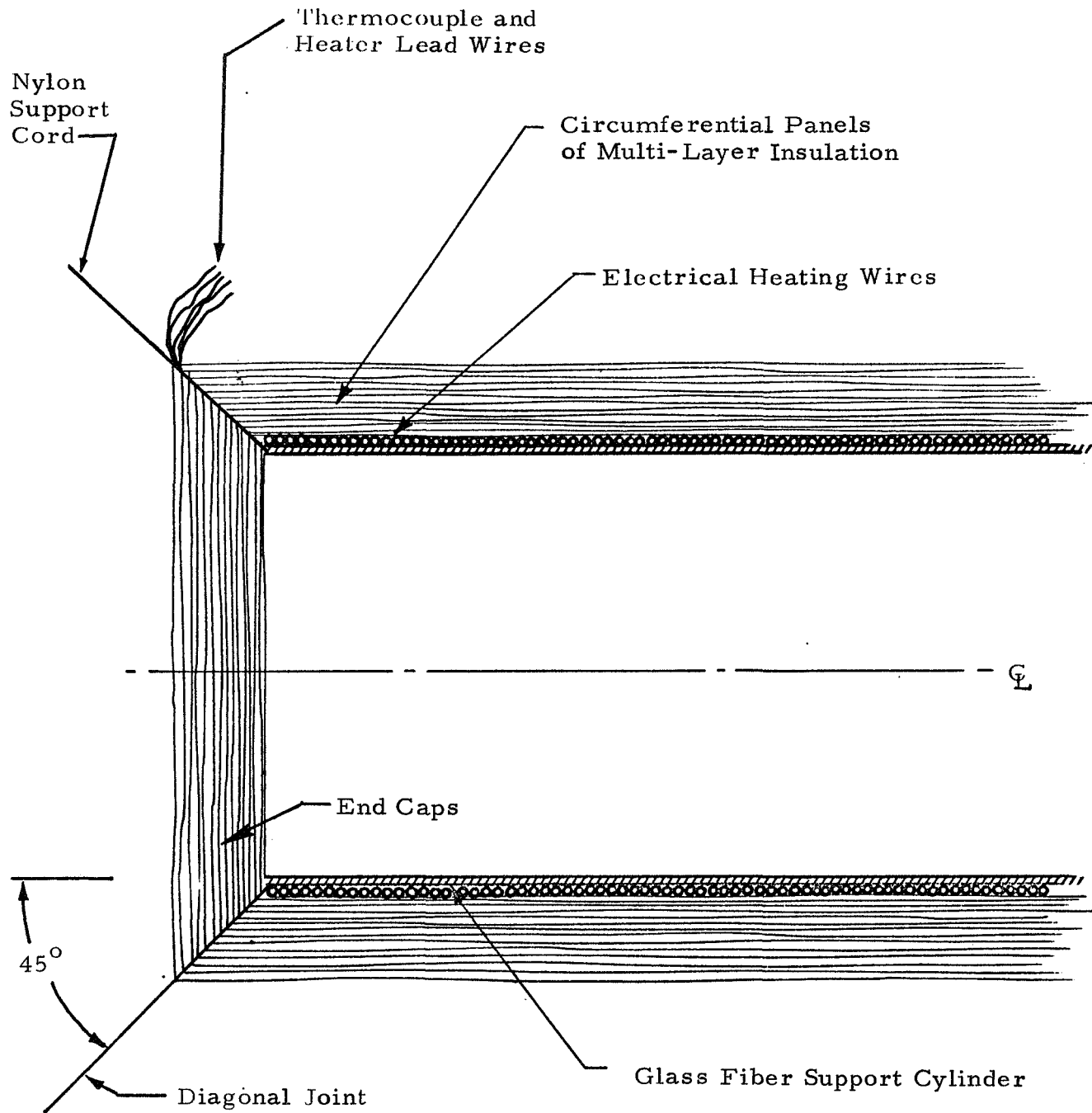


Figure 3 - Insulation Application Concept

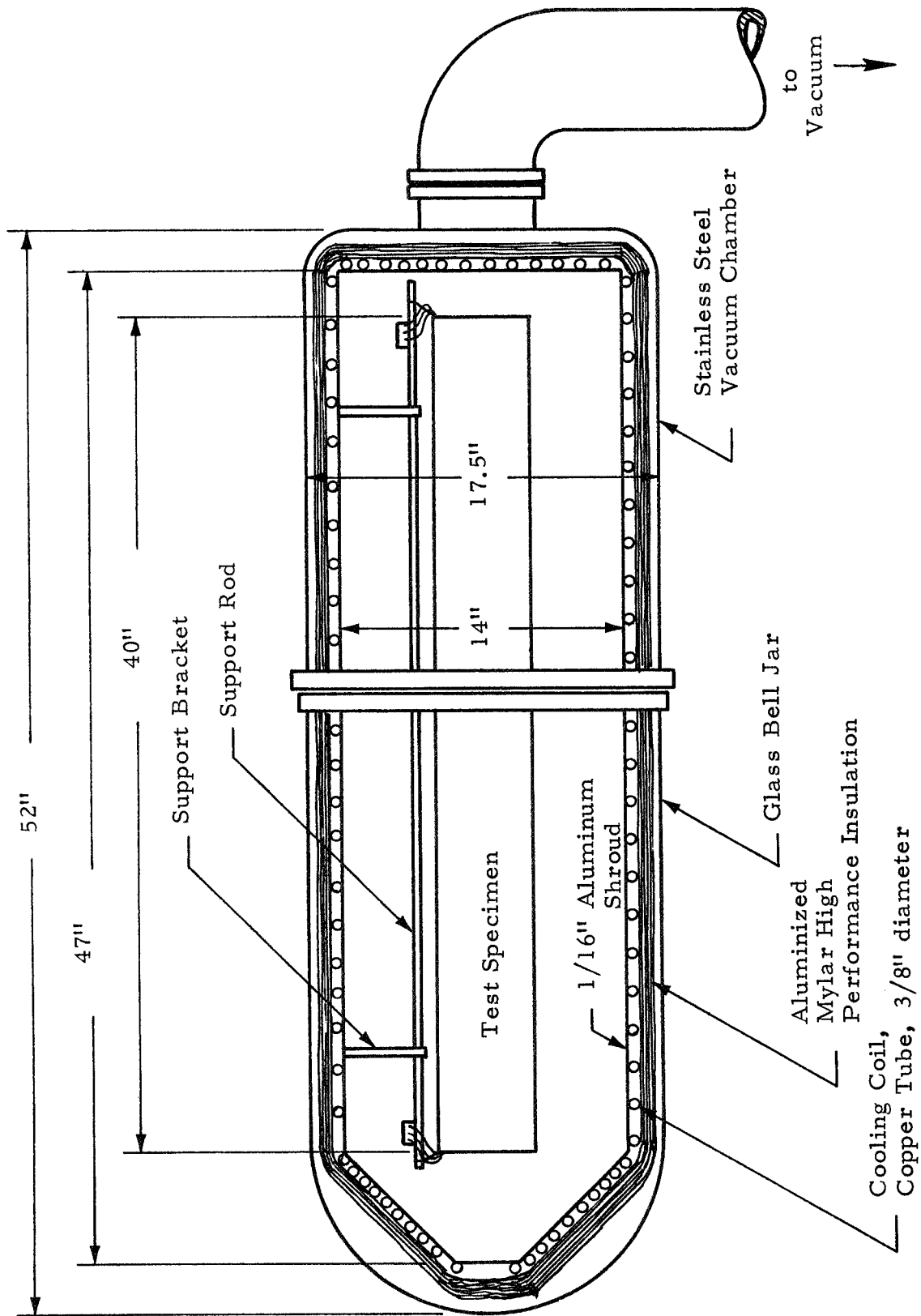


Figure 4 - Environmental Control and Vacuum Chamber System

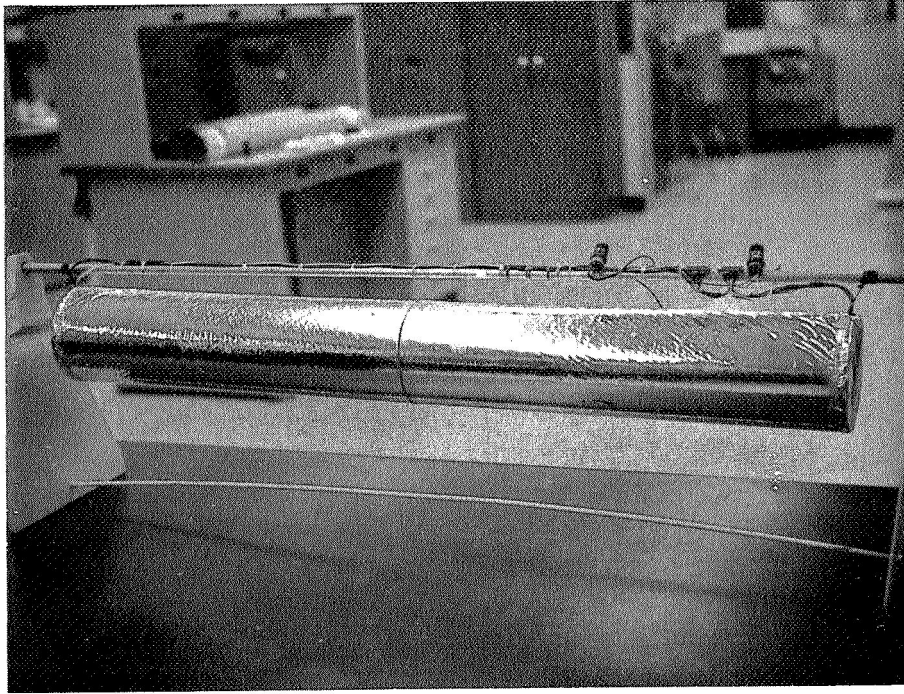


Fig. 5 - 1/4-mil Double Aluminized Mylar and Red Polyurethane Foam Specimen

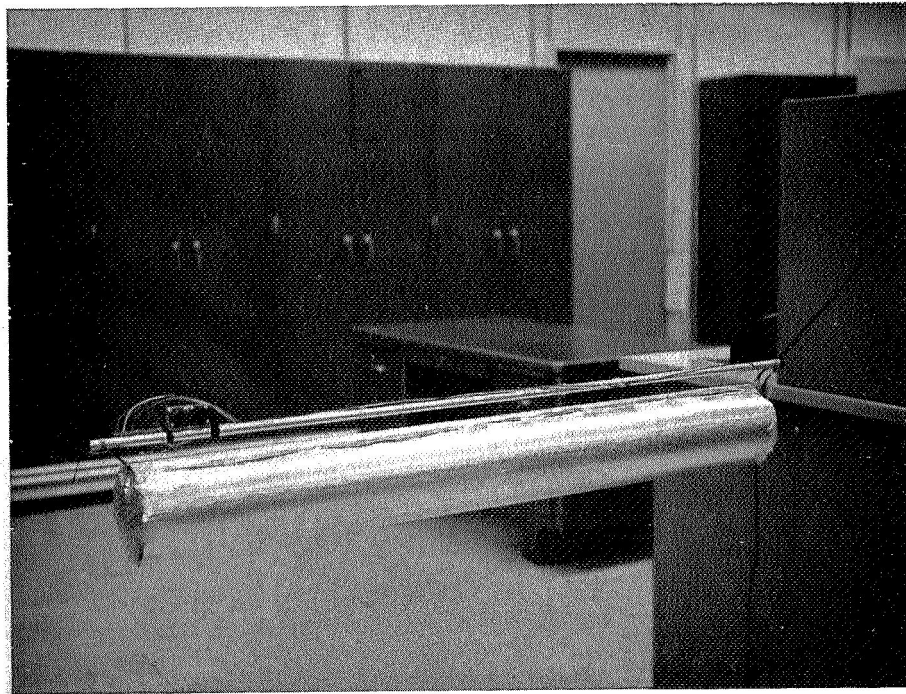


Fig. 6 - Embossed Singly Aluminized Mylar and Nylon Net

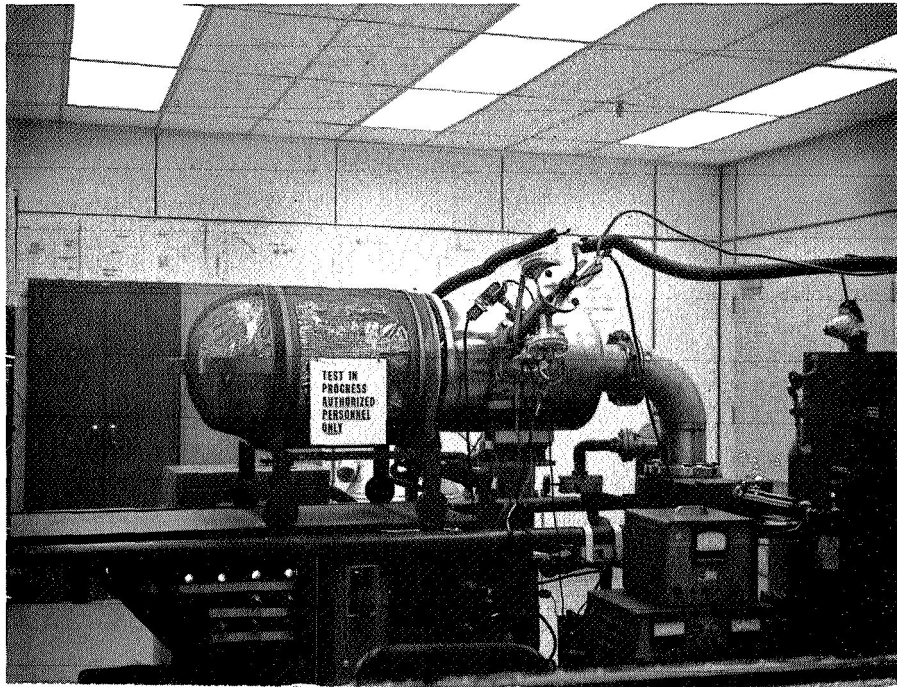


Fig. 7 - Vacuum Chamber System (View 1)

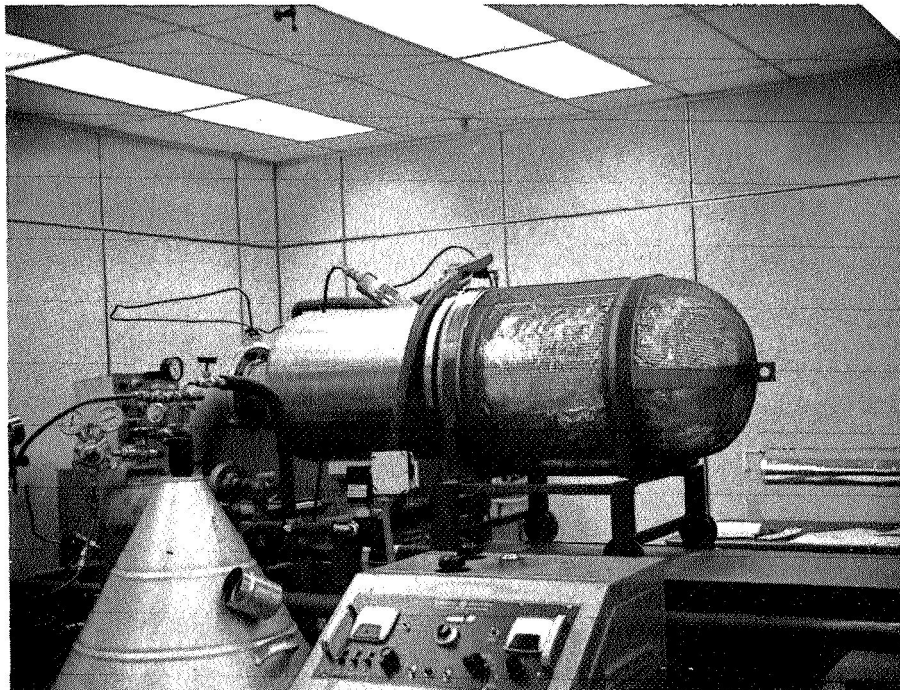


Fig. 8 - Vacuum Chamber System (View 2)

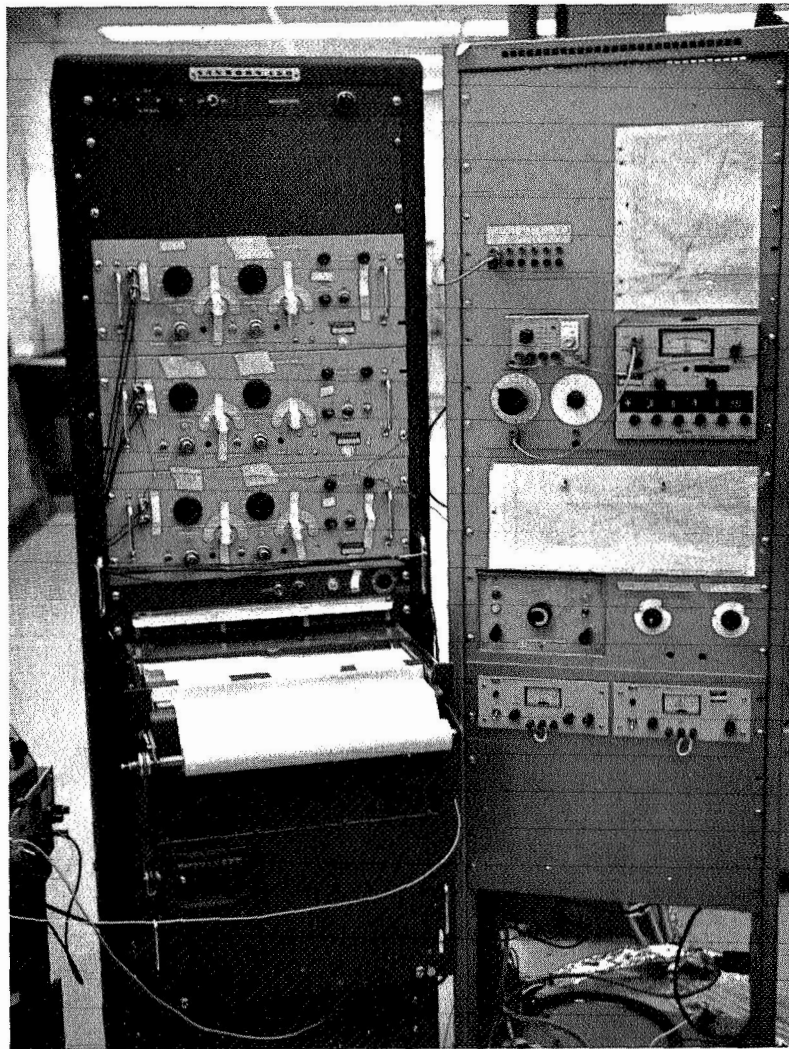


Fig. 9 - Electronic Automation Control Panel

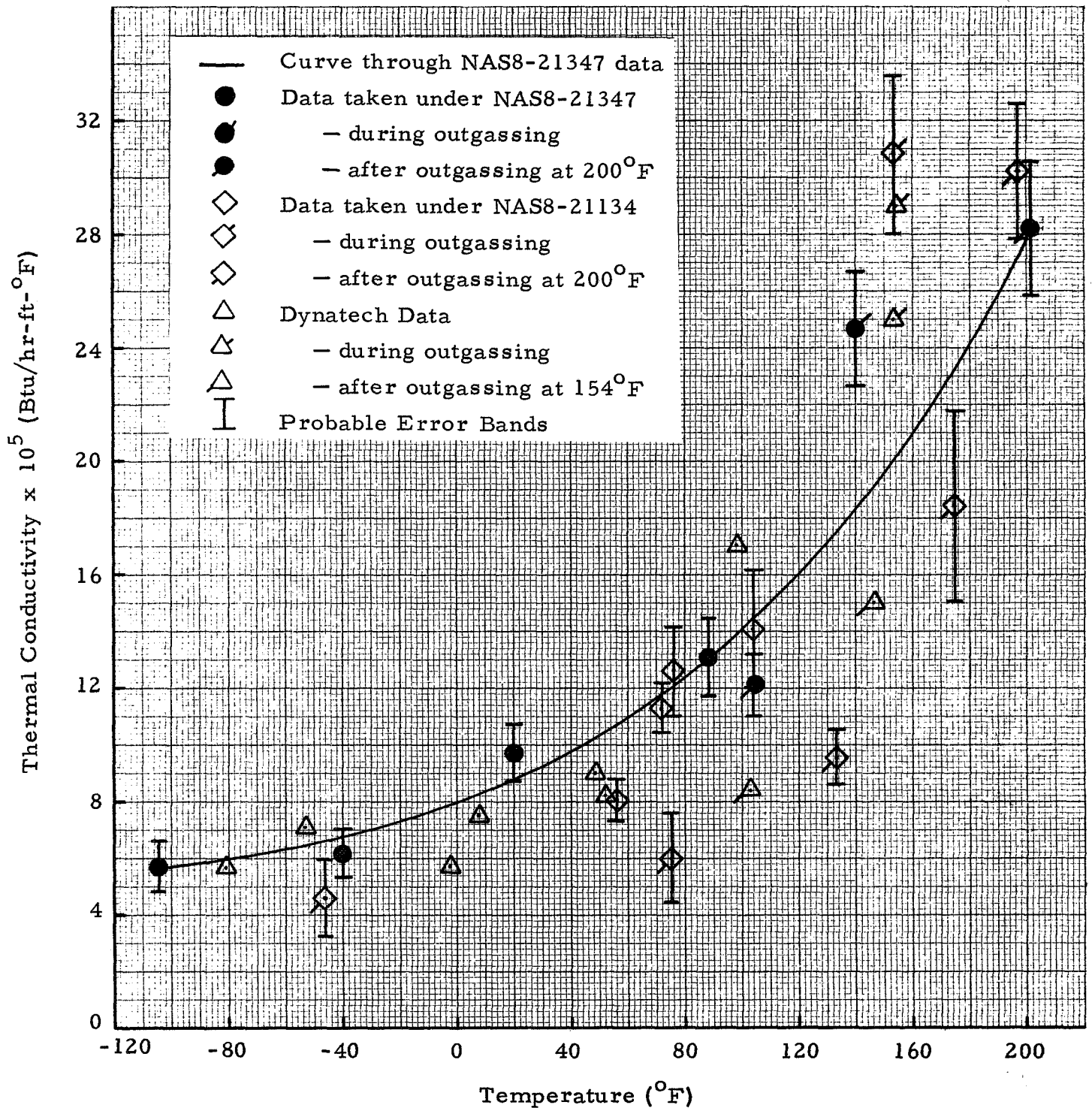


Figure 10 - Plot of Thermal Conductivity vs Temperature for Unperforated 1/4-mil Double-Aluminized Mylar and Red Polyurethane Foam

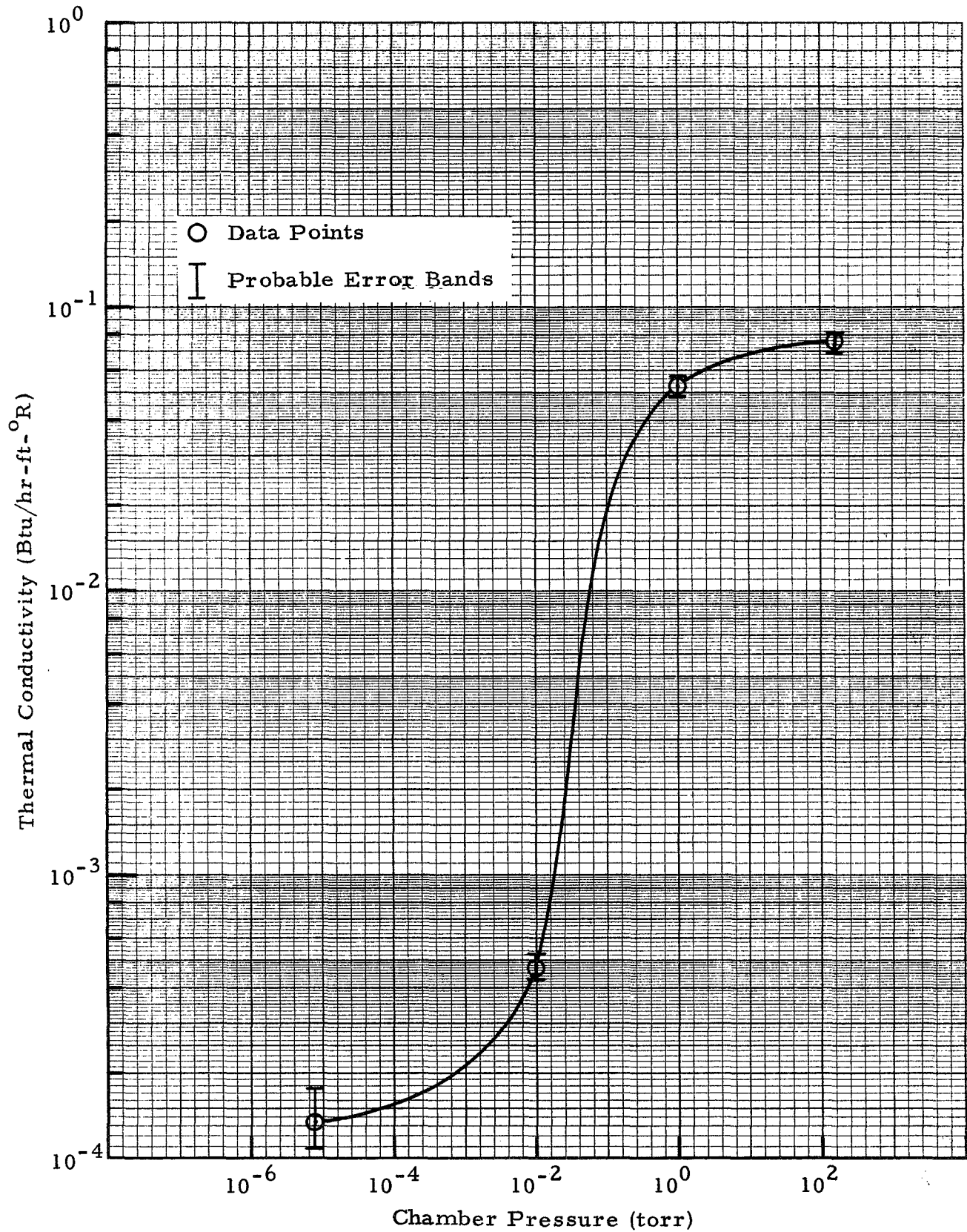


Figure 11 - Plot of Thermal Conductivity vs Chamber Pressure at Room Temperature for 1/4-mil Double-Aluminized Mylar and Red Polyurethane Foam Specimen

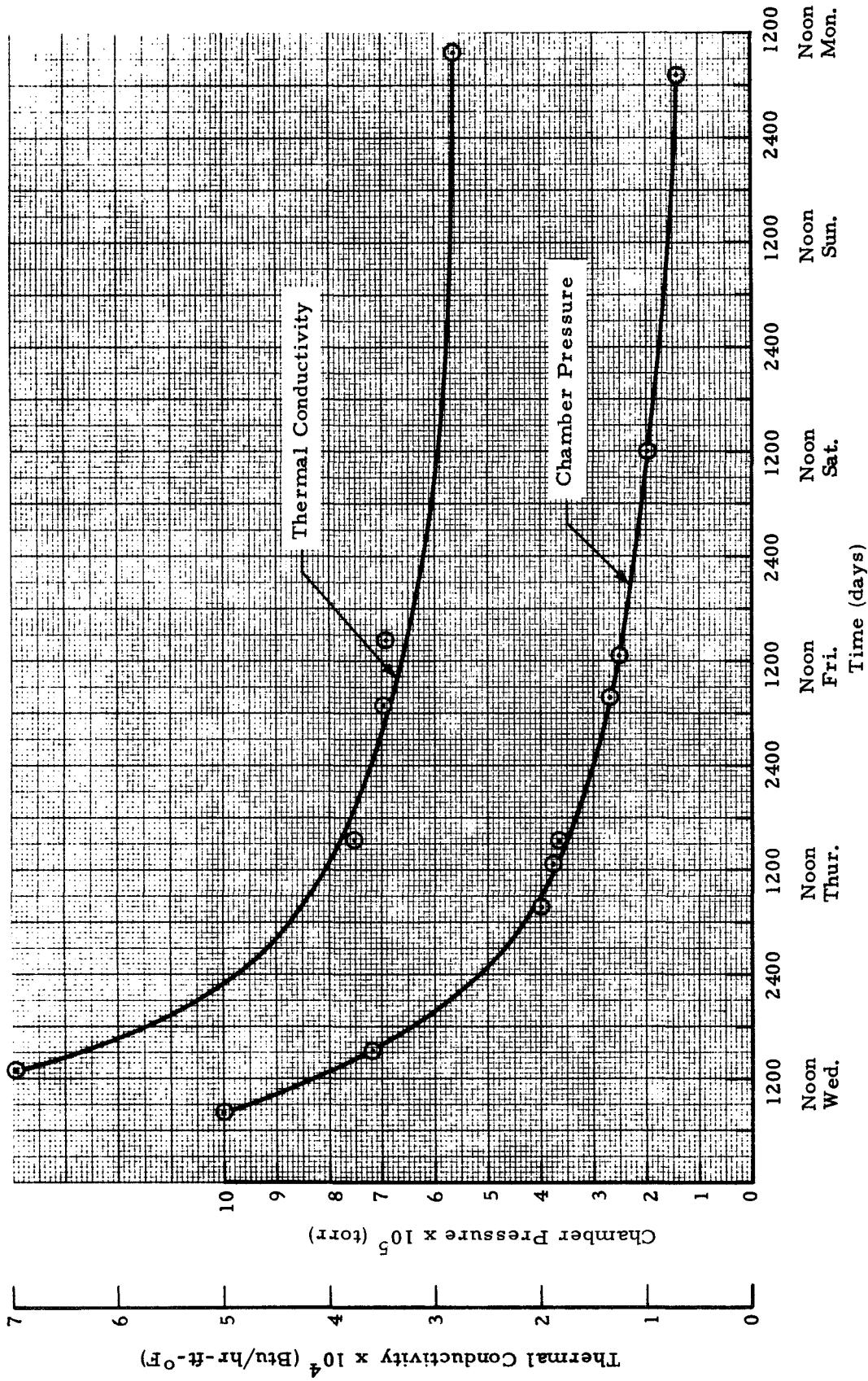


Figure 12 - Plot of Thermal Conductivity and Chamber Pressure versus Time for 200°F Data Point for Unperforated Goodyear Insulation

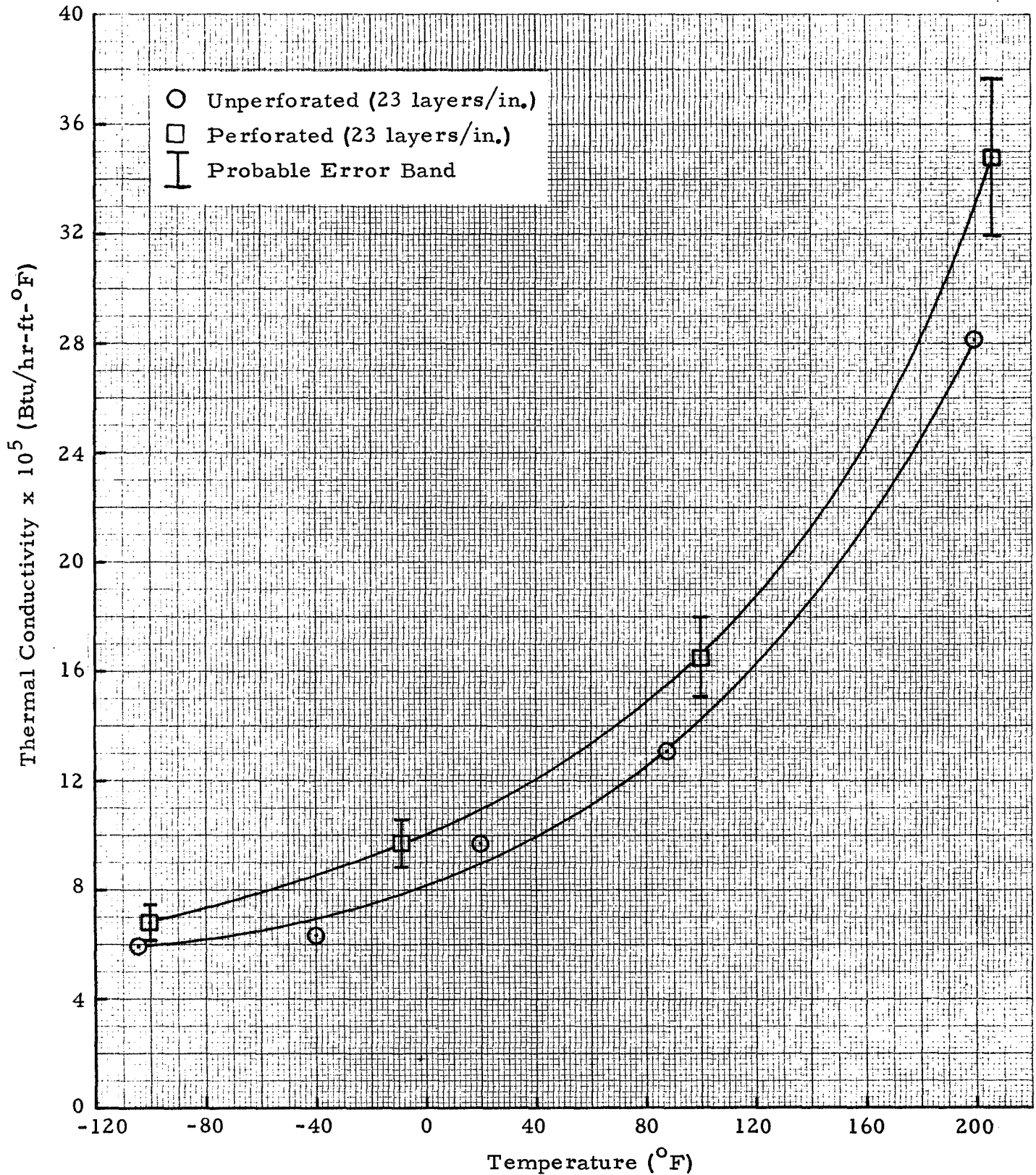


Figure 13 - Plot of Thermal Conductivity vs Temperature for Perforated and Unperforated 1/4-mil Double-Aluminized Mylar and Red Polyurethane Foam Specimen

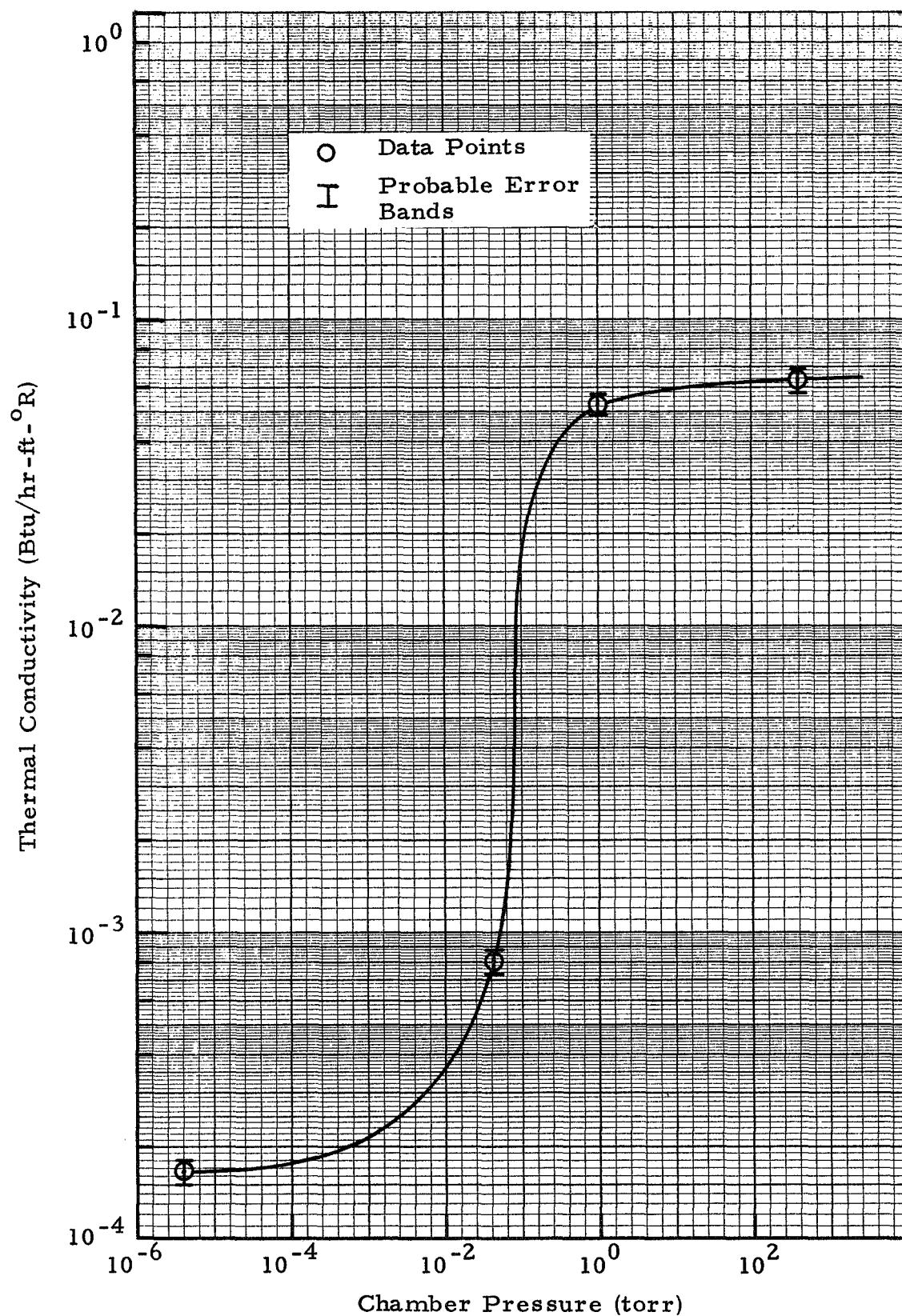


Figure 14 - Plot of Thermal Conductivity vs Chamber Pressure at Room Temperature for Perforated 1/4-mil Double-Aluminized Mylar and 0.030-Inch Red Foam Specimen

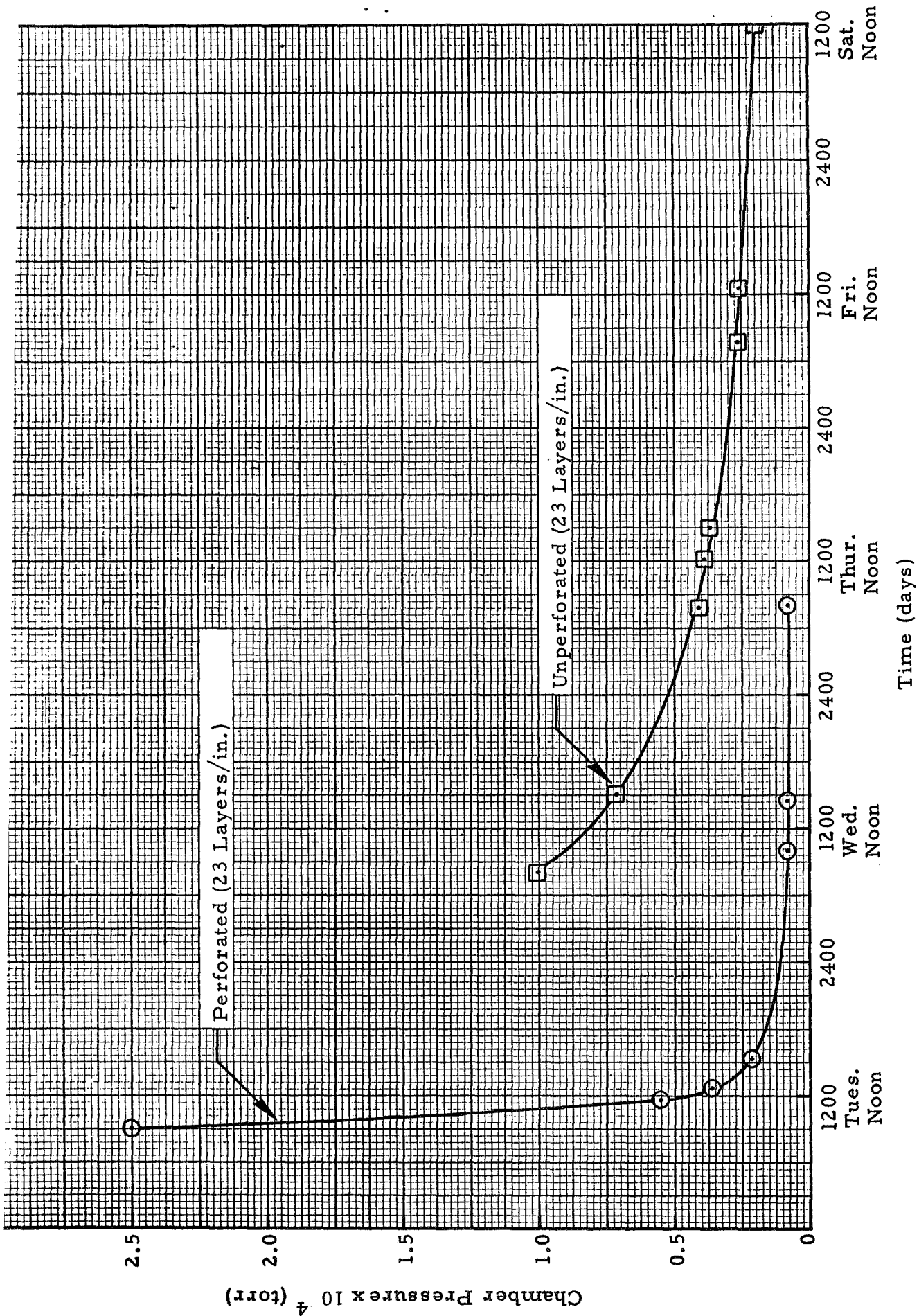


Figure 15 - Plot of Pressure vs Time for 200°F Data Point for Perforated and Unperforated 1/4-mil Double-Aluminized Mylar and Red Polyurethane Foam Specimen

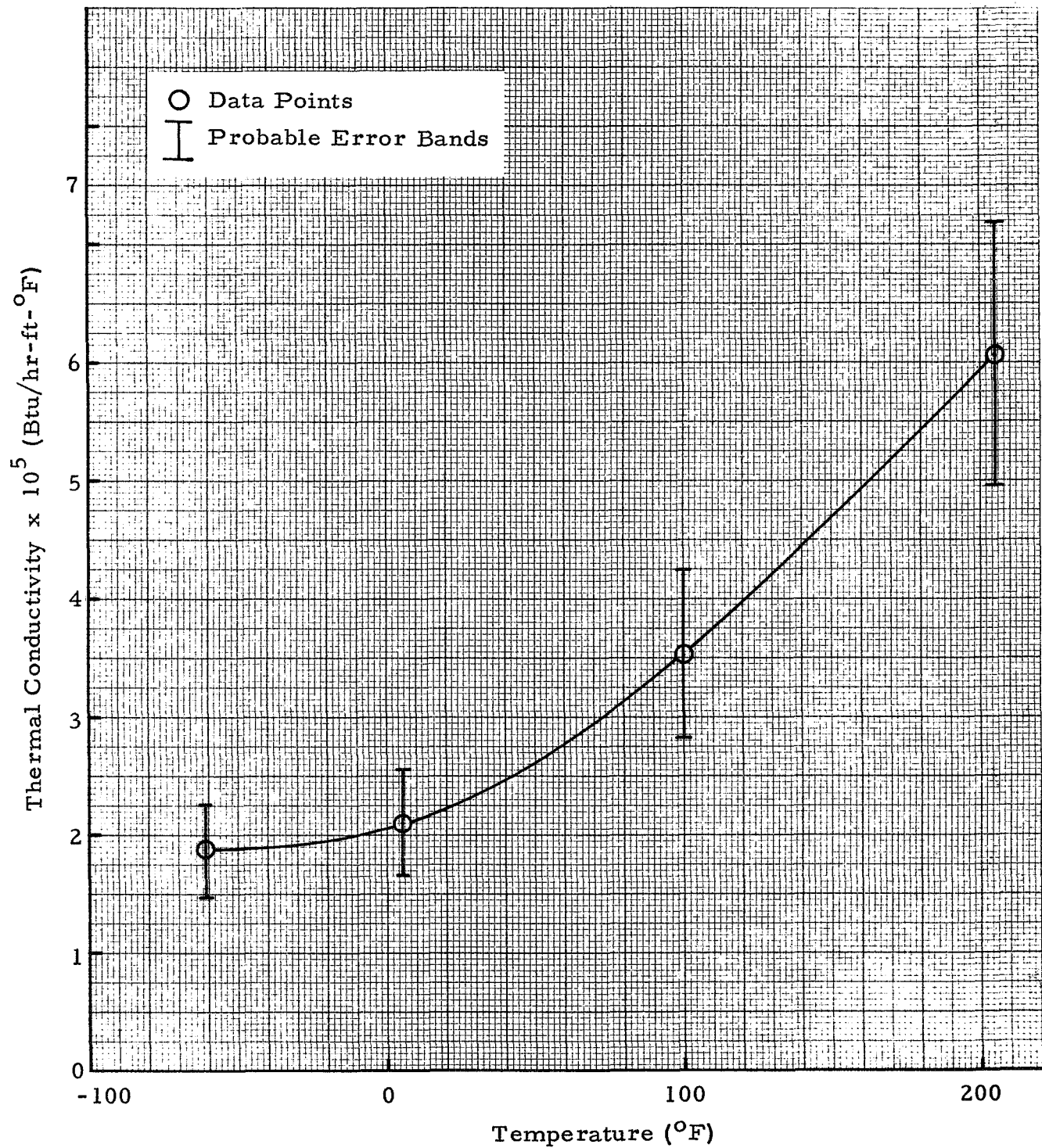


Figure 16 - Plot of Thermal Conductivity versus Temperature
for Embossed Aluminized Mylar at 162 Layers/Inch

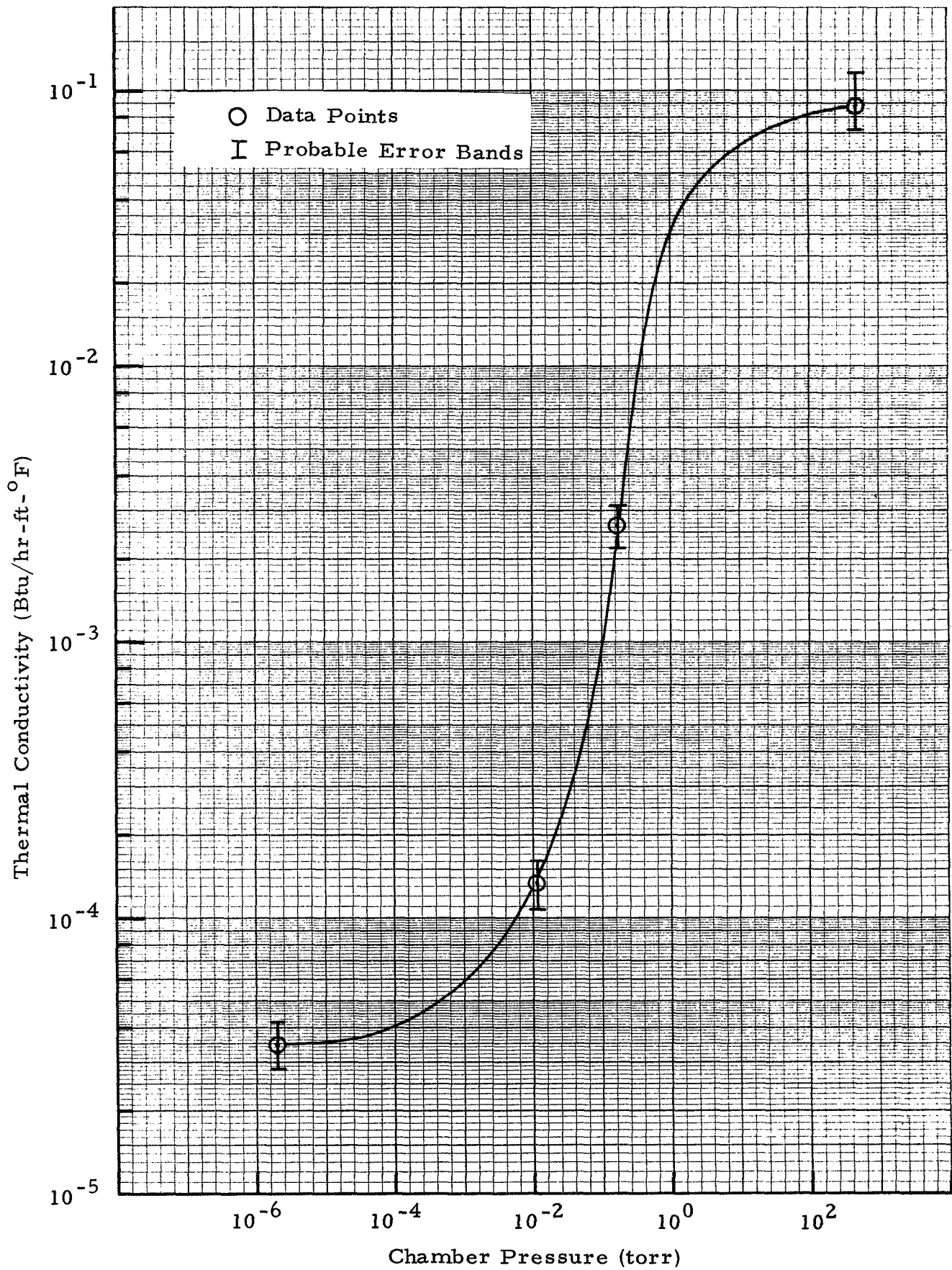


Figure 17 - Plot of Thermal Conductivity versus Chamber Pressure at Room Temperature for Embossed Aluminized Mylar at 162 Layers/Inch

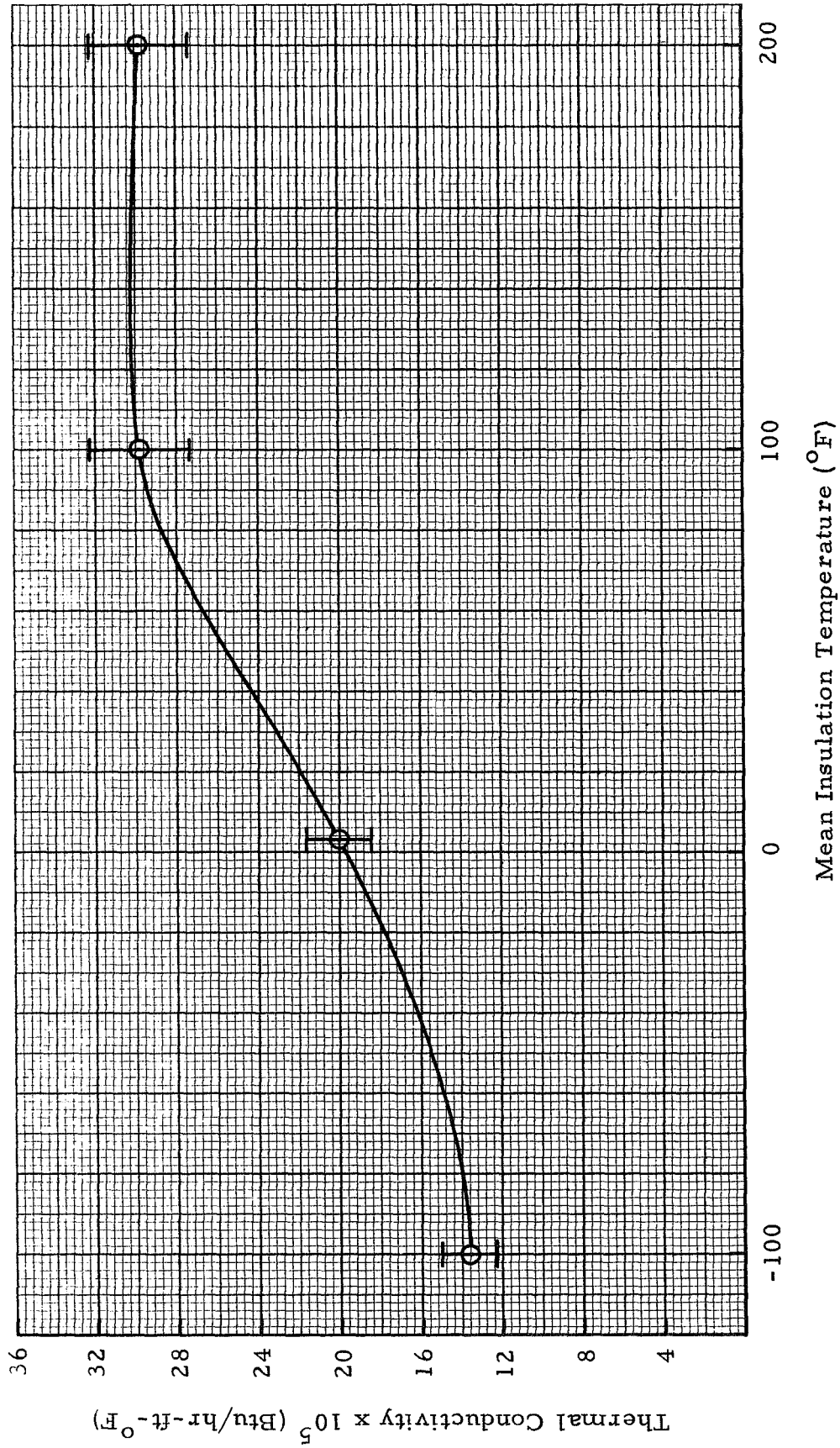


Figure 18 - Plot of Thermal Conductivity vs Temperature for Alternate Layers of Demplar and Embossed Aluminized Mylar at 19.15 Layers per Inch

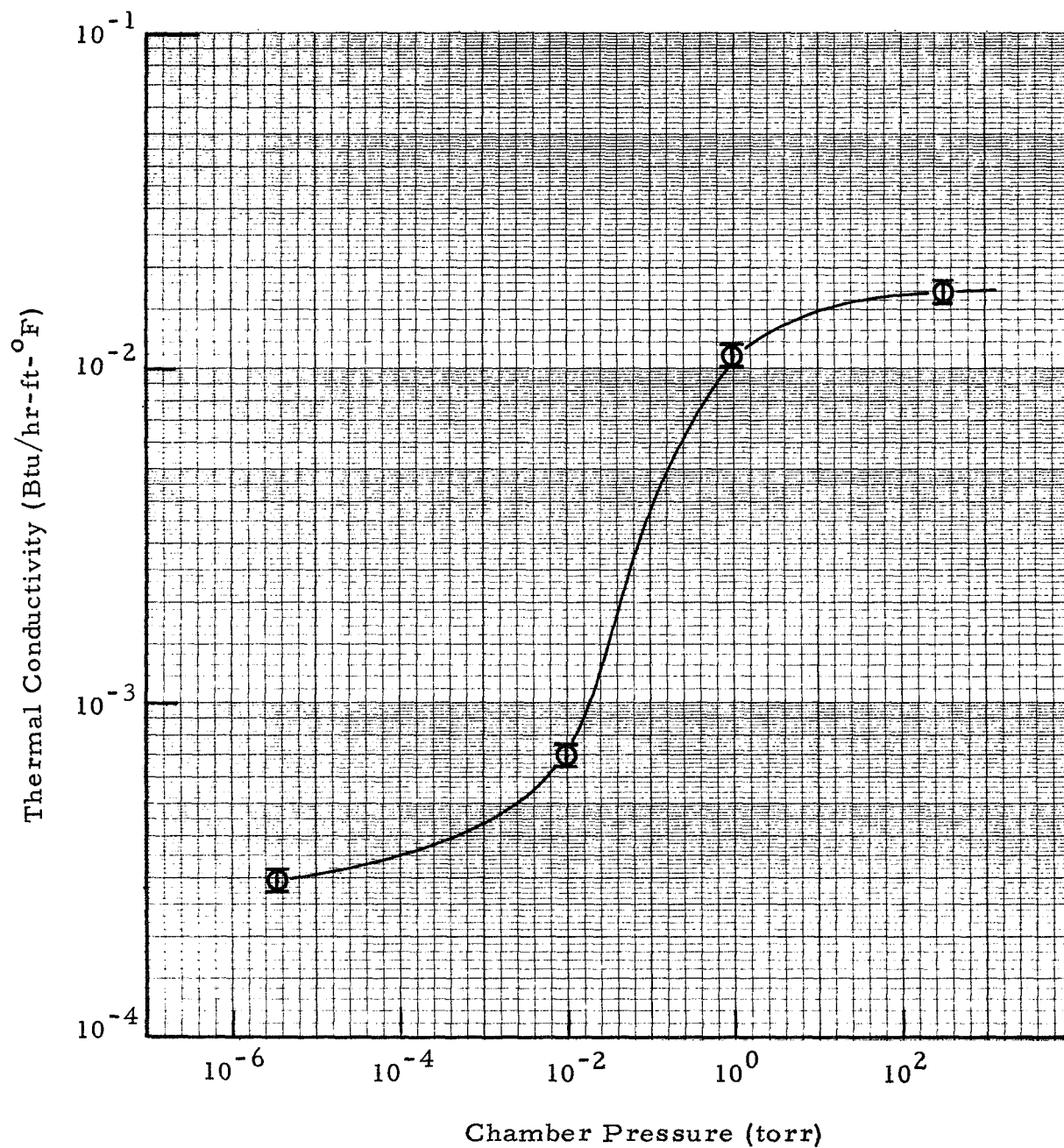


Figure 19 - Plot of Thermal Conductivity vs Chamber Pressure at Room Temperature for Alternate Layers of 1/4-mil Embossed Aluminized Mylar and Dimplar at 19.15 Layers/Inch

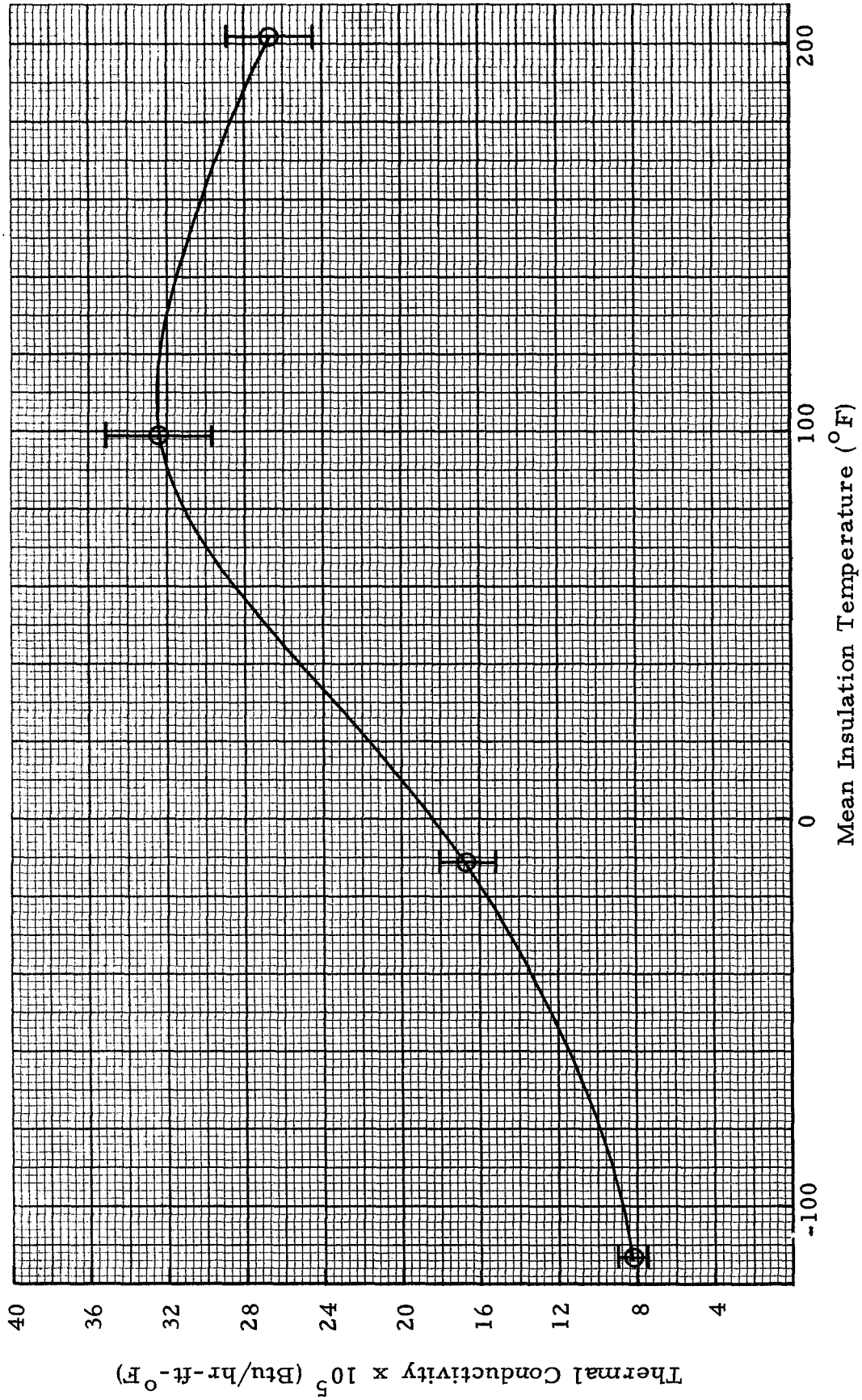


Figure 20 - Plot of Thermal Conductivity vs Temperature for Alternate Layers of 1/4-mil Embossed Aluminized Mylar and Nylon Net at 60 Layers Per Inch

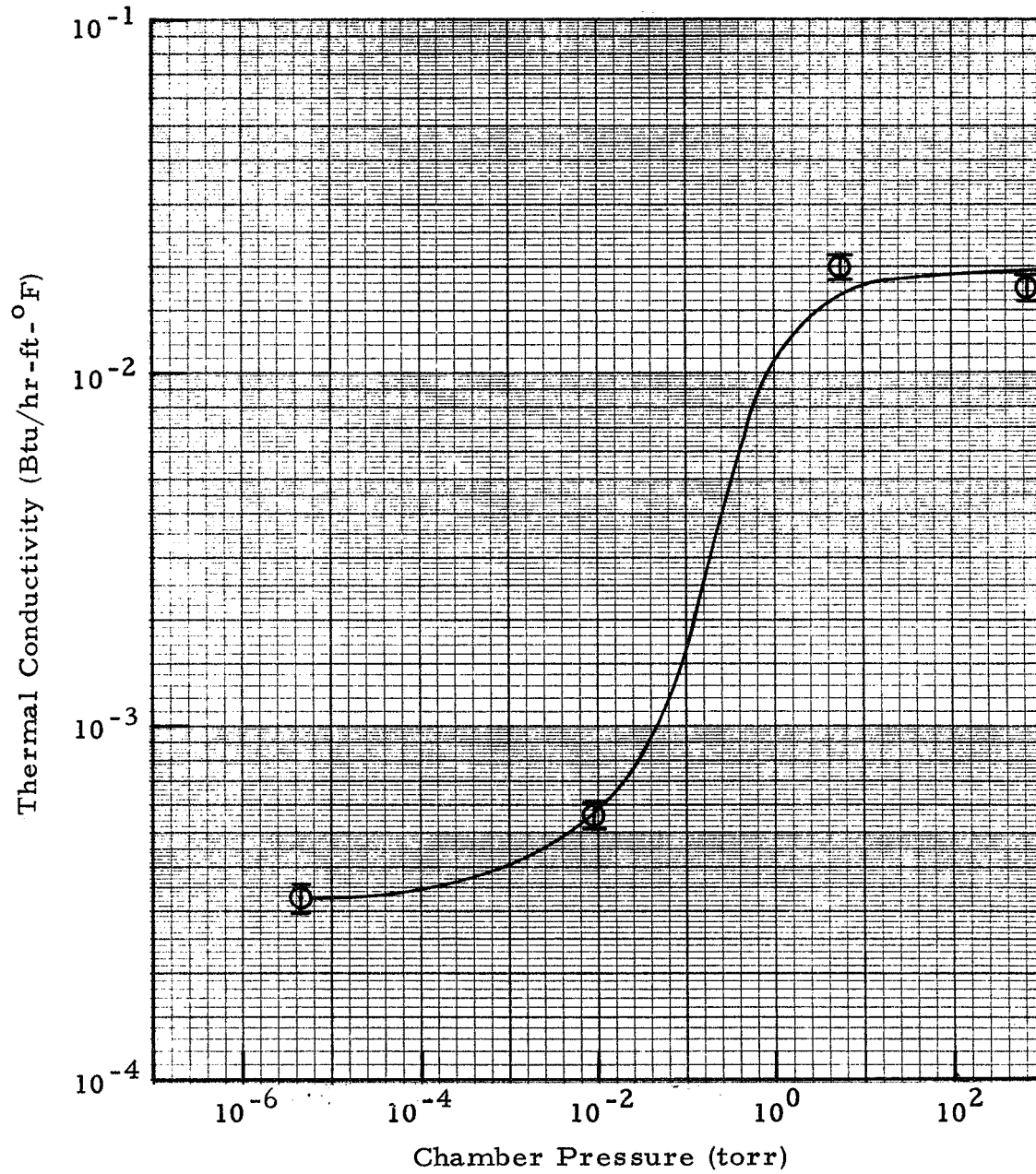


Figure 21 - Plot of Thermal Conductivity vs Chamber Pressure at Room Temperature for Alternate Layers of 1/4-mil Embossed Aluminized Mylar and Nylon Net at 60 Layers Per Inch

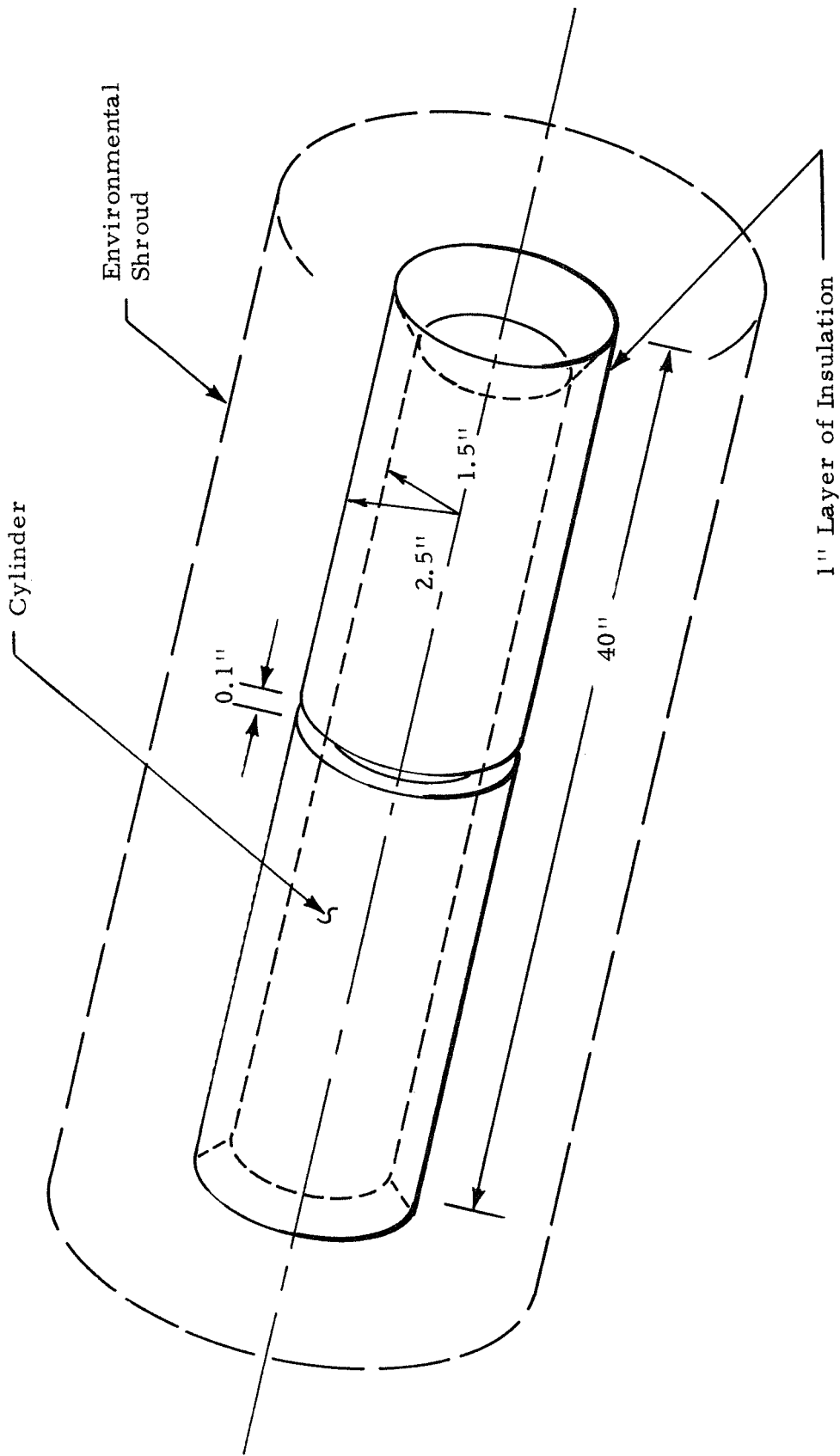


Figure 22 - Insulation Gap Test Schematic

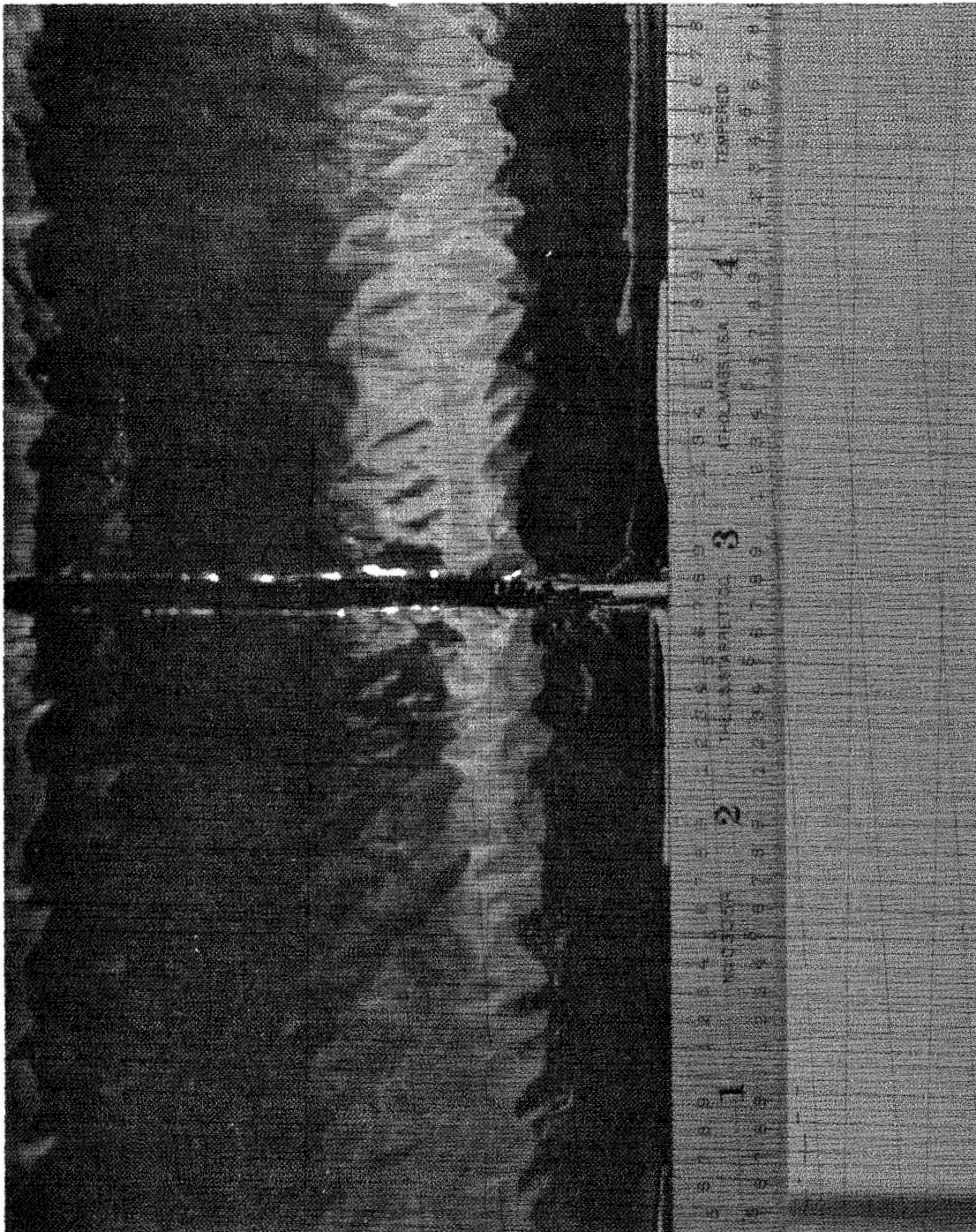


Figure 23 - Butt Joint with 1/10-Inch Separation

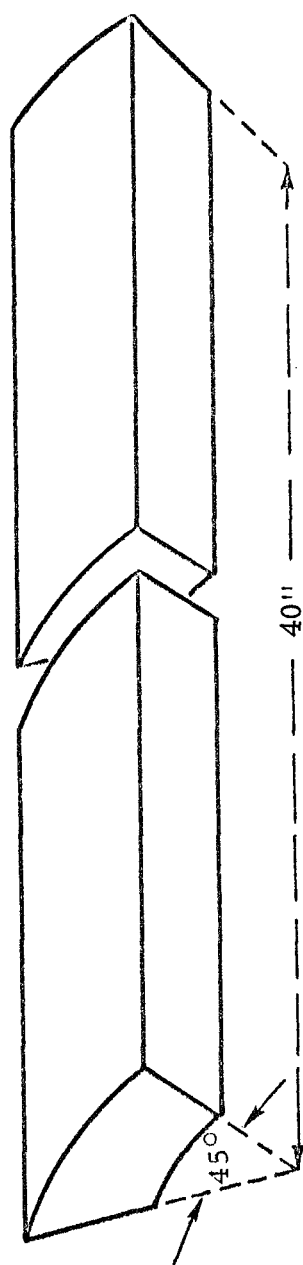


Figure 24 - Model Used for Thermal Analysis of Gap Test

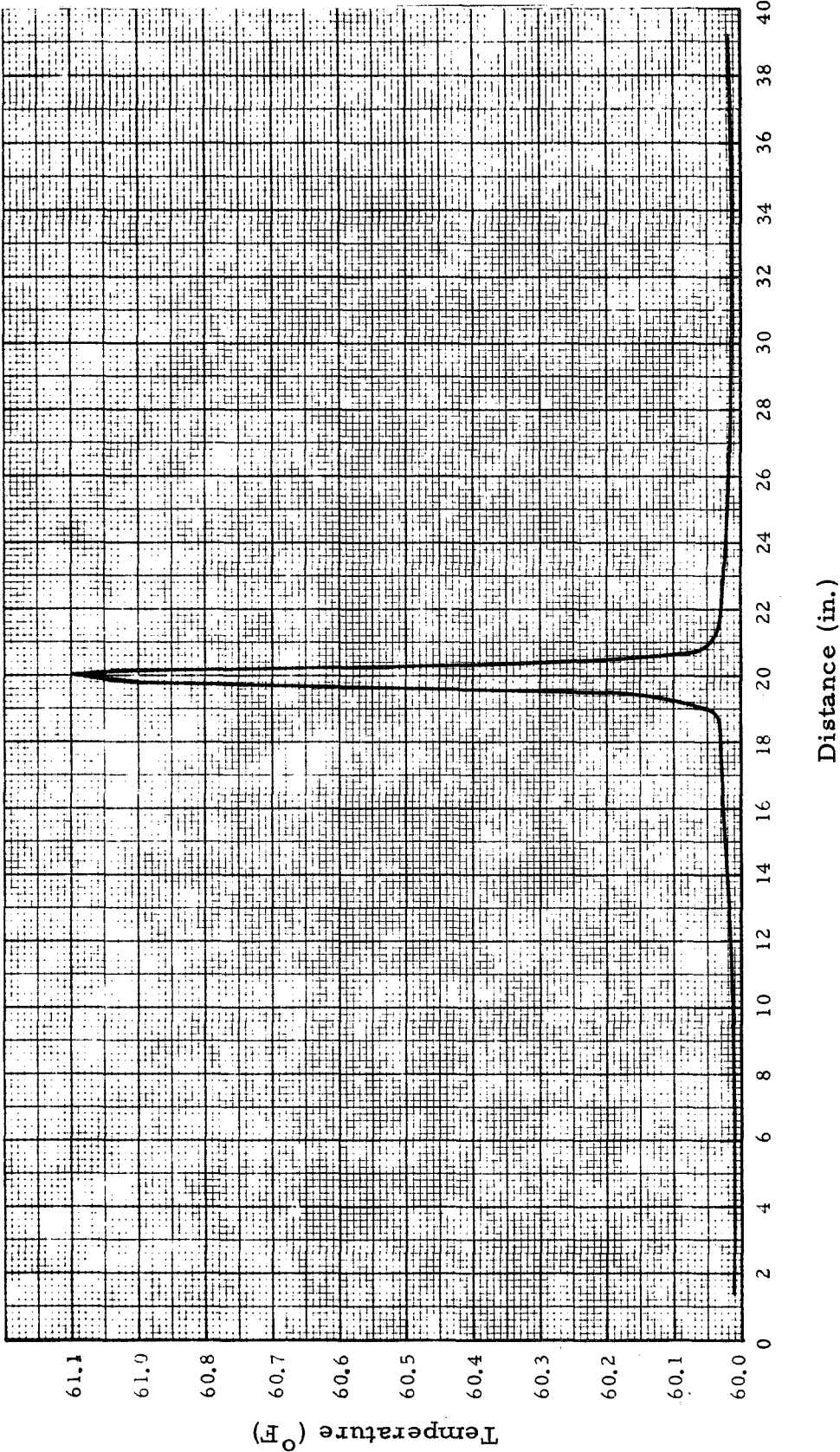


Figure 25 - External Surface Temperature Distribution on 1/10-Inch Gap Test Specimen for 1/4-mil Double-Aluminized Mylar and Red Polyurethane Foam 1-In. Thick at Room Temperature

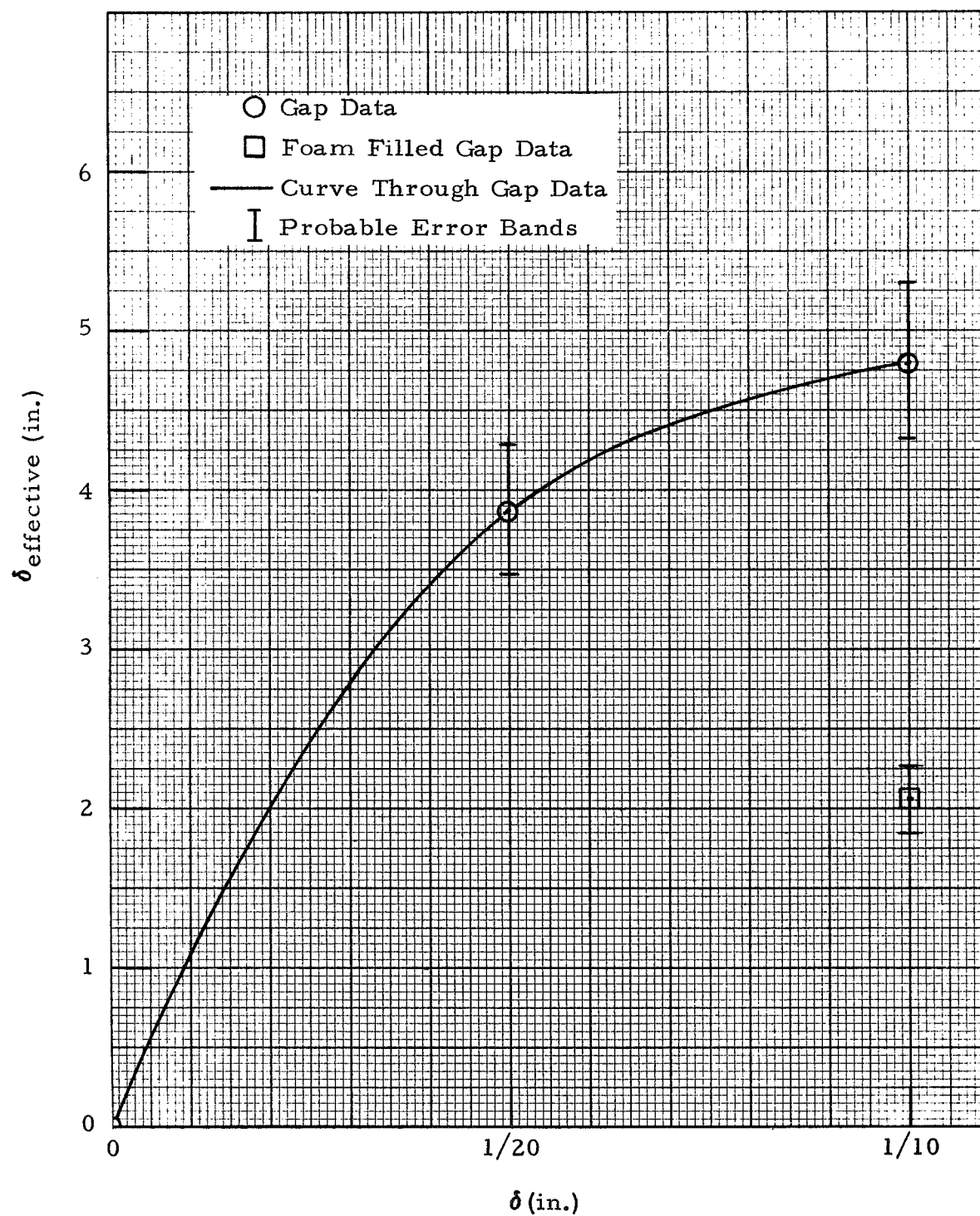


Figure 26 - Plot of Effective Gap Width versus Gap Width for Specimen of 1/4-mil Double-Aluminized Mylar and Red Polyurethane Foam 1-In. Thick at Room Temperature

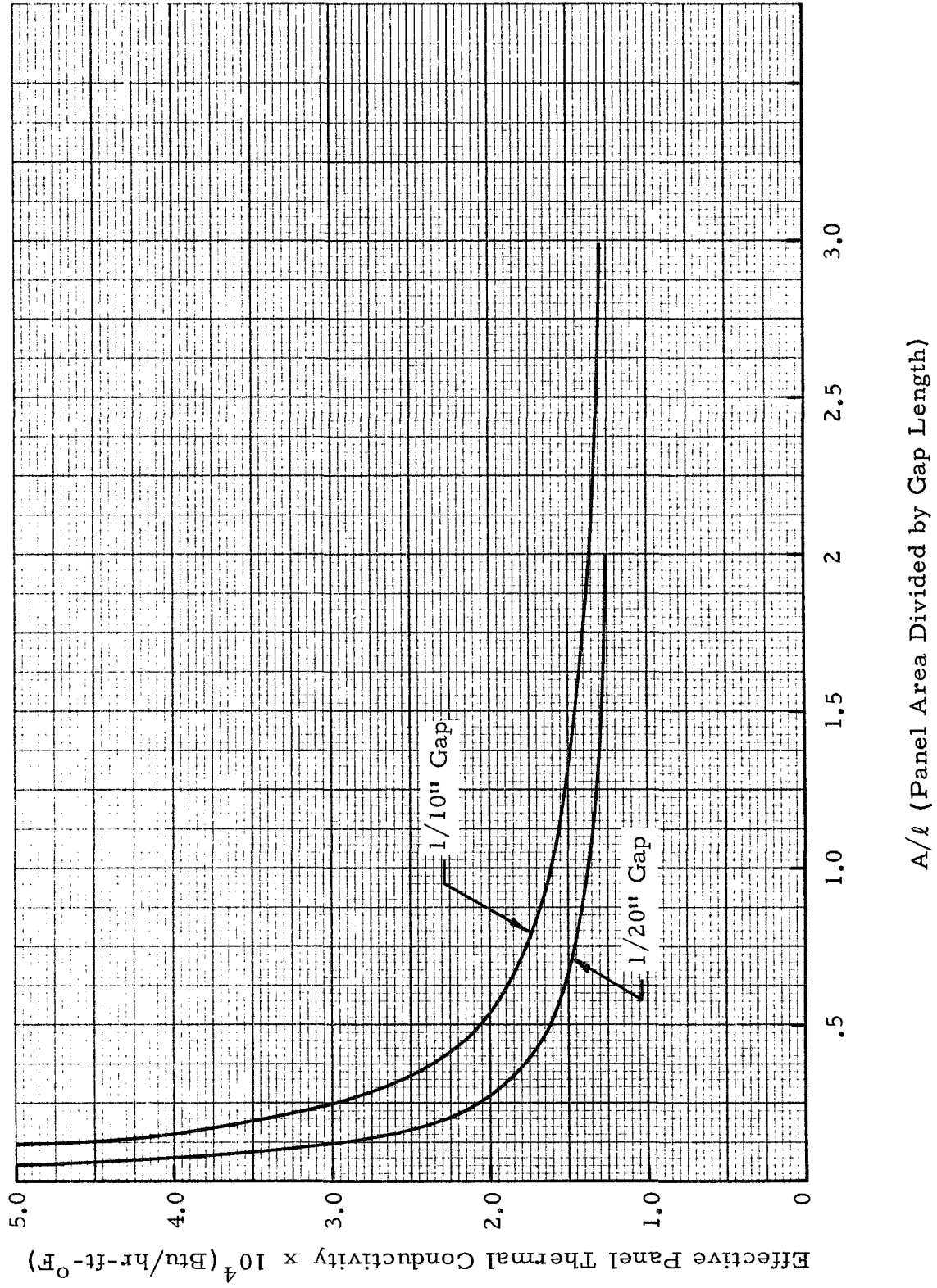


Figure 27 - Plot of Effective Panel Thermal Conductivity versus the Ratio of Panel Area to Gap Length for Double-Aluminized Mylar and Red Polyurethane Foam 1-Inch Thick at Room Temperature

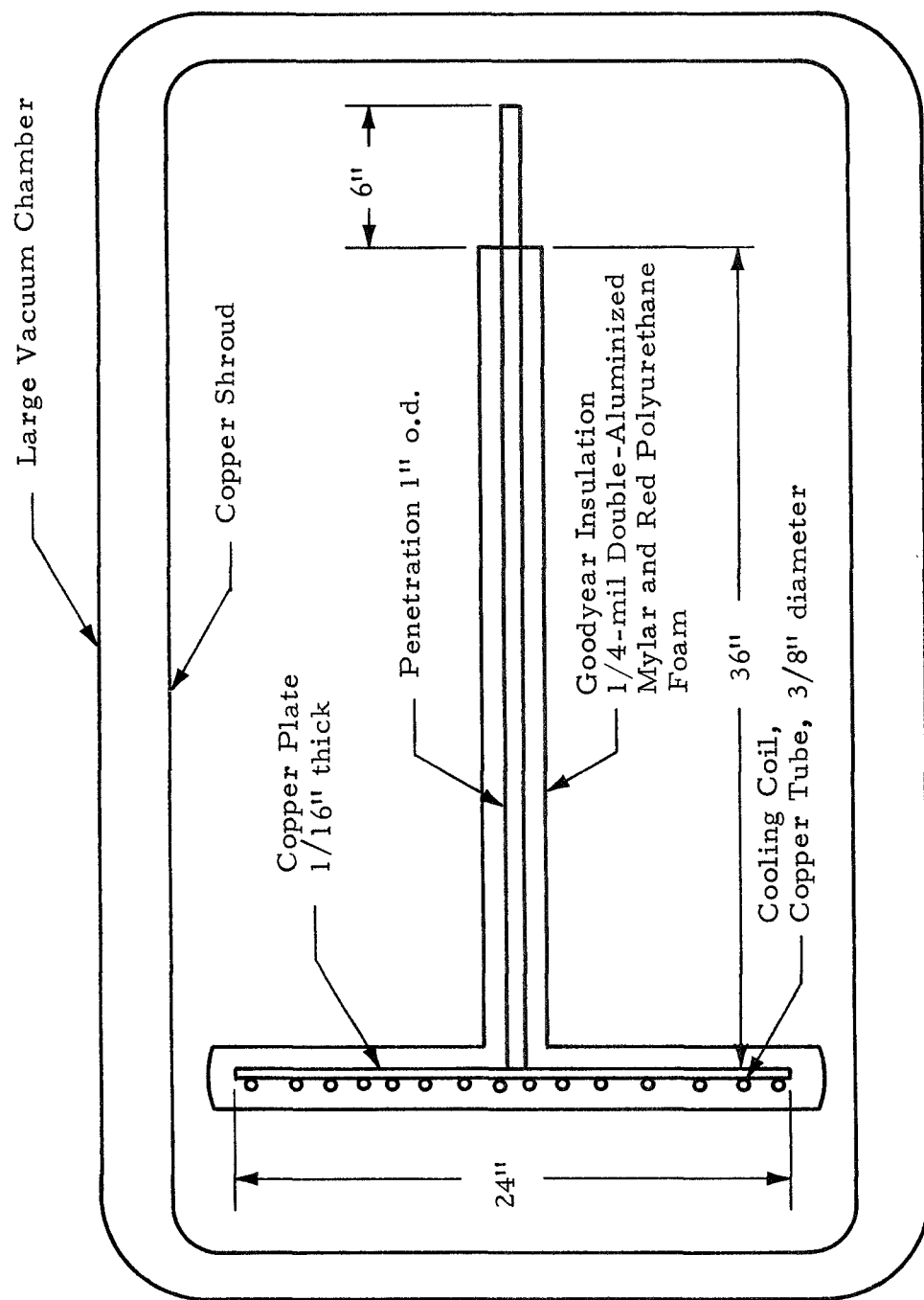


Figure 28 - Penetration Test Apparatus

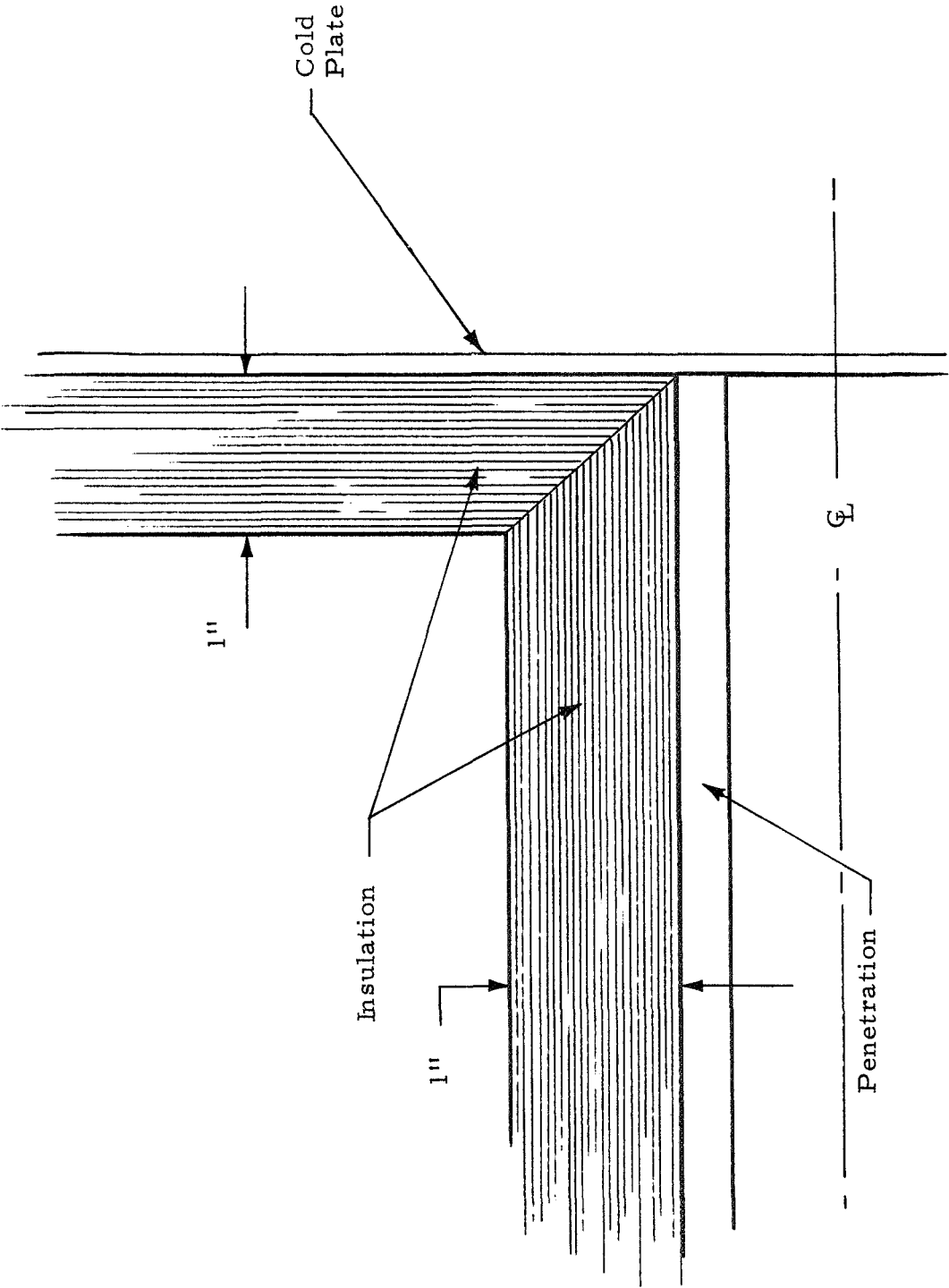


Figure 29 - Diagonal Joint Insulation Fit

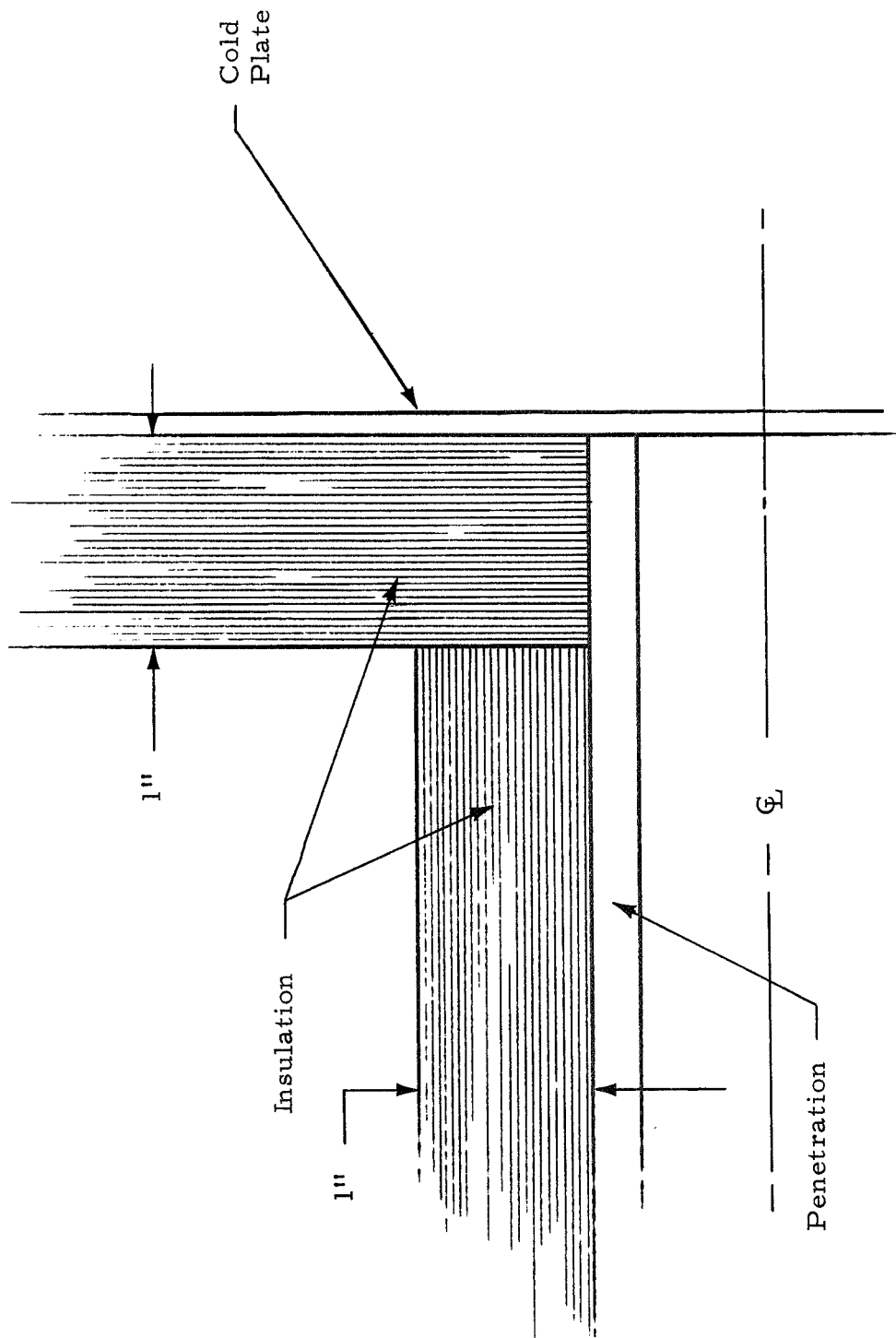


Figure 30 - Butt Joint Insulation Fit

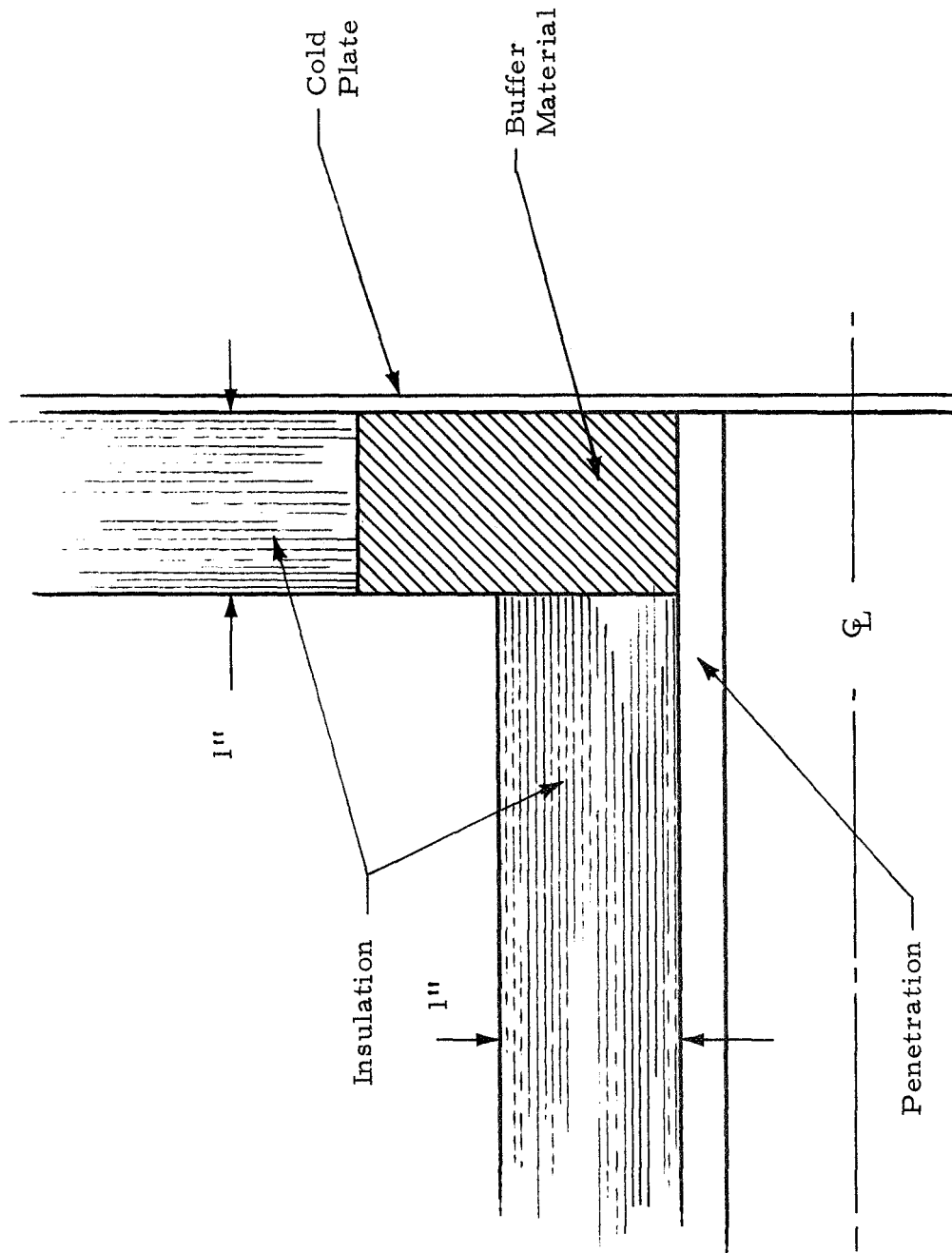


Figure 31 - Buffer Joint Insulation Fit



Fig. 32 - Penetration Test Apparatus During Wrapping Process

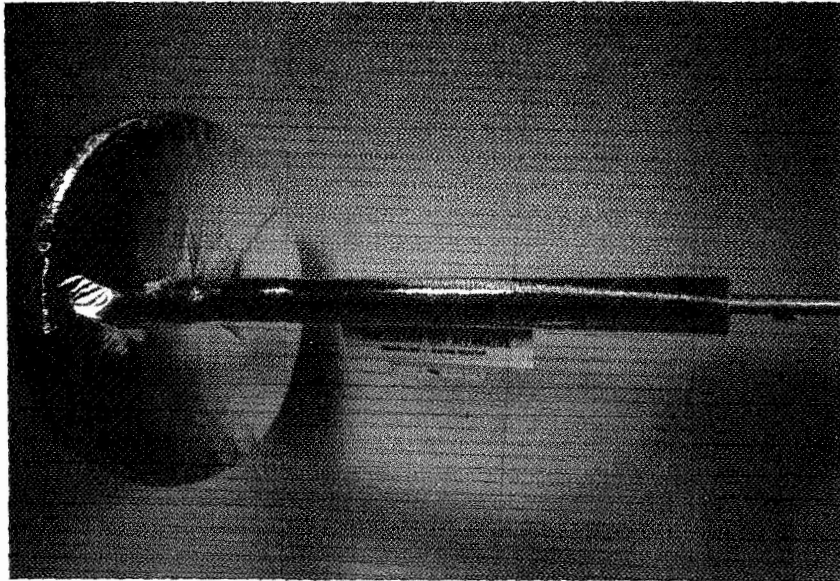


Figure 33 - Diagonal-Joint Insulation Specimen on Penetration Test Apparatus

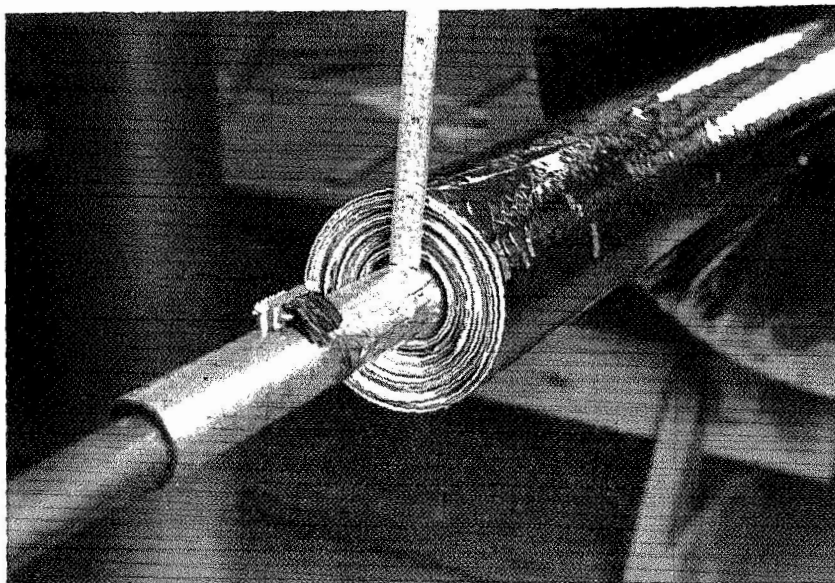


Figure 34 - Open End of Penetration Test Apparatus

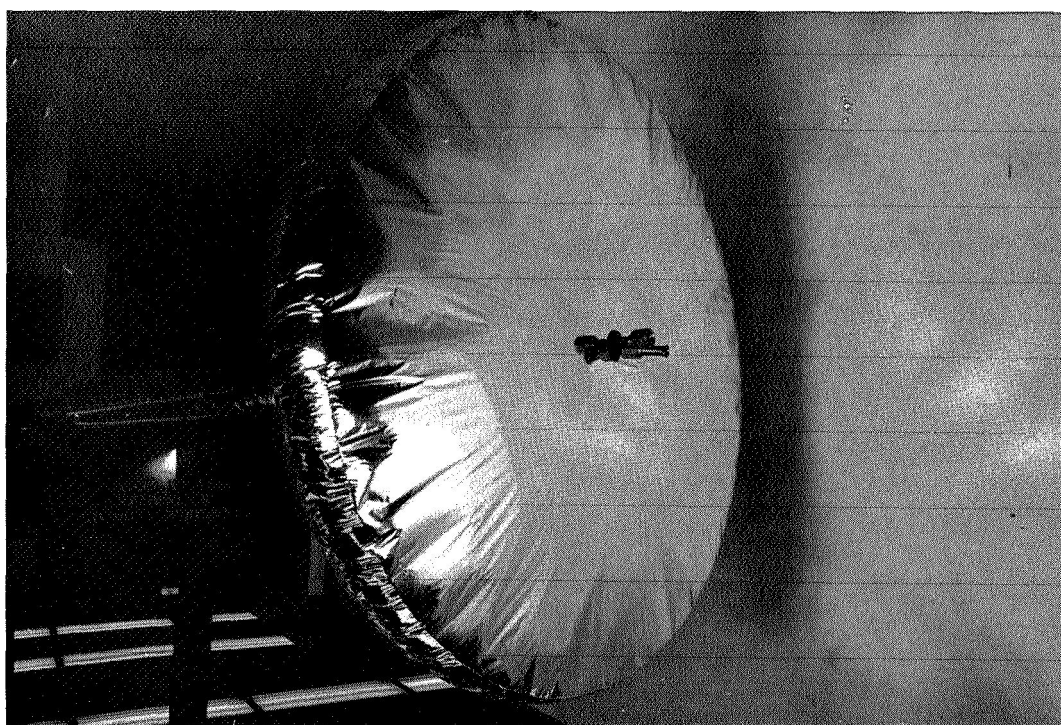


Fig. 35 - Backside of Penetration Test Apparatus

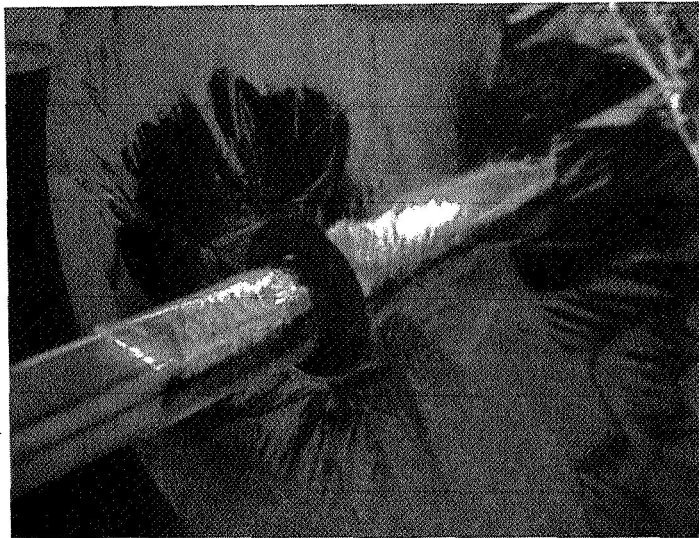


Figure 36 - Buffer-Joint Insulation Specimen on Penetration Test Apparatus

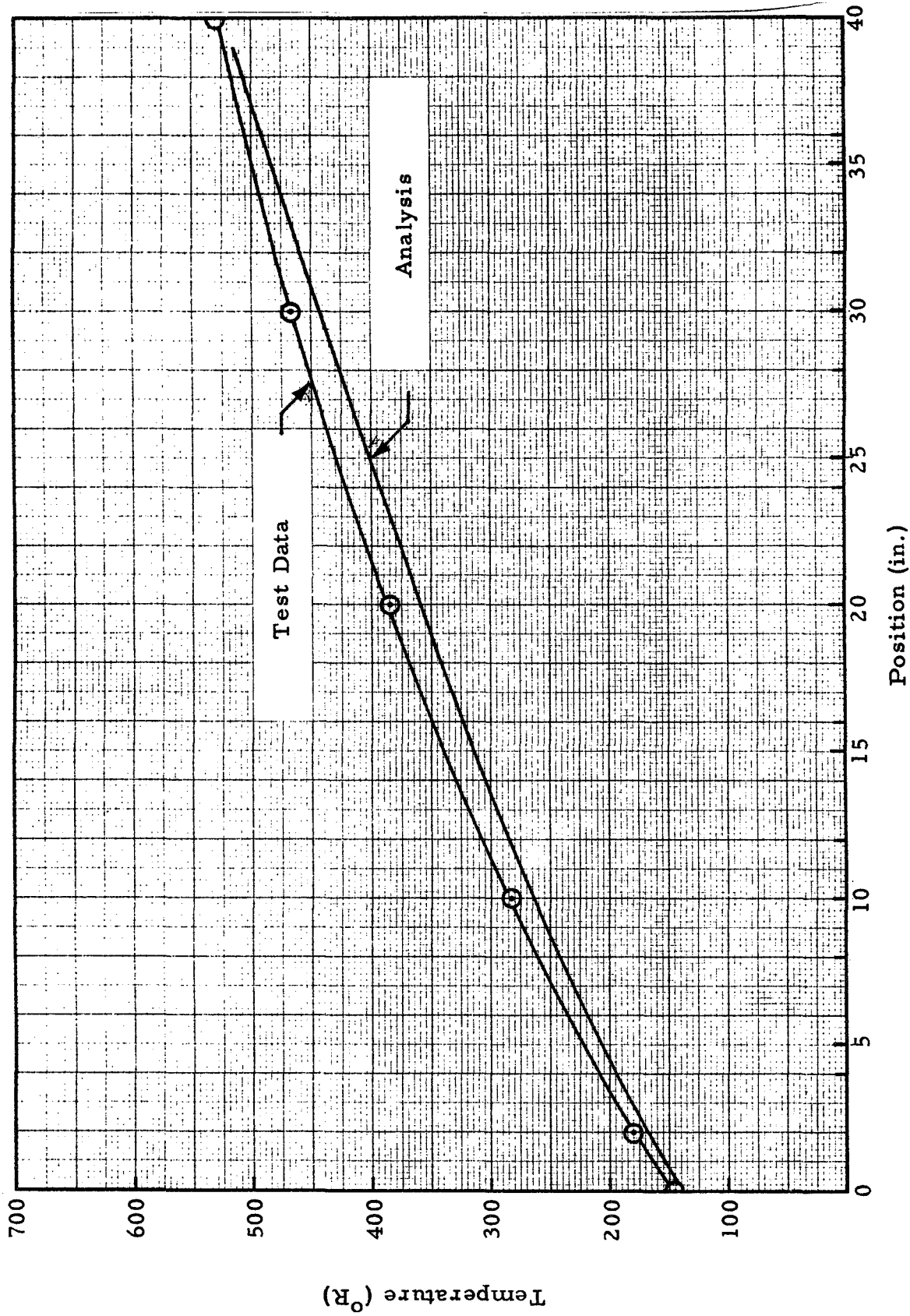


Figure 37 - Temperature Distribution Along Penetration for Diagonal Joint Insulation Specimen

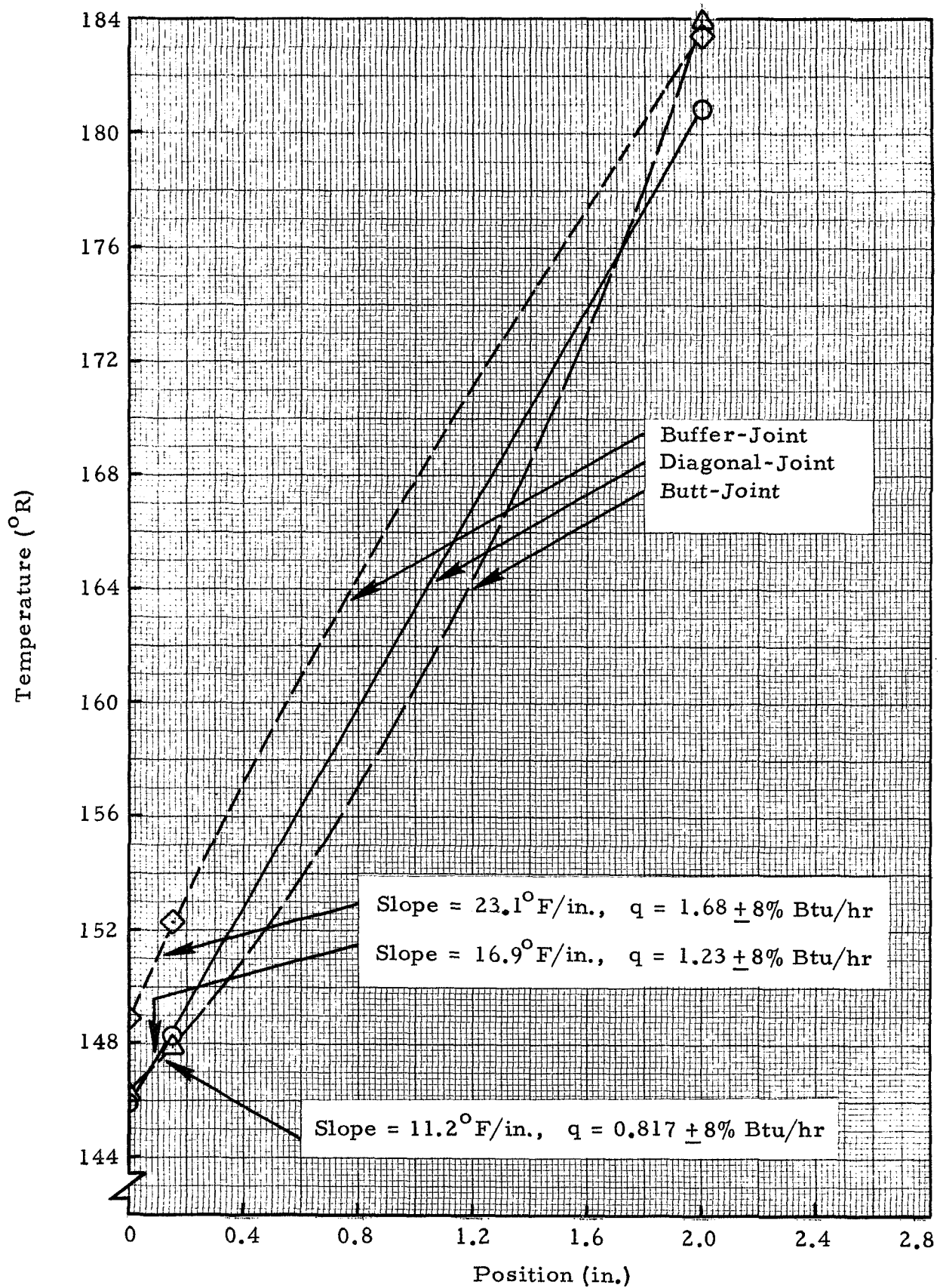


Figure 38 - Axial Temperature Distribution Along Base of Penetration for Diagonal, Buffer and Butt Insulation Specimen

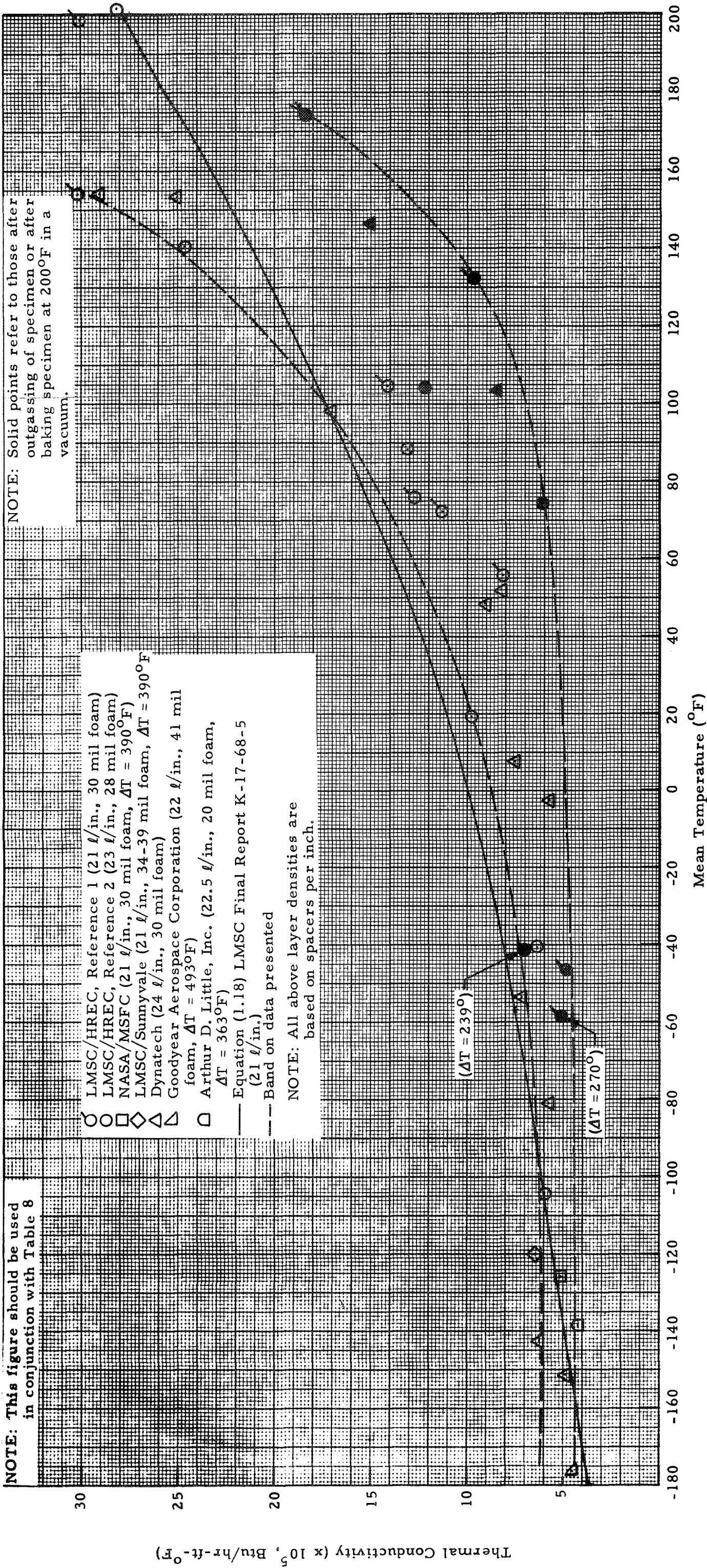


Figure 39
Plot of Thermal Conductivity vs Temperature
for Double Aluminized Mylar and Red Polyure-
thane Foam as Presented by Various Investigators

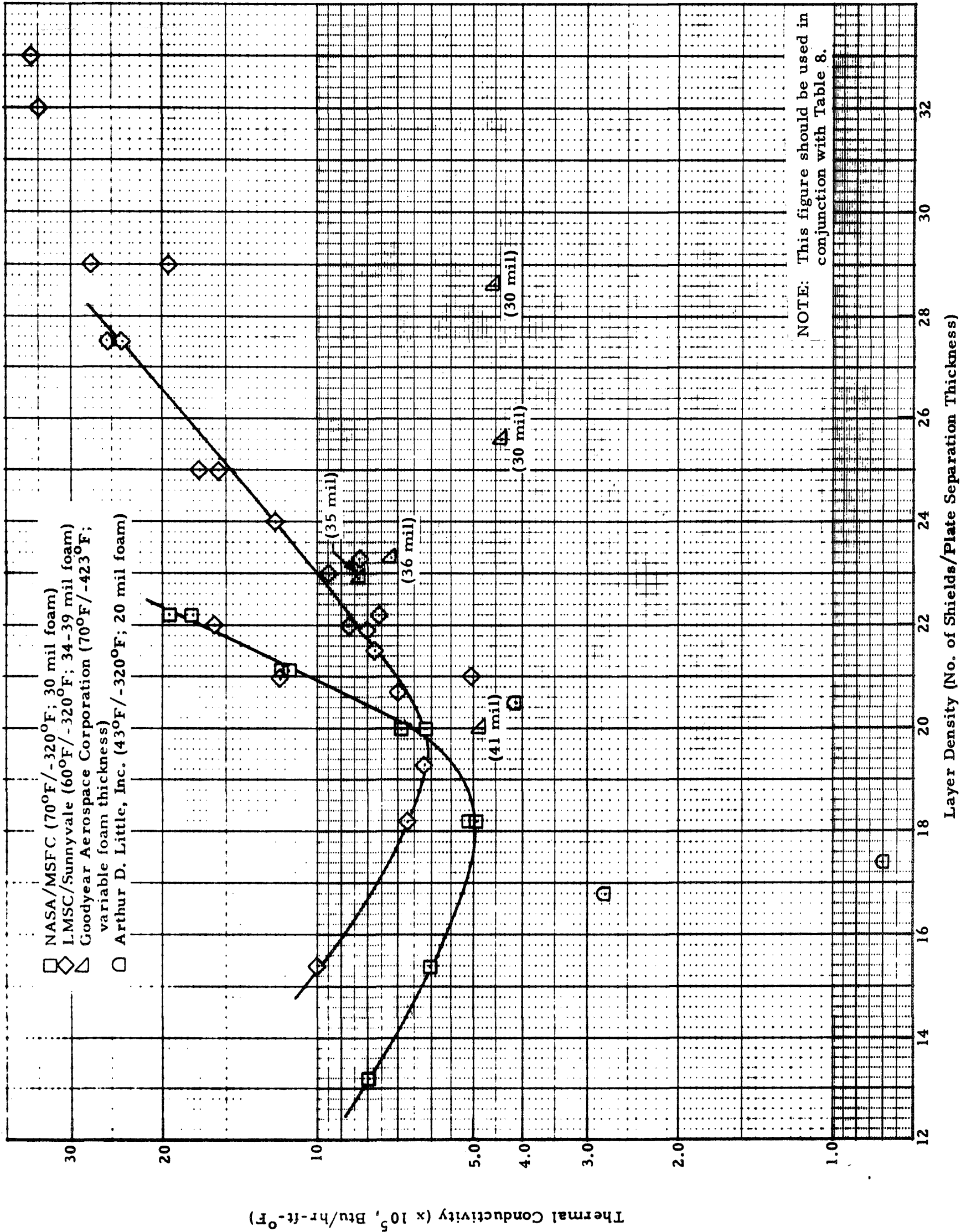


Figure 40
Plot of Thermal Conductivity vs Layer
Density for Double-Aluminized Mylar
and Red Polyurethane Foam as
Presented by Various Investigators

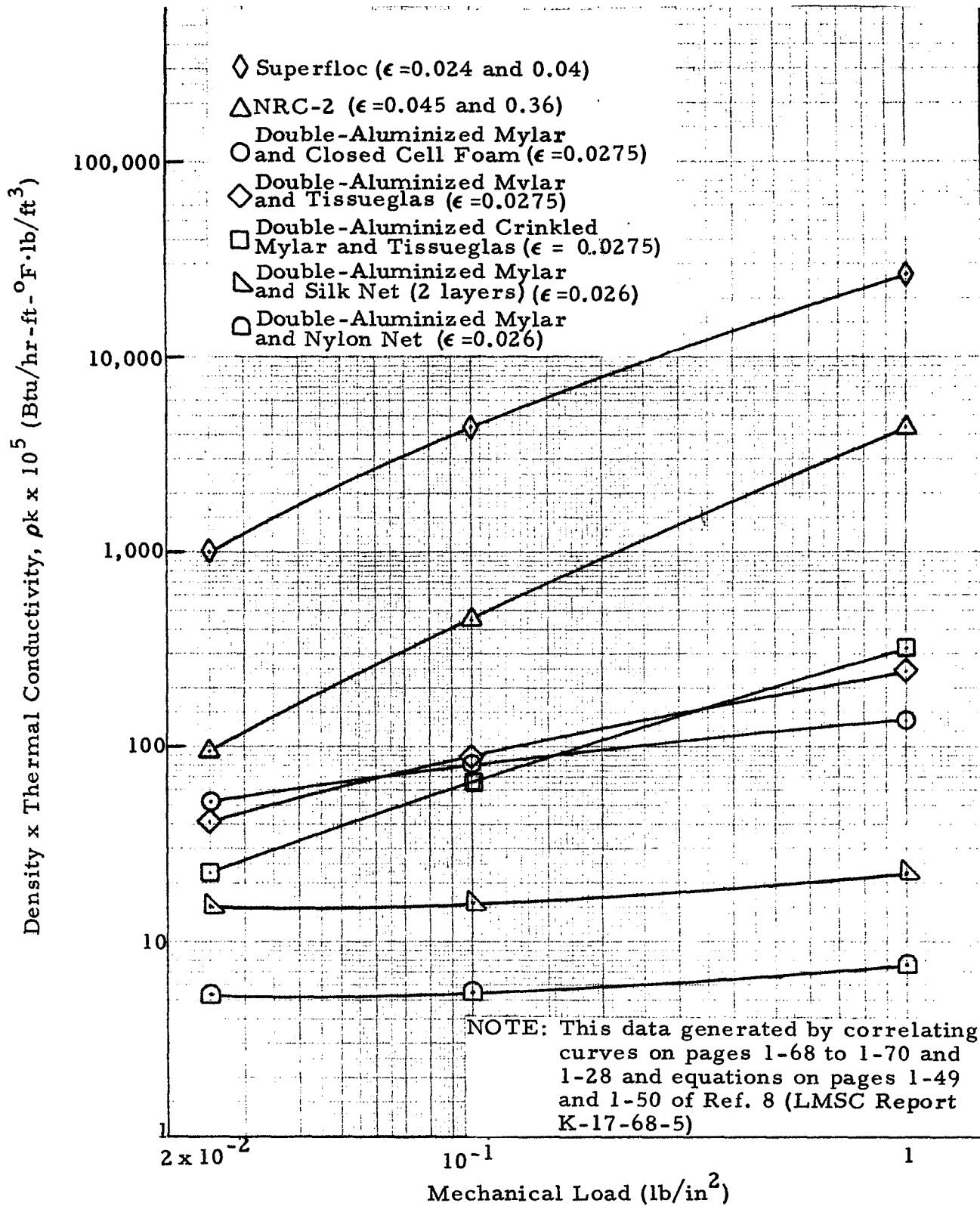


Figure 41 - Plot of Density x Thermal Conductivity vs Mechanical Load for Various HPI Materials at 0°F

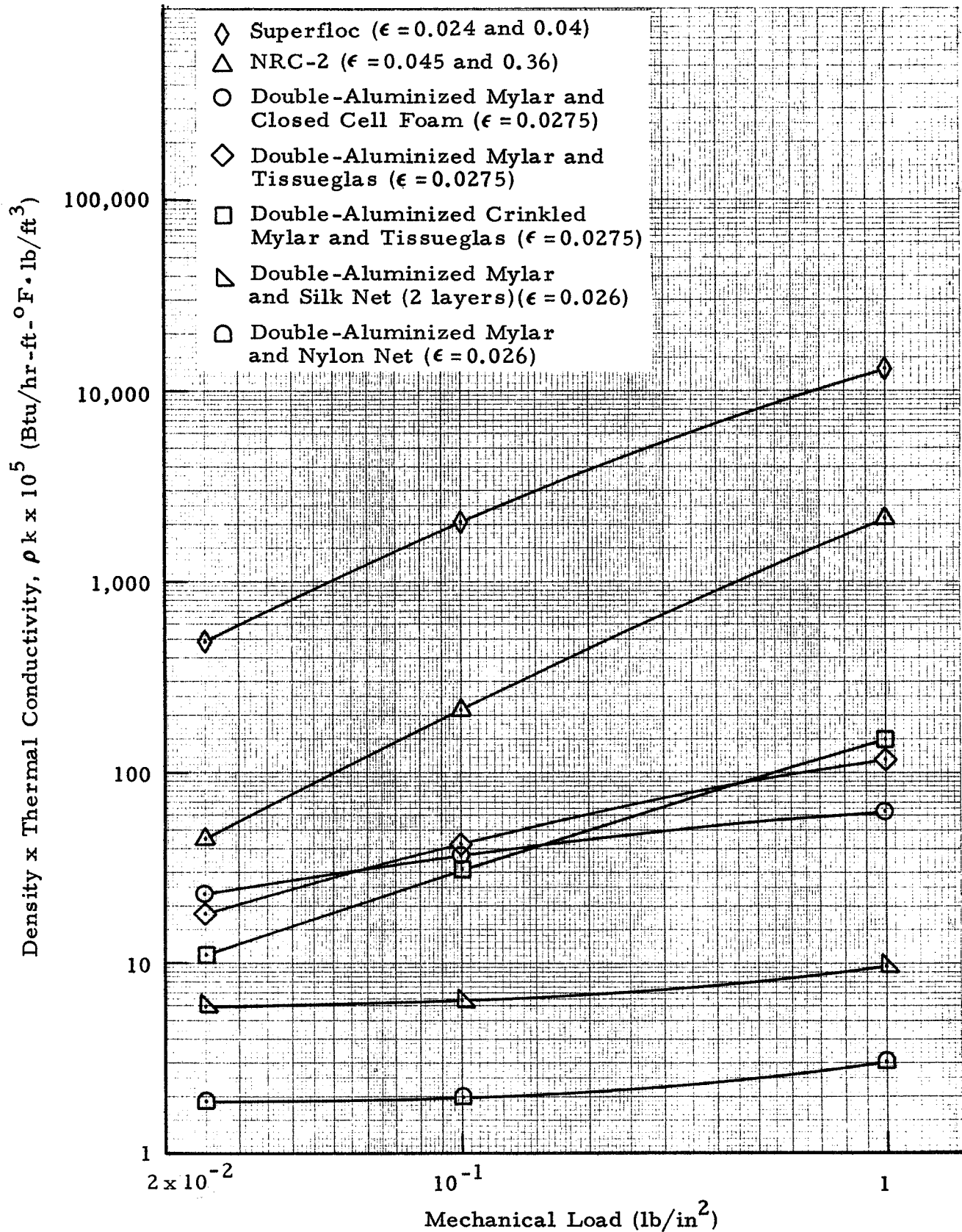


Figure 42 - Plot of Density x Thermal Conductivity vs Mechanical Load for Various HPI Materials at 400°R and 40°R Boundary Temperatures

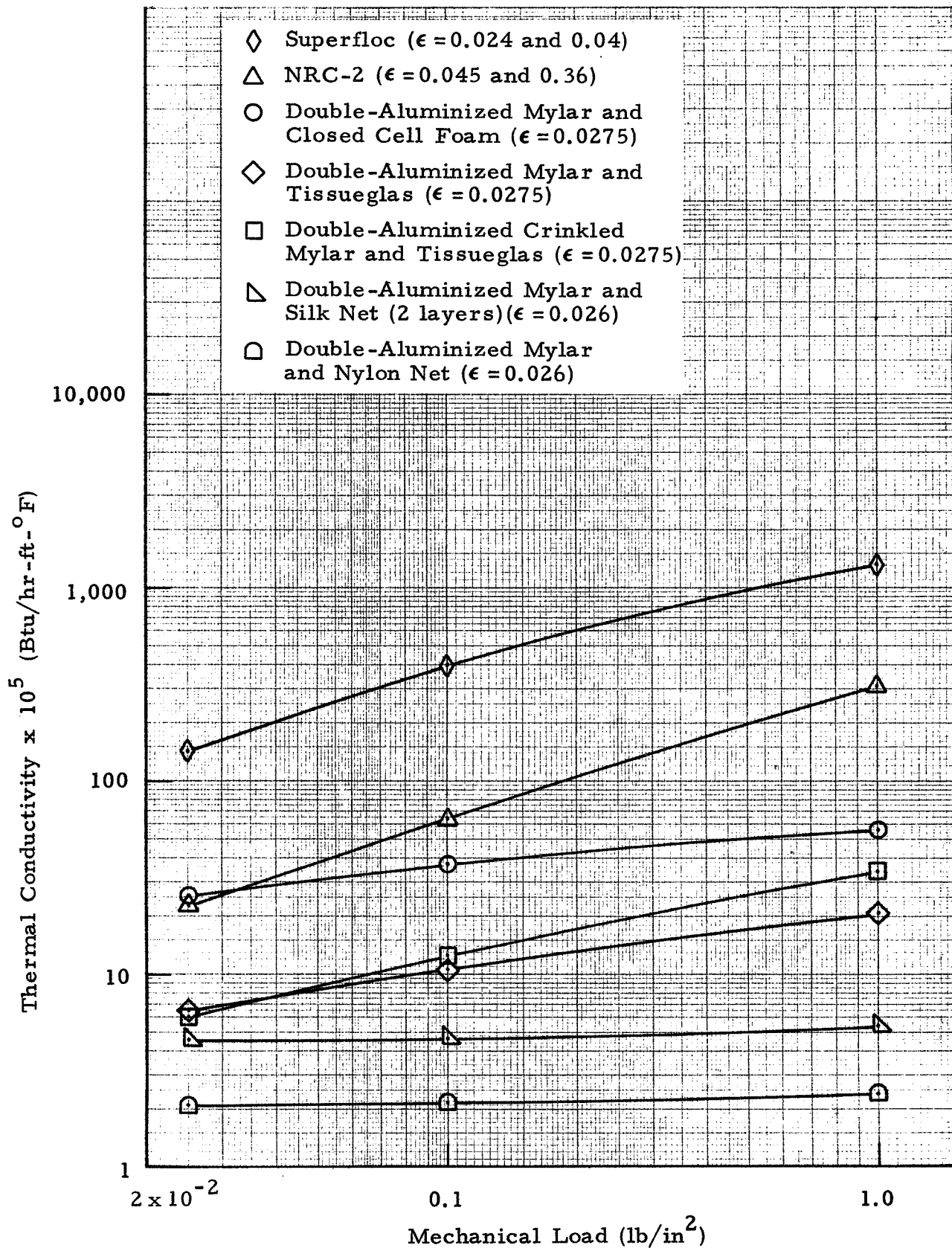


Figure 43 - Plot of Thermal Conductivity vs Mechanical Load for Various HPI Materials at 0°F

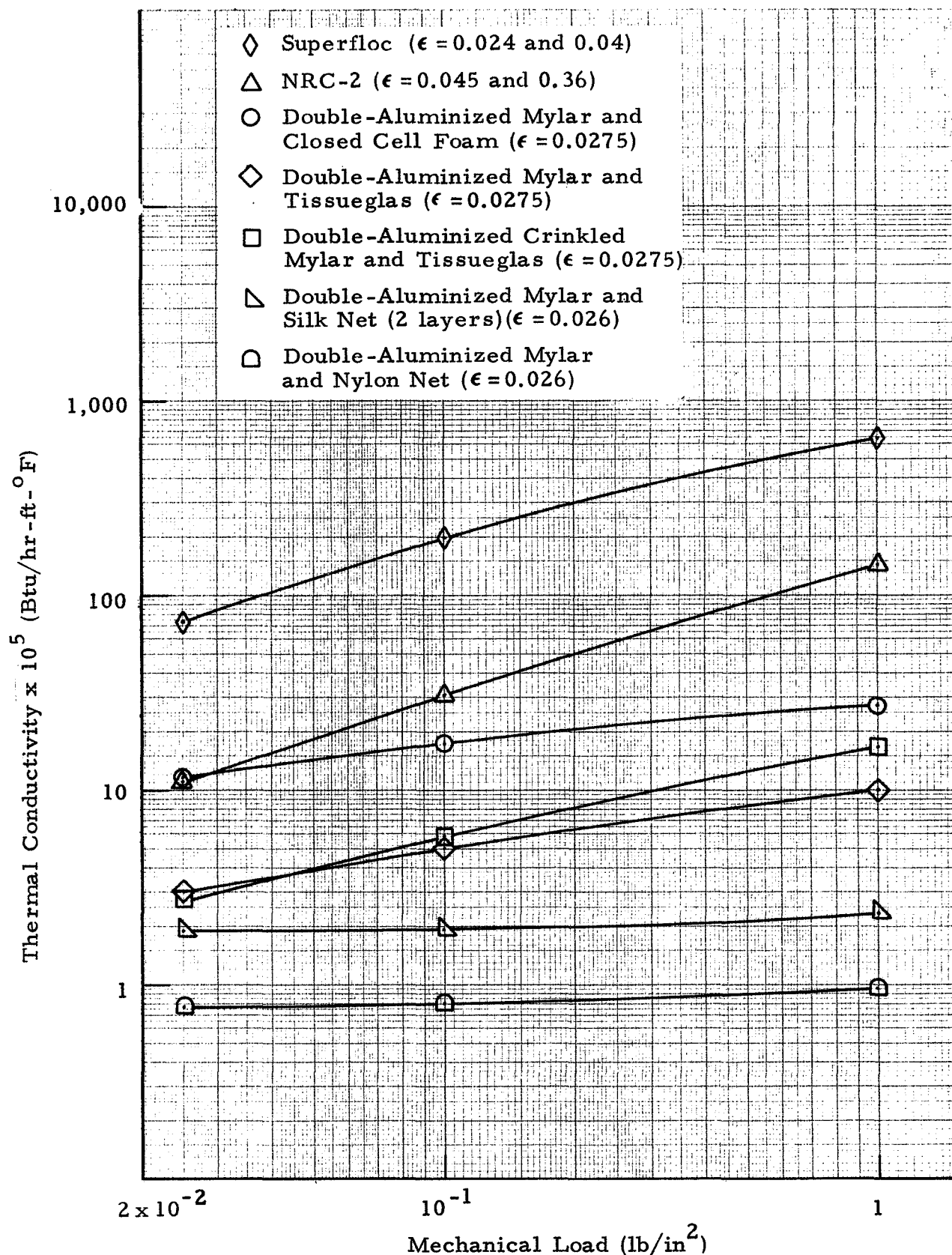


Figure 44 - Plot of Thermal Conductivity vs Mechanical Load for Various HPI Materials of 400°R and 40°R Boundary Temperatures

Appendix A
ERROR ANALYSIS

Appendix A ERROR ANALYSIS

The equation required to determine the thermal conductivity is

$$k(T) = \frac{q \ln \left(\frac{r_o}{r_i} \right)}{2 \pi L (T_i - T_o)}$$

where

$$T = \frac{T_o + T_i}{2}$$

$$q = P = IV$$

In order to determine the error in $k(T)$, the errors in q , r_o , r_i , L and $T_i - T_o$ must be determined and combined. The Kline-McClintock probable error analysis procedure shown in Appendix B is used to obtain the combined effect of the errors on k . The best estimate for the probable error for each parameter is determined below:

$$r_i = \frac{1.5}{12} \text{ ft}$$

$$dr_i = \frac{0.02}{12} \text{ ft}$$

$$r_o = \frac{2.5}{12} \text{ ft} \left(\frac{2.0}{12} \text{ for embossed aluminized Mylar} \right)$$

$$dr_o = \frac{0.1}{12} \text{ ft}$$

$$\begin{aligned} d \left(\frac{r_o}{r_i} \right) &= \left\{ \left(\frac{dr_o}{r_i} \right)^2 + \left(\frac{r_o dr_i}{r_i^2} \right)^2 \right\}^{1/2} \\ &= \left\{ \left(\frac{0.1/12}{1.5/12} \right)^2 + \left[\frac{(2.5/12)(0.02/12)}{(1.5/12)^2} \right]^2 \right\}^{1/2} \\ &= 0.0703 \end{aligned}$$

$$d \left(\ln \frac{r_o}{r_i} \right) = \frac{1}{\left(\frac{r_o}{r_i} \right)} \cdot d \left(\frac{r_o}{r_i} \right)$$

$$= \frac{0.0703}{\left(\frac{2.5/12}{1.5/12} \right)} = 0.0422$$

$$\frac{d \ln \left(\frac{r_o}{r_i} \right)}{\ln \left(\frac{r_o}{r_i} \right)} = \frac{0.0422}{0.51} = 8.3\% \quad \left(\begin{array}{l} 18\% \text{ for embossed} \\ \text{aluminized Mylar} \end{array} \right)$$

$$L = 1 \text{ ft} \quad dL = \frac{0.05}{12} \text{ ft}$$

$$\therefore \frac{dL}{L} = \frac{0.05/12}{1} = 0.00417 = 0.417\% \text{ (negligible)}$$

$$(T_i - T_o) \approx 40^\circ \text{R} \quad d(T_i - T_o) = 0.05^\circ \text{R}$$

$$\frac{d(T_i - T_o)}{(T_i - T_o)} = \frac{0.05}{40} = .00125 = 0.125\% \text{ (negligible)}$$

$$q = P = IV \quad dq = d(IV) \pm q_\ell \pm q_s$$

$$d(IV) = 0.0014 \text{ IV}$$

-

$$\frac{dIV}{IV} = 0.0014 = .14\% \text{ (negligible)}$$

The longitudinal heat loss, q_ℓ , is calculated using conduction in the glass fiber. Conduction down the insulation and the copper wire is small in comparison to that in the glass fiber. The largest temperature difference between the test and a longitudinal heater is $1/20^\circ \text{F}$.

$$q_\ell = k A_c \frac{\Delta T}{\Delta X}$$

where

$$k = 0.182 \text{ Btu/hr-ft-}^{\circ}\text{F}$$

$$\begin{aligned} A_c &= 2\pi r_i t \\ &= \frac{2\pi (1.5)(1/16)}{144} \text{ ft}^2 \end{aligned}$$

$$\frac{\Delta T}{\Delta X} = \frac{1/20^{\circ}\text{F}}{1 \text{ ft}} = 0.05$$

$$q_{\ell} = 0.000372 \text{ Btu/hr for one end}$$

$$\therefore q_{\ell} = \left[2 (0.000372)^2 \right]^{1/2} = 0.000525 \text{ Btu/hr for both ends}$$

The heat stored term q_s is calculated from the thermal mass of the test section of the calorimeter. During operation the largest temperature change with time of the calorimeter was 0.02°F/hr

$$q_s = \left(m_1 C_{p1} + m_2 C_{p2} \right) \frac{\Delta T}{\Delta \theta}$$

where

$$m_1 = 0.464 \text{ lbm}$$

$$C_{p1} = 0.27 \text{ Btu/lbm-}^{\circ}\text{F}$$

$$m_2 = 0.16 \text{ lbm}$$

$$C_{p2} = 0.1 \text{ Btu/lbm-}^{\circ}\text{F}$$

$$\frac{\Delta T}{\Delta \theta} = 0.02^{\circ}\text{F/hr}$$

$$q_s = \left[(0.464)(0.27) + (0.16)(0.1) \right] 0.02$$

$$= 0.00282 \text{ Btu/hr}$$

Now the combined probable error of q_l and q_s are calculated

$$\begin{aligned} dq &= (0.000525^2 + 0.00282^2)^{1/2} \\ &= 0.00288 \text{ Btu/hr} \end{aligned}$$

Since q varies from data point to data point,

$$\frac{dq}{q} \text{ is variable}$$

$$\therefore \frac{dq}{q} = \frac{0.00288}{q}$$

For each data point q is known and dq/q can be calculated.

Now all the errors are combined to obtain the error in thermal conductivity. The Kline McClintock rms method of combining errors is used. All the above errors except $d \ln(r_o/r_i) / \ln(r_o/r_i)$ and dq/q are insignificant in an rms summation. Therefore,

$$\frac{dk}{k} = \left\{ \left[\frac{d \ln \left(\frac{r_o}{r_i} \right)}{\ln \left(\frac{r_o}{r_i} \right)} \right]^2 + \left[\frac{dq}{q} \right]^2 \right\}^{1/2}$$

This calculation is done for each data point, and the resulting probable error is presented in the tables and figures.

Appendix B

KLINE-McCLINTOCK PROBABLE ERROR ANALYSIS PROCEDURE

Appendix B

KLINE-McCLINTOCK PROBABLE ERROR ANALYSIS PROCEDURE

If variables A and B have errors, a and b, respectively, then the propagation of these errors will be as follows:

For addition and subtraction of A and B, the resultant error P will be

$$P = \pm (a^2 + b^2)^{1/2}$$

For multiplication of A and B, the resultant error P will be

$$P = \pm \left[(A b)^2 + (B a)^2 \right]^{1/2}$$

For division of B by A, the resultant error P will be

$$P = \pm \left[\frac{\left(\frac{B a}{A} \right)^2 + b^2}{A^2} \right]^{1/2}$$